DIFFUSION OF DRAG REDUCING AQUEOUS POLYMER SOLUTIONS IN EXTERNAL FLOW

DIFFUSION OF DRAG REDUCING AQUEOUS POLYMER SOLUTIONS IN EXTERNAL FLOW

by

Ossama K. F. El Riedy, B.Sc.(Eng.)

A Thesis
Submitted to the School of Graduate Studies
in Partial Fulfilment of the Requirements
for the Degree
Master of Engineering

McMaster University

April 1975

MASTER OF ENGINEERING — McMASTER UNIVERSITY
(Mechanical Engineering) Hamilton, Ontario.

TITLE: Diffusion of Drag Reducing Aqueous Polymer Solutions in External Flow

AUTHOR: Ossama K. F. El Riedy, B.Sc. (Mech. Eng.)
(Cairo University,
Cairo, Egypt)

SUPERVISOR: Dr. B. Latto

NUMBER OF PAGES: x, 102

SCOPE AND CONTENTS:

This thesis describes an experimental study of the diffusion of dilute aqueous drag reducing polymers when ejected from a thin wall slot into a developing turbulent boundary layer (external flow).

A horizontal flat plate located in a 0.1524 m. (6 in.) I.D. plexiglass pipe was specifically designed for obtaining diffusion data. Water or aqueous polymer solutions which were dyed with a fluorescing dye were injected tangentially into the boundary layer through a slot situated near the leading edge of the flat plate. Samples were taken from the flow field and by using a spectrophotometer, concentration profiles were established. The investigation was carried out for a constant free stream velocity of 5.4 m./sec. for various injection flow rates and concentrations in the range 0 to 1500 w.p.p.m.

It was found that the diffusion rate will increase for very low polymer concentrations (of the order of 0.75 w.p.p.m.), while the diffusion rate will be reduced for higher concentrations. The resulting data have been compared to Newtonian diffusion phenomena as well as the available data for polymer additives.

Correlations for the concentration profiles, diffusion boundary layer growth, wall concentration and eddy diffusivity are presented. The research covers the four important zones of diffusion with emphasis on the earlier developing zones for which there are virtually no data available. The results indicate that a universal diffusion correlation exists which represents the data for both Newtonian and polymer solutions for the far region downstream but indicate decidedly different phenomena near the injection region, confirming a previously published theoretical analysis.

ACKNOWLEDGEMENTS

The author wishes to express his gratitude to his supervisor, Dr. B. Latto, for his valuable advice, continuous encouragement and assistance throughout the duration of the present investigation.

The author also expresses his appreciation to Ms. Betty Anne Bedell for typing the manuscript.

The financial support provided by the National Research Council through Grant A2937 and the Defence Research Board of Canada through Grant 9550-56 are also acknowledged.

TABLE OF CONTENTS

LIST OF FIGURES

NOMENCLATURE

SYMBOL	DESCRIPTION	UNIT
a, $\bar{a}_1$, $\bar{a}_2$,... a_1, a_2,...	Constants	
A	Constant: $\int_0^{\delta_m/\lambda} (\xi)^{\frac{1}{n}} f(\xi)\, d\xi$	
b, b_1, b_2,...	Constants	
B	Batchelor constant: $\frac{d\tilde{y}}{dx}/u(\tilde{y})$	sec,/m,
c	Polymer concentration in w.p.p.m.	
c_i	Value of c at injection slot fluid	
$\bar{c}$	Time average value of c at a point	
$\bar{c}_m$	Wall value of $\bar{c}$	
$\bar{c}_\infty$	The main stream mean concentration	
c'	Turbulent conditional average value of c at a point	
d	Hydraulic depth: (4 area/wetted perimeter)	m,
D	Molecular diffusivity	m^2/sec,
$D^{(t)}$	Eddy diffusivity	m^2/sec,
G_i	Volume flux of polymer solution per unit span	m^2/sec,
h	Slot thickness	mm,
K	Von Kármán constant	
K_1	$\int_0^{\delta_m/\lambda} \bar{u}\, \bar{c}\, dy/G_i\, c_i$ (correction factor)	
n	Velocity profile power law constant: 7	

Q_i	Volume flux of polymer solution	Lit./sec.
R	Radius of the test section	m.
Re	Reynolds number $(\frac{u_{max}\, x}{\nu})$	
t	time	sec.
u,v,w	x,y,z - components of the velocity vector	m./sec.
U_T	Local value of the friction velocity: $\sqrt{\tau_w/\rho}$	m./sec.
$\bar{u},\bar{v},\bar{w}$	Time average value of u,v,w at a point	m./sec.
u',v',w'	Turbulent conditional average value of u,v,w at a point	m./sec
$\bar{u}_{max}$	Mean free stream velocity	m./sec.
x,y,z	Rectangular coordinates; x measured along a surface in the flow direction from the injection slot; a normal distance from the surface; z span wise position	mm.
$\bar{x}$	Distance from the leading edge	mm.
$\bar{y}$	Mean vertical height of the particles	mm.
δ	Boundary layer thickness at which $\bar{u} = 0.99\ \bar{u}_{max}$	mm.
δ_π	Boundary layer thickness	mm.
δ_{av}	Mean boundary layer thickness: $\int_0^x \delta_\pi\, dx/\Delta x$	mm.
λ	Value of y at which $\bar{c}/\bar{c}_m = 0.5$	mm.
ξ	y/λ	
ρ	Water (or polymer solution) density, a constant	kg/m^3
τ_w	Local wall shear stress	N/m^2
ν	Kinematic viscosity	$m^2/sec.$

Subscripts

p	polymer
w	water

Abbreviations

w.p.p.m.	weight parts per million
O.D.	optical density
I.O.D.	injection optical density

CHAPTER 1

INTRODUCTION

That additives can considerably reduce drag in turbulent flow has been well established during the past twenty seven years since Tom's first publication on the subject. The actual mechanism involved has not been definitely established but it certainly appears that the suppression of high frequency turbulence in the inner wall or buffer zone of the boundary layer plays an important role. Consequently it is essential to efficiently get and keep the additive in the inner wall region.

A number of methods may be used to get the additive into the crucial wall region of the boundary layer. For example homogeneous dispersion, injection or additive coatings may be used. Homogeneous flows are only of practical value in closed loop or recirculating systems, whilst the latter approaches may be used on any practical system.

Obviously it is necessary to have available methods of determining the dispersion rate of the additives from a coating or injection area if design calculations or feasibility studies are to be made. This thesis is concerned with the subject of the turbulent diffusion rate of polymer solution injected into the turbulent developing external boundary layer.

Since the ejected polymer solution is greatly diluted by the turbulent mixing in the boundary layer, the drag reduction

is mainly determined by the diffusion rate of the polymer solution within the inner wall region. Thus the prediction of the mixing rate within the boundary layer becomes very important in evaluating a particular system.

Obviously the reduction of drag in real systems may have economic or practical advantages. For example, injection of polymer into the boundary layer on a submarine may facilitate a considerable increase in the maximum speed of the vessel. However, this may be an uneconomical operation when considering the cost of the polymers being used. But the running and capital costs of larger engines operating below their maximum efficiency would make use of the polymer additive economic from this point of view.

Unfortunately, the majority of research on polymer additives has been in drag reduction efficiency and methods of getting the polymer into the boundary layer. Very little research has been reported on the prediction of turbulent diffusion rates. Furthermore, very few papers have been published on empirical data, which are important if accurate methods of predicting dispersion rates and concentration levels are to be achieved. This research was investigated to help fill the gap in the available empirical knowledge especially regarding the near injection region as well as to verify existing though very sparse data for the far downstream conditions.

To this end, a small water tunnel in which a single flat plate model with injection facilities was located was constructed in which concentration measurements were made with maximum flow velocity of the order of 6 m./sec.

CHAPTER 2

LITERATURE SURVEY

As stated in the Introduction, it is important to have available reliable accurate information on the turbulent diffusion rates of polymers in order to assess the requirements for practical drag reduction systems in external flows. Unfortunately very little information is available in the open literature on this subject. The main emphasis during the past decade has been on the effect of drag reducing additives on the development of boundary layers and the mechanism involved.

In a study of the diffusion phenomena of drag reducing additives, it is necessary to compare the data with existing theories and data for Newtonian fluids. Consequently, pertinent research on all aspects of diffusion in turbulent fluid boundary layers must be considered.

Poreh and Cermak [1] studied the two-dimensional turbulent mixing of ammonia gas injected from a line source into a turbulent boundary layer formed on the wall of a wind tunnel. They found what appeared to be four zones of development of the mean concentration profile which were:

(1) The initial zone in which very large velocity and concentration gradients make it impossible to obtain reliable data. The length of this region is determined by the initial conditions near the source, physical

size of the source relative to the thickness of the sub-layer, the injection velocity and the magnitude of the molecular diffusivity.

(2) The intermediate zone in which longitudinal gradients are small compared to vertical gradients and the boundary layer approximation for the velocity and concentration profiles used. Within this zone the diffusing plume is totally submerged in the boundary layer, and the rate of growth of the vertical dimension of the plume is large compared to the rate of growth of the boundary layer itself. The mean concentration profiles can be described by the dimensionless universal curve:

$$\frac{\bar{c}}{\bar{c}_m} = f(\xi) \tag{2.1}$$

It appeared that the function $f(\xi)$ is independent of $\bar{u}_{max}$ and δ in this zone.

The data were fitted for longitudinal variation of λ using

$$\lambda = \bar{a}_1 (x)^{0.8} \tag{2.2}$$

and the variation of $\bar{c}_m \bar{u}_{max}$ could be approximated to

$$\bar{c}_m \bar{u}_{max} = \bar{a}_2 (x)^{-0.9} \tag{2.3}$$

The intermediate zone extends 20-40 boundary layer thicknesses downstream from the injection slot.

(3) The transient zone in which the effect of the mild mixing process in the ambient air decreases the rate of growth of the diffusion plume and gradually changes the shape of the concentration profile.

(4) The final zone in which the diffusion of matter beyond the boundary layer into the ambient fluid is controlled by the molecular action and the turbulent fluctuation in the ambient fluid. The concentration profiles within this zone can be described by

$$\frac{\bar{c}}{\bar{c}_m} = f\left(\frac{y}{\delta}\right) \tag{2.4}$$

$$\bar{c}_m = \bar{a}_3 \left(\bar{u}_{max}\, \delta\right)^{-1} \tag{2.5}$$

The major difference between the intermediate zone and the final zone is that the characteristics of the diffusion field are independent of the position of the source in the final zone.

Fabula and Burns [2] studied the mixing with and without friction reducing polymer solution in approximately two-dimensional open channel flow. Dyed polymer solution or dyed water was injected through a tangential wall slot extending across the channel near the effective start of the boundary layer. They applied the negative roughness analogy which is useful in the case of low polymer concentration and moderate wall stress. Samples were taken far enough downstream of the injection slot (5 and 12 m. from the injection slot) to ensure typical final zone behaviour. Good agreement was obtained between the

expression for $\frac{\bar{c}}{\bar{c}_m}$ described by Morkovin [3] and a correlation based on their own experimental results which was:

$$\frac{\bar{c}}{\bar{c}_m} = \exp\left[-0.693\ (\xi)^{2.15}\right] \qquad (2.6)$$

They used this expression for the concentration ratio together with the velocity defect similarity law of Coles [4] to obtain the following expression:

$$\frac{\bar{u}_{max}\ \delta_\pi\ \bar{c}_m}{G_i'\ c_i} = (0.606 - 313\ U_T/\bar{u}_{max})^{-1} \qquad (2.7)$$

The comparison between the predicted law and the experimental results supported the negative roughness analogy and showed good agreement between the calculated and experimental wall concentrations. The results for both the water and polymer solution injection flows were quite similar. However, there was large disagreement for λ between the calculated and the experimental values which showed that the agreement for $\bar{c}_m$ was partially accidental. They attributed this to the fact that either the flow was three-dimensional or that the approximation of substituting $\bar{u}\bar{c}$ for $\overline{uc}$ in their analysis produced a significant error. However, they recommended the three-dimensionalities effect as the primary reason for the difference. The dimensional comparison of prediction with experiment showed that there was qualitative agreement for the mean concentration profiles but a sizable underestimate of the concentration all across the profile. This was at least partly due to the large experimental

difference in the results between G_i c_i and the $\bar{uc}$ integral which should have been very nearly equal.

Jin Wu [5] measured the concentration profile for drag reducing polymer ejected from a thin wall slot into a developing turbulent boundary layer (external flow) using a laser phot-transistor unit. The research included tests of ejecting polymer solutions of various concentrations at various injection rates. The experiments were performed in a recirculating water channel and drag reduction studies were done at a constant free stream velocity. It has been observed that polymers thicken the viscous sub-layer which appreciably increases the flow rate in the sub-layer. Therefore, the turbulent mixing or the dilution of polymers outside of the sub-layer takes place with a smaller fraction of the ejected solution than for water injection. There is some disagreement between his concentration measurements and those reported earlier in [1] and [2]. His results indicated a suppression of the diffusion of drag reducing polymer within a turbulent boundary layer when the concentration of the ejected solution is greater than 100 w.p.p.m. and there is very little change in turbulent diffusion with polymer injection concentrations less than 100 w.p.p.m.

In a later work, Poreh and Hsu [6] calculated the diffusion in the intermediate zone when a fluid ejected from a continuous line source by using Poreh's previous data for ammonia air diffusion. They modified a method originally proposed on the basis of Lagrangian similarity conditions [7] to describe the mean position of an ensemble of particle release.

It was suggested, on the basis of the observed similarity of the concentration profiles downstream of a continuous line source at the ground level, that the mean vertical height $\bar{Y}$ of particles at a distance x from the source was approximately equal to the mean vertical height of an ensemble of single particle released having the same distance from the source. This theory was supported by [8]. Accordingly the rate of growth of the diffusing boundary layer had been calculated by integrating the equation:

$$\frac{d\bar{y}}{dx} = B\, U_T/u(\bar{y}) \qquad (2.8)$$

since $$\bar{y} = 0.76\, \lambda \qquad (2.9)$$

$$\bar{u}(y) = \bar{u}_{max}\ (y/\delta)^{\frac{1}{n}} \qquad (2.10)$$

Comparison with the experimental data [9] showed that 'B' is constant and approximately equal to the Von Karman constant K only when the diffusion boundary layer is completely submerged in the logarithmic layer of the velocity field (i.e., $\frac{y}{\delta} \leq 0.15$). When the thickness of the boundary layer becomes larger than this value, the diffusion rate decreases as a result of the reduced turbulent mixing in the outer region. Consequently the integration of Equation (2.8) should be done with $B = K\,(1 - \bar{y}/\delta)$ which gives a reasonable agreement with the experimental data of [1] throughout the intermediate zone. They studied the effect of roughness or polymer additives and found that the diffusion increased in the case of rough surfaces and decreased for drag reducing additives.

In a later work Porch and Hsu [10] analyzed the diffusion of diluted drag reducing polymers and the effect of the diffusing polymers on the development of the boundary layer. Their analysis suggested that both the diffusion rate and the drag were reduced. However in most practical situations, since the required concentration is small, the reduction in the diffusion rate will be small. In their analysis they concluded that except in very slowly moving ships, the initial stage of diffusion would be relatively short and insignificant. In the final zone of diffusion, on the other hand, there would be hardly any polymers left in the viscous sub-layer. Since the structure of the major portion of the turbulent boundary is not affected by the polymers, their prediction for the distribution in the final stage is expected to be similar to the distribution of inert tracers. Thus the main change would be in the intermediate zone. They found that the longer the plate the larger were the quantities of polymer required to achieve the same percentage of drag reduction (i.e., the absolute power saving due to the polymer ejecting did not decrease). Furthermore, they found that the drag reduction per unit discharge was larger for small values of Q_i, indicating that it might be more economical to obtain only small drag reduction. They also concluded that in high speed flows, the effect of the viscous sub-layer on the diffusion was limited to a short distance near the ejection line. Further downstream, diffusion was similar with and without polymers. In both cases the diffusion rate was proportional to the shear velocity and inversely proportional to the mean velocity. Thus

the diffusion rate was decreased in the case of drag reduction. The effect, however, was not very large and the polymers "fill" the entire boundary layer within a distance smaller than 100 times the boundary layer thickness.

Walters and Wells [11], [12] experimentally studied the mechanics of turbulent diffusion when uniformly injecting drag reducing polymer solution through a porous wall into fully developed pipe flow of water. Their data were obtained using very low injection rates and indicated an increase in the viscous sub-layer thickness which is accompanied by an increase in the diffusion sub-layer thickness. Furthermore, empirical diffusion coefficients were obtained. Their data showed that for the polymer diffusion, the diffusion rate in the region of the polymer deficient turbulent core is greater than the Newtonian fluid or water diffusion. Consequently there is a significant reduction in the turbulent diffusion near the wall which leads to a higher concentration there than for the case of water injection.

2.1. Summary

From the available data and analysis, it can be concluded that for diffusion from a line source into a two-dimensional turbulent boundary layer, the downstream diffusion may be divided into four zones:

1. Initial zone
2. Intermediate zone
3. Transient zone
4. Final zone

It was found that the main difference between the diffusion of polymers and other tracers would be in the intermediate zone. Furthermore, it was observed that the diffusion rate and drag were reduced. However, for most practical situations the reduction in the diffusion rate may be expected to be small. It is also suggested that the prediction of the negative roughness analogy is useful and that the drag reduction per unit discharge is larger for small values of the discharge rate.

Finally it is apparent that very few experimental studies have been completed, and those which have been done were mainly concerned with the diffusion far downstream from the injection site (i.e., for the final zone). Verification of Poreh et al.'s analytical studies as well as more extensive research for a greater range of velocities for the four proposed zones of diffusion needs to be done.

CHAPTER 3

EXPERIMENTAL APPARATUS

At the commencement of the research an experimental apparatus existed. However, the operating criteria were considerably changed from the previous requirements and consequently the apparatus is essentially a new design. As previously stated, the research was to obtain empirical data on the diffusion rate of drag reducing additives in two-dimensional external turbulent equilibrium boundary layers with no pressure gradient. To this end, an existing flat plate apparatus, see Figure 1, was redesigned to comply with the following criteria:

(1) To achieve the highest possible mean water flow velocity in the test section given an available static head of 3.3 m of water.

(2) Tangential injection of water or polymer solution at different flow rates and different concentrations.

(3) To be able to obtain velocity and concentration profile data in the longitudinal and vertical directions in the flow field.

(4) To simulate a semi-infinite flow field.

3.1. Test Section

The test section was comprised of a plexiglass pipe 1.3 m. long and 0.152 m. (6 in.) I.D. which permitted visual

observation. A horizontal flat plate 1.3 m. long by 0.152 m. wide with 12.7 mm. thickness was centrally located in the pipe with its large surfaces horizontal. At the leading and trailing ends of the plate, 63.5 mm. long wedges were fitted to minimize pressure gradients. A 76.2 mm. (3 in.) wide by 0.64 mm. (0.025 in.) deep transverse injection slot, see Figure 2, located 0.137 m. downstream from the leading edge on the upper face of the flat plate was used to tangentially inject the solutions into the boundary layer. The solution to be injected was supplied to both ends of a transverse chamber situated behind the injection slot in an attempt to obtain a uniform injection velocity profile. In order to obtain liquid samples in the longitudinal direction, 36 locations for probes 31.8 mm. (1.25 in.) apart along the centerline on the top of the pipe were produced. These probes, which could be used either for concentration or velocity measurements, were attached to a crossbar which could be moved vertically. The location of the bar with respect to the flat plate was measured with two micrometers, having an accuracy of 0.025 mm. (0.001 in.), which were located at the ends of the bar. At three cross-section sections 0.44 m. (17.5 in.) apart, provisions were made to locate 4 probes around the upper semi-circular periphery, as shown in Figure 3, such that one probe was at the top, two at 45^{o} to the horizontal and one 5^{o} to the horizontal. The first cross section was at 95.25 mm. from the injection slot. These probes were used to obtain cross-sectional concentration profiles, total and static pressures required for the calculation of the velocity profiles and the pressure drop

over the test section. Right angle probes with 0.5 mm. I.D. and 1 mm. O.D. were used to collect the samples and also to obtain velocity profiles. The sampling stations, see Figure 4, were at distances of 0.050 , 0.146 , 0.304 , 0.558 and 0.844 m. (2, 5.75, 12, 22 and 33.25 in.) downstream from the injection slot and could cover the four zones of diffusion previously defined in Chapter 2. The probe stations for measuring the velocity were at distances of 0.095 , 0.539 and 0.984 m. (3.75, 21.25 and 38.75 in.) downstream from the injection slot.

3.2. The Water Flow System

The water flow system could either be open circuit or closed loop, the latter arrangement, see Figure 3, was used when the flow rates were greater than that which could be accommodated by the drains. The system was comprised of a 50.0 m^3 capacity in-ground storage reservoir (sump tank), from which the water was pumped to a 7.5 m^3 capacity constant head header tank situated above the apparatus. This arrangement produced a maximum of 3.3 m. static head at the test section. An axial single stage centrifugal pump*, driven by a three-phase a.c. motor+, pumped the water from the sump tank to the header tank. The water then flowed through a 0.203 m. (8 in.) diameter pipe vertically down to a cylindrical plenum chamber thence to a plexiglass tubular test section. A cylindrical-type brass

---

* Canada Pumps Limited, 1400 U.S. gal/min., 1150 r.p.m., 20 ft. head, 10 H.P.

\+ Robbins and Meyers Company, 30, 55 V, 11A, 1140 r.p.m. 10 H.P., continuous duty.

screen at the entrance to the 0.203 m. (8 in.) vertical pipe inside the constant head tank stopped foreign matter from entering the test section and also reduced the tendency to produce entrance vortices. The flow area of the screen was higher than the area of the pipe which avoided excessive losses. Furthermore, a cross piece was fixed in the 0.203 m. (8 in.) vertical pipe at the exit from the constant head tank to avoid vortices being generated in the constant head tank with the consequent air injection. A butterfly valve situated in the 0.203 m. (8 in.) vertical pipe before the plenum chamber was used to control the mass flow rate and consequently the velocity of the water inside the test section. An upstream cylindrical plenum chamber situated prior to the test section was used to ensure damping the vortices, and to avoid excessive boundary layer thickness in the test section and thus produce cored flow in the test section. At the entrance to the plexiglass pipe a honeycomb was used to align the flow going to the test section. The velocity was measured at the inlet to the test section using a pitot static tube. At the exit from the test section an inverted 'U' type elbow and bend was used to ensure that the flow would fill all the test section, the flow then discharged to the sump.

After the assembly of the apparatus, the velocity distribution vertically across the test section just upstream of the test plate was measured. It was found that the velocity at the top half of the plexiglass pipe was much smaller than expected. After several trials, it was found that the smaller velocity was mainly due to eddies and disturbances at the inlet

to the plexiglass pipe from the plenum chamber. This was virtually eliminated by changing the entrance from reentrant to sharp edged.

3.3. The Polymer Solution Flow System

The supply of the polymer solution, see Figure 3, was from a pressurized storage vessel, which was connected to a constant 689.5 KN/m^2 (100 lb_f/in^2) pressure air supply. The air pressure inside the vessel could be maintained at any desired value using a pressure regulator. The compressed air above the polymer solution was used to discharge the solution to the apparatus via a pipeline at the bottom of the vessel. The pressurized vessel was fitted with a safety valve set for 103.4 KN/m^2 (15 lb_f/in^2). A rotameter type flow meter which had been precalibrated with various polymer solution concentrations was used in the polymer solution flowline to measure the injection flow rate. The solution being injected to the opposite ends of the injection slot, in an attempt to obtain a uniform velocity profile at the exit from the slot. The polymer solution was pre-prepared in plastic lined bins and supplied to the pressurized vessel by means of a variable speed peristalic pump*, driven by a three-phase a.c. motor+.

---

* All speeds Limited, type A16FS, 1 H.P.

\+ Brook Motors Limited, 3-ϕ, 865 r.p.m., 1 H.P.

3.4. Measuring Instrumentation

(1) Mean velocity profiles were measured at four locations. The first location was just prior to the test plate using a pitot static tube while the other three locations were along the plate. The measurements were made using the difference between the total head measured by the pitot tubes in the centerline and the static head at the same section using a mercury in glass U tube manometer.

(2) The pressure drop along the upper half of the test section was measured using a U tube manometer filled with carbon tetrachloride dyed with iodine.

(3) The discharge rate of the injected solution was measured using a rotameter which was calibrated prior to the experiments for various polymer concentrations.

(4) Concentration profile measurements were made using the total head probes to obtain samples which were collected in small test tubes. The flow rate into the small bore sampling tubes was sufficiently low that no disturbance in the flow would occur. The samples were taken at different locations and different heights above the flat plate downstream of the injection slot. The local concentration measurements of the injection fluid in the test section was based on the measurements of the concentration of a fluorescent tracer dye solution mixed with the injected fluid and detected in the samples. The fluorescent concentration

in the samples was measured using a spectrophotometer* which gave excellent sensitivity of the order of 0.005 w.p.p.m. and specificity at very low concentrations. The level of fluorescent radiation is usually in direct proportion to the concentration of the fluorescing molecules and linear response is possible over a broad range of concentrations. Rhodamine WT was used as a fluorescent tracer which gave linear response in the range of 0 to 8 w.p.p.m. which covers the range used in the experiments.

3.5. Experimental Procedures

3.5.1. System Preparation

It was initially necessary before each experiment to drain off the water from the header tank and the sump and then refill the system with clean untreated mains water to reduce the accummulation of the dye in the water system. This was usually done 12 hours or more before the test. The water was circulated through the system prior to the experiments to ensure isothermal conditions.

3.5.2. Additive Solution Preparation

The solutions were prepared in plastic cans each having a capacity of 60 Kg. of water. The plastic bag was replaced prior to the preparation of each new solution after which the solution was pumped into the storage vessel.

---

* Gilford Instrument Laboratories Inc., Oberlin, Ohio, Automatic recording spectrophotometer model 2400, Form No. 04-2400-6-1-69.

(a) Water Injection

The experimental measurements were performed by injecting an aqueous rhodamine solution through the injection slot into the boundary layer over the flat plate. The concentration of the injected rhodamine WT solution was 100 w.p.p.m. and the solution was prepared 6 hours before a test run.

(b) Polymer Injection

The additive used was Reten 423 (obtained from Hercules Inc.) which is an anionic acrylic polymer with an assessed molecular weight of between 10^7 to 10^8 and is known to have high resistance to sheer degradation. The experimental test runs were performed by injecting a mixture of aqueous polymer and rhodamine WT dye solution. The polymer solution was prepared by carefully weighing an appropriate quantity of polymer, then dispersing it in a small quantity of alcohol and gradually adding this to the homogeneous rhodamine water mixture. (The polymer should not be added to the water all at once since it does not disperse and flacculates.) The mixture was then periodically stirred. This procedure reduces the time required to obtain a homogeneous solution and the alcohol has little effect on the solution if only small quantities are used. The solution was prepared between one and three days before the test to ensure complete mixing.

3.6. Test Procedures

The header tank and sump were filled with untreated mains water 12 hours before the test and circulation of the water continued until steady state isothermal conditions were achieved. The velocity data were taken vertically across the test section at four locations using the pitot static tube in conjunction with the total and static head probes. The vertical location of the probes was obtained from the micrometers.

After starting the main flow and allowing a steady state condition to be reached, the discharge valve from the polymer solution vessel was turned on and the rhodamine or polymer-rhodamine solution was then injected at a constant predetermined discharge rate which was achieved by adjusting the air pressure to a desired constant value. In order to avoid the effect of the decreasing solution level inside the polymer solution vessel on the flow rate. A fine adjustment valve controlled the polymer solution flow rate. The system was operated for some time to achieve steady state conditions.

To prevent the effect of eddies and disturbances created behind each probe on the diffusion data, the samples were collected at only one longitudinal location each time. The samples were collected within the boundary layer for each longitudinal location. In addition, samples were collected at the top part of the test section to check the free stream concentration. The location of the sample points above the flat plate was determined using the micrometers.

The capacity of the injection vessel was such that it was only possible to obtain samples in five longitudinal locations before it emptied. At least two samples were taken at each location to check reproducibility of data at given flow conditions.

CHAPTER 4

THEORY

4.1. Velocity Profiles

In order to avoid the necessity of using numerical data in subsequent calculations and correlations, the velocity data were correlated using standard techniques. A simple power law relationship was initially used and subsequently was found suitable for the range of Reynolds numbers used in the experiments. That is, the velocity profile correlation which was found to best fit the experimental data was the well established seventh power law. [14].

$$\frac{\bar{u}}{\bar{u}_{max}} = \left(\frac{y}{\delta_\pi}\right)^{\frac{1}{n}} \qquad (4.1)$$

where $n = 7$

4.2. Concentration Profiles

In a turbulent boundary layer over a flat plate any quantity such as the instantaneous local concentration of the polymer or the dye will be a function of the location compared to the injection source, the time t, the injection rate and concentration, and the free stream velocity, thus

$$c = c(x, y, z, Q_i, c_i, u_{max}, t) \qquad (4.2)$$

For two-dimensional flows and taking time average values, the mean concentration will be independent of z, i.e.,

$$\bar{c} = \bar{c}\ (x,\ y,\ Q_i',\ c_i,\ u_{max}) \tag{4.3}$$

Introducing a convenient dimensional characteristic of the diffusion boundary layer λ, defined by

$$\frac{\bar{c}}{\bar{c}_m} = 0.5 \quad \text{at } y = \lambda$$

and also the mean concentration on the wall which will be a function of $(Q_i,\ c_i,\ x,\ \bar{u}_{max})$, we obtain an equation for the mean concentration as a function of $(x,\ \lambda,\ \bar{c}_m)$, i.e.,

$$\bar{c} = \bar{c}(x,\ \lambda,\ c_m)$$

From dimensional analysis and similarity to the velocity profile within the boundary layer over a flat plate, we may expect that

$$\frac{\bar{c}}{\bar{c}_m} = f\ \left(\frac{y}{\lambda}\right) = f\ (\xi) \tag{4.4}$$

Morkovin [3] developed the following expression which describes the data of Poreh and Cermak [1] for $(\bar{c}/\bar{c}_m)$ versus (y/λ) with the following expression,

$$\frac{\bar{c}}{\bar{c}_m} = \exp\ [-0.693\ (\xi)^a] \tag{4.5}$$

where a = constant which depends on the diffusion zone which

will satisfy the intermediate, transient and final zones.

4.3. The Continuity Equation

Assuming that the flow is approximately two dimensional and that steady state conditions prevail, the continuity equation between the injection slot and any location downstream may be written as

$$G_i c_i = \int_0^\infty \overline{u c}\, dy \qquad (4.6)$$

where $u = \bar{u} + u'$

and $c = \bar{c} + c'$

assuming $\bar{c}'$ and $\bar{u}'$ tend to zero.

Then

$$G_i c_i = \int_0^\infty (\bar{u}\,\bar{c} + \overline{u'\,c'})\, dy$$

since

$$\overline{u'\,c'} \ll \bar{u}\,\bar{c}, \text{ then } \overline{u'\,c'} \approx 0$$

This is a reasonable assumption since even if u' and c' were "perfectly correlated", i.e., if $|\overline{u'\,c'}| = (\overline{u'^2}\ \overline{c'^2})^{1/2}$ and if the relative root mean square amplitudes of u' and c' were each about 20% of the mean value, the error in neglecting $\overline{u'\,c'}$ compared to $\bar{u}\,\bar{c}$ would be only about 4% at the most. Thus neglecting $\overline{u'\,c'}$ is reasonable.

Therefore

$$G_i\, c_i = \int_0^{\infty} \bar{u}\, \bar{c}\, dy$$

$$= \int_0^{\delta_\pi} \bar{u}_{max} \left(\frac{y}{\delta_\pi}\right)^{\frac{1}{n}} \bar{c}_m\, f(\xi)\, dy + \int_{\delta_\pi}^{\infty} \bar{u}_{max}\, \bar{c}_m\, f(\xi)\, dy$$

Since λ is independent of y,

$$\frac{G_i\, c_i}{\bar{u}_{max} \lambda \bar{c}_m} = \left(\frac{\lambda}{\delta_\pi}\right)^{\frac{1}{n}} \int_0^{\frac{\delta_\pi}{\lambda}} (\xi)^{\frac{1}{n}} f(\xi)\, d\xi + \int_{\frac{\delta_\pi}{\lambda}}^{\infty} f(\xi)\, d\xi \qquad (4.7)$$

4.4. The Eddy Diffusivity.

The continuity equation of the dye without chemical reaction can be written as follows:

$$\frac{\partial \bar{c}}{\partial t} = -\left(\frac{\partial}{\partial x}\bar{u}\bar{c} + \frac{\partial}{\partial y}\bar{v}\bar{c} + \frac{\partial}{\partial z}\bar{w}\bar{c}\right) - \left(\frac{\partial}{\partial x}\overline{u'c'} + \frac{\partial}{\partial y}\overline{u'c'} + \frac{\partial}{\partial z}\overline{w'c'}\right)$$

$$+ D\left(\frac{\partial^2 \bar{c}}{\partial x^2} + \frac{\partial^2 \bar{c}}{\partial y^2} + \frac{\partial^2 \bar{c}}{\partial z^2}\right) \qquad (4.8)$$

For steady state conditions and two-dimensional flow the continuity equation can be reduced to

$$u\frac{\partial \bar{c}}{\partial x} + v\frac{\partial \bar{c}}{\partial y} + \bar{c}\left(\frac{\partial \bar{u}}{\partial x} + \frac{\partial \bar{v}}{\partial y}\right) = \frac{\partial}{\partial x}\left(D\frac{\partial \bar{c}}{\partial x} - \overline{u'c'}\right) + \frac{\partial}{\partial y}\left(D\frac{\partial \bar{c}}{\partial y} - \overline{v'c'}\right)$$

(4.9)

The continuity equation of an incompressible mixture can be written as follows:

$$\frac{\partial \bar{u}}{\partial x} + \frac{\partial \bar{v}}{\partial y} + \frac{\partial \bar{w}}{\partial z} = 0$$

For two-dimensional flow the continuity can be reduced to:

$$\frac{\partial \bar{u}}{\partial x} + \frac{\partial \bar{v}}{\partial y} = 0 \tag{4.10}$$

From Equations (4.9) and (4.10) the continuity equation for the diffusion of the injected Newtonian (dyed) solution will be

$$\bar{u} \frac{\partial \bar{c}}{\partial x} + v \frac{\partial \bar{c}}{\partial y} = \frac{\partial}{\partial x} \left(D \frac{\partial \bar{c}}{\partial x} - \overline{u'c'}\right) + \frac{\partial}{\partial y} \left(D \frac{\partial \bar{c}}{\partial y} - \overline{v'c'}\right)$$

Except near the source, a boundary layer approximation becomes possible [13] and gives

$$\bar{u} \frac{\partial \bar{c}}{\partial x} + \bar{v} \frac{\partial \bar{c}}{\partial y} = \frac{\partial}{\partial y} \left(D \frac{\partial \bar{c}}{\partial y} - \overline{v'c'}\right) \tag{4.11}$$

Integration of Equation (4.11) may be achieved by using the distribution function of the concentration obtained from the experiments. Furthermore, by dividing Equation (4.4) by Equation (4.7), the following equation can be obtained

$$\bar{c} = \frac{G_i \, c_i}{\bar{u}_{max} \, \lambda} \; \frac{f(\xi)}{\left(\frac{\lambda}{\delta_\pi}\right)^{\frac{1}{n}} A + \int_{\frac{\delta_\pi}{\lambda}}^{\infty} f(\xi) \, d\xi}$$

If we assumed that the diffusion will only be within the boundary layer, i.e.,

$$f\left(\frac{\delta_\pi}{\lambda}\right) \to 0$$

$$\therefore \quad \bar{c} = \frac{G_i\, c_i}{\bar{u}_{max}\,\lambda A}\left(\frac{\delta_\pi}{\lambda}\right)^{\frac{1}{n}} f(\xi) \tag{4.12}$$

$$\therefore \quad \bar{u}\,\frac{\partial \bar{c}}{\partial x} = \frac{G_i c_i f(\xi)(\xi)^{\frac{1}{n}}}{A}\cdot\left(\frac{d\lambda}{dx}\right)\left(\frac{\frac{1}{n}\left(\frac{\lambda}{\delta_\pi}\right)\frac{d\delta_\pi}{d\lambda} - \left(\frac{n+1}{n}\right)}{\lambda^2}\right)$$

$$- \frac{G_i\, c_i\, f'(\xi)\,(\xi)^{\left(\frac{1}{n}+1\right)}}{A}\cdot\left(\frac{d\lambda}{dx}\right)\cdot\left(\frac{1}{\lambda^2}\right) \tag{4.13}$$

From the continuity equation for the mixture

$$\bar{v} = -\int_0^y \frac{\partial \bar{u}}{\partial x}\, dy.$$

$$= -\frac{1}{n}\,\bar{u}_{max}\int_0^y \frac{y^{\frac{1}{n}}}{(\delta_\pi)^{\frac{1}{n}+1}}\,\frac{d\,\delta_\pi}{dx}\,dy$$

$$= \frac{1}{n+1}\,\bar{u}_{max}\,(\xi)^{\frac{n+1}{n}}\cdot\left(\frac{\lambda}{\delta_\pi}\right)^{\frac{n+1}{n}}\frac{d\,\delta_\pi}{dx} \tag{4.14}$$

From Equations (4.12) and (4.14)

$$\bar{v}\,\frac{\partial \bar{c}}{\partial y} = \frac{1}{n+1}\,\frac{G_i\, c_i}{A}\cdot\frac{f'(\xi)(\xi)^{\frac{1}{n}+1}}{\delta_\pi\,\lambda}\,\frac{d\,\delta_\pi}{dx} \tag{4.15}$$

By introducing Equations (4.13) and (4.15) into Equation (4.11)

$$\therefore \frac{\partial}{\partial y}\left(D\frac{\partial \bar{c}}{\partial y} - \overline{v'c'}\right) = \frac{G_i\, c_i}{A}\left(\frac{d\lambda}{dx}\right)\left\{\frac{f(\xi)(\xi)^{\frac{1}{n}}\left[\frac{1}{n}\left(\frac{\lambda}{\delta_\pi}\right)\frac{d\delta_\pi}{d\lambda} - \left(\frac{n+1}{n}\right)\right]}{\lambda^2}\right.$$

$$\left. - \frac{f'(\xi)(\xi)^{\frac{1}{n}+1}}{\lambda^2} + \frac{1}{n+1}\,\frac{f'(\xi)(\xi)^{\left(\frac{1}{n}+1\right)}}{\delta_\pi\,\lambda}\,\frac{d\,\delta_\pi}{d\lambda}\right\} \qquad (4.16)$$

By partial integration, Equation (4.16) can be reduced to:

$$D\,\frac{\partial \bar{c}}{\partial y} - \overline{v'c'} = -\frac{G_i\, c_i}{\lambda\, A}\left(\frac{d\lambda}{dx}\right) f(\xi)\,(\xi)^{\left(\frac{1}{n}+1\right)}\left[1-\frac{1}{n+1}\left(\frac{\lambda}{\delta_\pi}\right)\frac{d\delta_\pi}{d\lambda}\right] \qquad (4.17)$$

Since the molecular diffusion is very low compared to the turbulent diffusion, it is justified to neglect the molecular diffusion except near the surface. An equation for the turbulent diffusion can be deduced as follows:

$$\overline{v'c'} = \frac{G_i\, c_i}{\lambda\, A}\,\frac{d\lambda}{dx}\, f(\xi)\,(\xi)^{\left(\frac{1}{n}+1\right)}\left[1 - \frac{1}{n+1}\,\frac{\lambda}{\delta_\pi}\,\frac{d\,\delta_\pi}{d\lambda}\right]$$

The order of the dimensionless factor $\left[\frac{1}{n+1}\,\frac{\lambda}{\delta_\pi}\,\frac{d\,\delta_\pi}{d\lambda}\right]$ will be much smaller than one where,

$$n = 7 \quad . \quad \frac{\lambda}{\delta_\pi} = 0 \rightarrow 0.6 \quad \text{at the most}$$

$\frac{d\,\delta_\pi}{d\lambda}$ is much smaller than one and equal to zero at the final zone.

Therefore it is justified to reduce the equation of the turbulent diffusion to

$$\overline{v'c'} = \left(\frac{G_i\ c_i}{\lambda\ A}\right)\left(\frac{d\lambda}{dx}\right)\ f(\xi)\ (\xi)^{\frac{1}{n}+1} \tag{4.18}$$

By introducing the eddy diffusivity defined by

$$D^{(t)} = -\left[\overline{v'c'}/(\partial\bar{c}/\partial y)\right] \tag{4.19}$$

Treating Equations (4.12), (4.18) and (4.19) simultaneously we obtain

$$D^{(t)} = -\lambda\ \bar{u}_{max}\left(\frac{d\lambda}{dx}\right)\left(\frac{\lambda}{\delta_\pi}\right)^{\frac{1}{n}}\ (\xi)^{\frac{1}{n}+1}\ \frac{f(\xi)}{f'(\xi)} \tag{4.20}$$

Equations (4.18) and (4.20) give the turbulent diffusion and the eddy diffusivity at any location in the longitudinal or vertical directions, and is valid except near the injection slot or at the surface where the molecular diffusivity will be prominent. Equation (4.20) shows that the eddy diffusivity is proportional to the diffusion boundary layer growth where it can be used for diluted polymer solutions at low concentations.

By introducing Equation (4.5) into Equation (4.20), the following general equation for the eddy diffusivity at the different zones can be obtained.

$$D^{(t)} = \frac{1}{0.693a}\ \lambda\ \bar{u}_{max}\left(\frac{d\lambda}{dx}\right)\ \left(\frac{\lambda}{\delta_\pi}\right)^{\frac{1}{n}}\ (\xi)^{\left(2+\frac{1}{n}-a\right)} \tag{4.21}$$

CHAPTER 5

RESULTS

In this chapter the experimental data are presented with some explanatory comment. The experimental data are tabulated in Appendix 2.

Figure 5 shows a plot of non-dimensional velocity profiles, i.e., $\bar{u}/\bar{u}_{max}$ versus height over the flat plate for a location upstream of the test section and at three locations over the test section for a fully opened inlet valve. Also shown in this graph is the boundary layer growth profile together with a 1/7th power law profile [14]. Figure 6 shows a plot of non-dimensional $\bar{u}/\bar{u}_{max}$ versus non-dimensional height y/δ_π at the three locations over the test section together with a 1/7th power law. It is apparent from all the velocity profiles and the boundary layer thickness growth diagrams that a 1/7th power law quite accurately describes the empirical data, thence the velocity profile and the boundary layer thickness can be approximated by the following equations.

$$\frac{\bar{u}}{\bar{u}_{max}} = \left(\frac{y}{\delta_\pi}\right)^{\frac{1}{n}} \tag{5.1}$$

$$\frac{\delta_\pi}{\bar{x}} = 0.037\ (Re_x)^{-0.2} \tag{5.2}$$

Figures 7, 8, 9, 10, 11 and 12 show plots of the concentration profiles $\bar{c}/c_i$ versus the height over the flat plate within the test section at five locations downstream from the injection slot for water and polymer solution injection at different injection flow rates and concentrations. It is seen that for water injection all the concentration profiles have the same trend, whereas the concentration profiles for polymer solution injection can be divided into at least two zones. The first zone is one in which the concentration gradient is very steep and the second is a zone in which the concentration gradient tends to approach that of the water injection. It seems that the length of the first zone is a function of the polymer injection concentration and the injection flow rate. Figure 13 shows a plot of non-dimensional concentration profile $\bar{c}/\bar{c}_m$ versus the non-dimensional height y/λ at the five locations for water injection. It is apparent that the non-dimensional concentration profile $\bar{c}/\bar{c}_m$ for the water injection is a function of the non-dimensional height ξ only and independent of the location from the injection slot. It is seen that the result can be presented by the following equation:

$$\frac{\bar{c}}{\bar{c}_m} = \exp\left[-0.693\left(\frac{y}{\lambda}\right)^a\right] \tag{5.3}$$

where a = constant.

Figure 22 shows a plot of non-dimensional wall concentration $\frac{\bar{c}_m\ \bar{u}_{max}}{c_i\ u_i}$ versus the non-dimensional location $(\frac{x}{h})$ for the water injection. The result can apparently be presented by the

equation:

$$\frac{\bar{c}_m \, \bar{u}_{max}}{c_i \, u_i} = b_1 \left(\frac{x}{h}\right)^{a_1} \qquad (5.4)$$

Figure 23 shows the growth of a representative diffusion thickness defined by λ versus the location downstream from the injection slot for water injection. It is apparent that within the velocity ratio $(\bar{u}_{max}/u_i)$ used in the experiments that λ is a function of only the location downstream from the injection slot, and the results can be presented by the equation:

$$\lambda = b_2 \, (x)^{a_2} \qquad (5.5)$$

Figure 24 shows a plot for the growth of a representative diffusion thickness with respect to the boundary layer thickness (λ/δ_π) versus the non-dimensional location defined by (x/δ_{av}) from which it is apparent that $(\frac{\lambda}{\delta_\pi})$ tends to approach a constant value of 0.45 at $\frac{x}{\delta_{av}} = 15$.

Figures 14, 15, 16, 17, 18, 19, 20 and 21 which are only for the developed concentration profiles show plots of non-dimensional concentration $\bar{c}/\bar{c}_m$ versus a non-dimensional height y/λ for injections of polymer concentrations of 50, 100, 250, 500 and 1500 w.p.p.m. It is apparent that there are four zones that may be described within the test section length. The length of those zones depends on a number of factors.

Figure 25 shows a plot of non-dimensional wall concentration $(\bar{c}_m \, \bar{u}_{max}/c_i \, u_i)$ versus the non-dimensional location down-

stream from the injection slot $(\frac{x}{h})$ for polymer injection concentrations of 50 and 100 w.p.p.m. The data of this can be presented by an equation of the form:

$$\frac{\bar{c}_m \bar{u}_{max}}{c_i u_i} = b_3 \left(\frac{x}{h}\right)^{a_3} \tag{5.6}$$

Figure 26 shows the growth of a representative diffusion thickness λ versus the location x for a polymer injection concentration of 50 w.p.p.m. It is seen that λ is a function of the location downstream from the injection slot for the range of $\bar{u}_{max}/\bar{u}_i$ used in the experiments.

Figure 27 shows a ratio of a non-dimensional polymer wall concentration compared to the non-dimensional water wall concentration defined by

$$\left(\frac{\bar{c}_m \bar{u}_{max}}{c_i u_i}\right)_p \Big/ \left(\frac{\bar{c}_m \bar{u}_{max}}{c_i u_i}\right)_w$$

versus the location x for polymer injection concentrations of 50 and 100 w.p.p.m. in which case the wall concentration for polymer solution injection is smaller than for water injection. This means that the diffusion rate for polymer injection is higher than for water injection for the low injection concentration used in these experiments.

Figure 28 shows the relation between the ratio of non-dimensional concentration

$$\left(\frac{\bar{c}_m \bar{u}_{max}}{c_i u_i}\right)_p \Big/ \left(\frac{\bar{c}_m \bar{u}_{max}}{c_i u_i}\right)_w$$

versus the non-dimensional polymer injection flow rate

$$\frac{G_i\ c_i}{\bar{u}_{max}\ d}$$

It appears that the wall concentration for the polymer injection flow low polymer injection flow rates will decrease when compared to water injection as mentioned previously and will increase again as the polymer injection flow rate is progressively increased.

Figure 29 shows the non-dimensional diffusion boundary layer growth $\frac{\lambda}{\delta_\pi}$ and the wall concentration versus the non-dimensional polymer injection flow rate

$$\frac{G_i\ c_i}{\bar{u}_{max}\ x}$$

It appears that the representative diffusion boundary layer thickness λ will increase in the region on the graph representing the low dimensionless polymer injection flow rate and then decrease again for the higher non-dimensional polymer injection flow rate. The representative boundary layer growth can be approximated by the following straight line equation:

$$\frac{\lambda}{\delta_\pi} = b_4 \left(\frac{G_i\ c_i}{\bar{u}_{max}\ x}\right) + a_4 \quad \text{for} \quad \frac{G_i\ c_i}{\bar{u}_{max}\ x} \geq 10^{-8}$$

It seems that the wall concentration will be proportional to the non-dimensional polymer injection flow rate such that

$$\bar{c}_m = b_5 \left(\frac{G_i\ c_i}{\bar{u}_{max}\ x}\right) \quad \text{for} \quad \frac{G_i\ c_i}{\bar{u}_{max}\ x} \leq 4 \times 10^{-8}$$

where for higher values of the non-dimensional polymer injection flow rate, the wall concentration will increase very rapidly. Unfortunately, there are insufficient data available to determine the exact shape of the curve for values of

$$\frac{G_i\, c_i}{\bar{u}_{max}\, x} > 5 \times 10^{-6}$$

Figure 30 shows a plot for the ratio of the calculated injection mass flow rate to the measured value versus the location x. It appears that the calculated mass flow rate will decrease for higher values of x, which means that the diffusion will extend outside the hydrodynamic boundary layer.

CHAPTER 6

ANALYSIS AND DISCUSSION

In this section the results will be discussed in detail. For convenience, the data have been defined by the following:

Series 1	smallest injection flow rate
Series 2	medium injection flow rate
Series 3	highest injection flow rate
Location 1	x = 0.050 m.
Location 2	x = 0.146 m.
Location 3	x = 0.304 m.
Location 4	x = 0.558 m.
Location 5	x = 0.844 m.

Furthermore, the deductions are made with respect to the experimental range of the parameters which are:

$\frac{x}{\theta_{av}}$ varies between 12.5 to 82

$\frac{\bar{u}_{max}}{u_i}$ varies between 6 to 36

The concentration profiles, see Figure 7, for dyed water injection at various injection flow rates and at the five locations downstream from the injection slot can be transformed into a universal diagram as shown in Figure 13, where

it is apparent that the mean concentration distribution $\bar{c}/\bar{c}_m$ within the experimental scatter is a function of the dimensionless height y/λ alone and is independent of the location and the injection flow rate. There are no distinct zones in the longitudinal range used, contrary to what might be expected from [1] which indicated four zones within the same range. This is mainly because the non-dimensional velocity defined by $\frac{\bar{u}_{max}}{u_i}$ is very high which means that the dispersion as a result of the high velocity ratio will play an active role in the diffusion in the initial three zones and will reduce the length of these zones enormously. It is found that the equation obtained by Morkovin [3] based on the collected data of Poreh and Cermak [1] for the final zone of the diffusion from the line slot can be used to represent the present data as shown in Figure 13 by the following equation:

$$\frac{\bar{c}}{\bar{c}_m} = \exp\left[-0.693\ \left(\frac{y}{\lambda}\right)^{2.15}\right] \tag{6.1}$$

which fits the data with an accuracy of better than +4%.

It was found that the mean velocity profile within the hydrodynamic boundary layer can be represented by the following equation:

$$\frac{\bar{u}}{\bar{u}_{max}} = \left(\frac{y}{\delta_\pi}\right)^{\frac{1}{7}} \tag{6.2}$$

By substituting Equations (6.1) and (6.2) into the continuity equation (4.7), we can obtain the following equation:

$$\frac{G_i\, c_i}{\bar{u}_{max}\, \lambda\, c_m} = \left(\frac{\lambda}{\delta_\pi}\right)^{\frac{1}{7}} \int_0^{\frac{\delta_\pi}{\lambda}} (\xi)^{\frac{1}{7}} \exp\left[-0.693\ (\xi)^{2.15}\right] d\xi + \int_{\frac{\delta_\pi}{\lambda}}^{\infty} \exp\left[-0.693\ (\xi)^{2.15}\right] d\xi \qquad (6.3)$$

in which the numerical value of the second term approaches zero. The function

$$\int_0^{\frac{\delta_\pi}{\lambda}} (\xi)^{\frac{1}{7}} \exp\left[-0.693\ (\xi)^{2.15}\right] d\xi = \text{constant value}$$

since from the experiments $\frac{\lambda}{\delta_\pi} \cong 0.45$ and G_i, c_i and $\bar{u}_{max}$ are also constants for a given test run. The continuity equation, Equation (6.3), therefore may be reduced to

$$\lambda\, \bar{c}_m = \text{constant} \qquad (6.4)$$

By substituting the values of λ and $\bar{c}_m$ from Figure 7 into Equation (4.4), it was found that the value of $(\lambda\, \bar{c}_m)$ is a function of the location downstream from the injection slot, that is,

$$\lambda\, \bar{c}_m = a_6\, (x)^{b_6}$$

where $b_6 < 0$ and therefore, the value $(\lambda\, \bar{c}_m)$ is decreasing in the longitudinal direction downstream from the injection slot. This means that the flow is either three-dimensional or that

Equation (6.1) is not valid for the high values of the dimensionless height ξ, since $\lambda \bar{c}_m$ should be a constant.

Measurements of the mean concentration in the transverse direction indicated that although the injection velocity was not strictly uniform, the flow field was approximately two dimensional since the concentration ratio between two longitudinal locations for the same height was independent of z. It is apparent that Equation (6.1) is not valid for high values of the non-dimensional height ξ. This is mainly because of the effect of the high value of the dimensionless velocity $\frac{\bar{u}_{max}}{u_i}$ which will reduce the length of the first three zones. Consequently the injected solution will fill all the boundary layer at $\frac{x}{\delta_{av}} = 12.5$ and then diffuse out of the boundary layer which explains why at the first location that the continuity equation is approximately satisfied by Equation (6.1). Thus the concentration c_∞ in the mainstream when $y/\delta_\pi \to \infty$ may represent not only the upstream concentration coming with the recirculated water but also the diffused solution from the injection slot. Since the area of the test section is about ten times that of the diffusion area described by Equation (6.1), the concentration of the diffused solution outside of the boundary layer will be negligibly small. Hence the continuity equation can be written as follows:

$$\frac{G_i \, c_i}{\bar{u}_{max} \, \lambda \, \bar{c}_m} = K_1 \left(\frac{\lambda}{\delta_\pi}\right)^{\frac{1}{7}} \int_0^\infty (\xi)^{\frac{1}{7}} \, \text{Exp} \left[-0.693 \, (\xi)^{2.15}\right] d\xi \qquad (6,5)$$

where $K_1 = 0.31 \, (x)^{0.26}$ (6.6)

From the plot of Figure 24 of $\frac{\lambda}{\delta_\pi}$ versus $\frac{x}{\delta_{av}}$ it is apparent that $\frac{\lambda}{\delta_\pi}$ approaches a constant value of 0.45 at $\frac{x}{\delta_{av}} \cong 15$,

i.e., $$\frac{\lambda}{\delta_\pi} \cong 0.45 \tag{6.7}$$

which is the condition of the final zone described by [1] where $\frac{\lambda}{\delta_\pi}$ approaches a constant value of 0.58 at $\frac{x}{\delta_{av}} \cong 60$. This explains why a universal equation can be used. Comparison of the present data and the data of [1] shows that the condition of the final zone should be close to the injection slot. This is mainly, as mentioned previously, because the length of the first three zones is reduced. Consequently the value of $\frac{\lambda}{\delta_\pi}$ will be reduced as a result of the diffusion outside of the hydrodynamic boundary layer.

From the plot of Figure 22 of non-dimensional wall concentration

$$\frac{\bar{c}_m \bar{u}_{max}}{c_i u_i}$$

versus $(\frac{x}{h})$, it is apparent that the value of $\bar{c}_m$ is proportional to c_i and u_i and can be approximated by:

$$\frac{\bar{c}_m \bar{u}_{max}}{c_i u_i} = 25.63 \left(\frac{x}{h}\right)^{-0.834} \tag{6.8}$$

The rate of decrease of $\bar{c}_m$ in the longitudinal direction is in good agreement with the experimental data of [1] for the intermediate zone and is much higher than the experimental

data of [1] for the final zone. Consequently, the diffusion rate outside of the hydrodynamic boundary layer will be higher than for the case of [1] for the final zone since the diffusion of the additives beyond the hydrodynamic boundary layer into the mainstream will be mainly controlled by the turbulence there which seems much higher than for the case of [1].

From the plot of Figure 23 of λ versus x, it appears that λ is approximately independent of the velocity ratio $\frac{\bar{u}_{max}}{u_i}$, and can be approximated by:

$$\lambda = 0.284\ (x)^{0.47} \qquad (6.9)$$

The rate of growth of λ from Equation (6.9) for the final zone is smaller than that described by [1] in the intermediate zone, and higher than that described by [1] in the final zone. Consequently, as mentioned previously, the rate of diffusion is higher than that for the case of [1] in the final zone.

Attempts to obtain a universal relationship between the concentration distribution $\bar{c}/\bar{c}_m$ as a function of $\frac{y}{\lambda}$ for a 50 w.p.p.m. polymer injection concentration gave considerable scatter of points which infers that there is more than one zone within the longitudinal length. Since it is seen from the concentration profiles, Figure 8, that the initial zone would be prior to the first location in which there is a very large concentration gradient. This suggests that the longitudinal range represents the intermediate, transient and final zones. It was found that the concentration profile, Figure 14, for $\bar{c}/\bar{c}_m$

for the first location for all injection rates, and the second and third locations for the third series can be represented by the following equation:

$$\frac{\bar{c}}{\bar{c}_m} = \exp\ [-0.693\ (\xi)^{1.7}] \qquad (6.10)$$

It appears that the length of the intermediate zone is dependent on $\frac{\bar{u}_{max}}{u_i}$ and Q_i, but the intermediate zone will only cover the first location for the first two series and will cover the first three locations for the third series. This can mainly be attributed to a decreased eddy diffusivity as the injection rate increases. Determining the length of the transient zone is difficult because it requires excessive data to cover the longitudinal length completely.

It was found that the concentration profile $\bar{c}/\bar{c}_m$ for polymer injection as shown in Figure 15 for the other locations downstream can be represented by the following equation:

$$\frac{\bar{c}}{\bar{c}_m} = \exp\ [-0.693\ (\xi)^{2.15}] \qquad (6.11)$$

which is the same for water injection data for the final zone. It appears from the previous two equations, Equations (6.10) and (6.11), that for the intermediate and final zones, the following general equation may cover the intermediate, transient and final zones:

$$\frac{\bar{c}}{\bar{c}_m} = \exp\ [-0.693\ (\xi)^{a}] \qquad (6.12)$$

The constant 'a' will be dependent on the location downstream from the injection slot and the non-dimensional velocity ratio ($\bar{u}_{max}/u_i$) and is expected to be dependent on the slot height h and the injection concentration such that,

$$a = f\left(\frac{\bar{u}_{max}\, x}{u_i\, c_i\, h}\right) \tag{6.13}$$

From the concentration profiles, Figure 9, of c_i = 100 w.p.p.m. for polymer injection, it appears that all the zones are represented. The initial zone exceeds the first location in the first two series and the second location in the third series. Unfortunately, a general equation for this zone cannot be obtained since an exact value for $\bar{c}_m$ cannot be accurately obtained by extrapolation when the concentration gradient adjacent to the wall is very large. Consequently, λ cannot be determined in this zone. It is seen that the length of the initial zone will be dependent upon $\bar{u}_{max}/u_i$ and Q_i. and a higher Q_i, u_i will be accompanied by a longer initial zone. The intermediate zone, Figure 16, covers the second location in the first series, the second and third locations in the second series, and the third location in the third series. In the last case, the intermediate zone can be represented by Equation (6.10) which is the same as that used for a c_i of 50 w.p.p.m. in the intermediate zone. The final zone, Figure 17, will be the same as for the case of water injection and extends downstream for the rest of the test section. The general equation, Equation (6.11), can be used to describe the final zone

for a c_i of 100 w.p.p.m. of polymer injection.

In the case of a c_i of 250 w.p.p.m. of polymer injection, Figure 10, the initial zone extends up to the third location for all values of Q_i, and the intermediate zone, Figure 18, covers the fourth location for the second and third series. It also appears that the intermediate zone is confined between the third and fourth locations in the first series. The general equation, Equation (6.10), used previously to describe the intermediate zone can also be used for the case of a c_i of 250 w.p.p.m. The final zone, Figure 19, will extend to the rest of the test section. The same general equation, Equation (6.11), for the final zone is applicable for this case which fits the data within an accuracy of $\pm$ 3%, which is in good agreement with the data of [2].

In the case of a c_i of 500 w.p.p.m., Figure 11, the initial zone stretches to cover a distance up to the third location in the first two series and the fourth location in the third series. The fourth location in the first two series will not satisfy the general equation, Equation (6.10), for the intermediate zone. It is apparent that the fourth location is somewhere between the initial and intermediate zones. Under these conditions, the final zone, Figure 20, will include the fifth location only for all values of Q_i. The same general equation, Equation (6.11), will satisfy the final zone which fits the data within an accuracy of $\pm$ 3%. The data is in good agreement with [2]. It is apparent that by increasing the quantity of the polymer injected, the initial zone will be greatly

extended compared to the intermediate and the transient zones. This is mainly because the bulk of the additives will be submerged in the viscous sub-layer and since the molecular diffusivity of the high polymer solution concentration is very small, it is expected that the diffusion rate will be very small which will result in a greater length for the initial zone.

In the case of a c_i of 1500 w.p.p.m., Figure 12, the initial zone covers up to the third location for all values of Q_i. It seems that the condition of the intermediate zone described by Equation (6.10) will not be achieved within the longitudinal range and the equation describing the last location as shown in Figure 21 is:

$$\frac{\bar{c}}{\bar{c}_m} = \exp\left[-0.693\ (\xi)^{1.5}\right] \qquad (6.14)$$

i.e., the last location will be somewhere between the initial and intermediate zones. Equation (6.14) supports the hypothesis mentioned previously that the general equation, Equation (6.12), will satisfy all of the zones.

A comparison between water injection and polymer solution injection can be made. The first three zones in the case of water injection will be relatively short and insignificant. The first three zones and especially the initial zone, will be very significant particularly for high injection concentrations and flow rates which disagrees with the analysis made by [6].

The wall concentration for c_i's of 50 and 100 w.p.p.m. shown in Figure 25 can be approximated by the following equation:

$$\frac{\bar{c}_m \bar{u}_{max}}{c_i u_i} = 17.668 \left(\frac{x}{h}\right)^{-0.794} \qquad (6.15)$$

From the plot of Figure 27 of

$$\left(\frac{\bar{c}_m \bar{u}_{max}}{c_i u_i}\right)_p / \left(\frac{\bar{c}_m \bar{u}_{max}}{c_i u_i}\right)_w$$

versus x for c_i's of 50 and 100 w.p.p.m. showed that $(\bar{c}_m)_p$ is smaller than that for water injection. This means that for very low $(\bar{c}_m)_p$ in the range of 0 to 0.75 w.p.p.m. that the diffusion rate will be greater for polymer injection than for the self diffusion of pure water which is in agreement with [12].

From the plot of Figure 26 of λ versus x for c_i = 50 w.p.p.m., it is apparent that λ is approximately independent of the velocity ratio $\bar{u}_{max}/u_i$, and is only a function of x and can be approximated by:

$$\lambda = 0.186 \, (x)^{0.55} \qquad (6.16)$$

It is apparent by comparing λ for c_i = 50 w.p.p.m. to that for water injection that at low values of x near the injection, that λ for water injection is higher than for the polymer solution. Then λ will be the same for both water and polymer injection if $(\bar{c}_m)_p$ approaches 0.75 w.p.p.m. where λ for polymer injection

starts to be higher than that of water injection. However the change in the diffusion rate is small.

From the plot of Figure 28 for the ratio of the dimensionless wall concentration of the polymer and water injections

$$\left(\frac{\bar{c}_m\ \bar{u}_{max}}{c_i\ u_i}\right)_p \Big/ \left(\frac{\bar{c}_m\ \bar{u}_{max}}{c_i\ u_i}\right)_w$$

versus $\frac{G_i\ c_i}{\bar{u}_{max}\ d}$ indicates that the diffusion rate starts to decrease when $(\bar{c}_m)_p > 0.75$ w.p.p.m. A general equation for

$$\left(\frac{\bar{c}_m\ \bar{u}_{max}}{c_i\ u_i}\right)_p \Big/ \left(\frac{\bar{c}_m\ \bar{u}_{max}}{c_i\ u_i}\right)_w$$

as a function of $\frac{G_i\ c_i}{\bar{u}_{max}\ d}$ cannot be obtained because of the scatter of the points in the graph, however, the trend of increasing diffusion for low polymer concentration and then decreasing diffusion for high wall concentration is shown in the graph.

From the plot of Figure 29 for $\frac{\lambda}{\delta_\pi}$ versus $\frac{G_i\ c_i}{\bar{u}_{max}\ x}$ the following approximate general equation can be obtained:

$$\frac{\lambda}{\delta_\pi} = 0.5275 - 0.18 \times 10^8 \left(\frac{G_i\ c_i}{\bar{u}_{max}\ x}\right) \qquad (6.17)$$

for $\frac{G_i\ c_i}{\bar{u}_{max}\ x} \geq 10^{-8}$

Equation (6.17) is only valid for a location downstream from the injection slot where $\frac{x}{\delta_{av}} \geq 50$, i.e., for the final zone.

This graph shows that λ increases for low $(Q_i\ c_i)$ and then decreases for high $(Q_i\ c_i)$, which supports the hypothesis that the diffusion rate will increase for low $(\bar{c}_m)_p$ and decrease for high $(\bar{c}_m)_p$. The wall concentration as a function of $(\frac{G_i\ c_i}{\bar{u}_{max}\ x})$ can be obtained from the same graph by the following equation:

$$\bar{c}_m = 0.81 \times 10^8 \left(\frac{G_i\ c_i}{\bar{u}_{max}\ x}\right) \text{ w.p.p.m.} \qquad (6.18)$$

for

$$\frac{G_i\ c_i}{\bar{u}_{max}\ x} \leq 3.5 \times 10^{-8}$$

$$\frac{x}{\delta_{av}} \geq 50$$

Unfortunately, there are not enough data to obtain an appropriate equation for $\frac{G_i\ c_i}{\bar{u}_{max}\ x} > 3.5 \times 10^{-8}$, since in this region $\bar{c}_m$ will increase very rapidly. This can be attributed to the fact that the initial zone will prevail over large distances of the test section which leads to a high $\bar{c}_m$ in the final zone. However, Figure 29 is very useful for the design purpose. For a $(\bar{c}_m)_p$ required to achieve maximum drag reduction at a given x, a value for $(Q_i\ c_i)$ can be determined from the graph. Hence the values for $(\bar{c}_m)_p$ for the entire surface can be obtained from the appropriate relationship between $\bar{c}_m$ and x. Hence the drag reduction over the surface can be obtained. In this case, a comparison should be made to obtain an optimum design, keeping in mind that increasing the polymer injection flow rate

will lead to a longer initial zone and a very high $\bar{c}_m$, which may increase the drag in that area but still achieves the required optimum concentration downstream. However, decreasing the injection flow rate will reduce the length of the initial zone but $\bar{c}_m$ downstream may be lower than the optimum value for the drag reduction. In this type of analysis, the cost of the polymer should be included.

6.1. The Eddy Diffusivity

From Equation (4.21), the eddy diffusivity can be written as follows:

$$D^{(t)} = \frac{1}{0.693a} \lambda \bar{u}_{max} \frac{d\lambda}{dx} \left(\frac{\lambda}{\delta_\pi}\right)^{\frac{1}{n}} (\xi)^{2+\frac{1}{n}-a} \qquad (6.19)$$

where a = 2.15 for the final zone.

By introducing the correction factor K_1 into the continuity equation, Equation (4.7), Equation (6.19) can be modified for the final zone as follows:

$$D^{(t)} = 0.67\, K_1 \lambda \bar{u}_{max} \frac{d(K_1^{\frac{n}{n+1}} \lambda)}{dx} \left(\frac{\lambda}{\delta_\pi}\right)^{\frac{1}{n}} (\xi)^{-0.07} \qquad (6.20)$$

Therefore, within the boundary layer, it is apparent from the above equation that the eddy diffusivity is approximately independent of the height above the flat plate, but is a function of λ. In the final zone, $(\xi)^{-0.07}$ approaches one for water or polymer injection. For water injection, by substituting the values of λ, $\frac{\lambda}{\delta_\pi}$ and K_1 from Equations (6.9), (6.7),

and (6.6) into Equation (6.20), the following equation can be obtained.

$$D^{(t)} = 3.8 \times 10^{-6} \, x^{0.43} \, \bar{u}_{max} \quad m^2/sec. \qquad (6.21)$$

where x is in mm. and $\bar{u}_{max}$ is in m./sec.

Hence the eddy diffusivity is apparently proportional to $\bar{u}_{max}$ and x.

For polymer injection with a c_i of 50 w.p.p.m. in the final zone the eddy diffusivity can be obtained, as before, from the following equation:

$$D^{(t)} = 1.8 \times 10^{-6} \, x^{0.59} \, \bar{u}_{max} \quad m^2/sec. \qquad (6.22)$$

where x is in mm. and $\bar{u}_{max}$ is in m./sec.

A general equation can be deduced for the eddy diffusivity for each of the different zones. There are insufficient data to obtain the correction factor for the initial zones. Hence, an equation for the eddy diffusivity in the final zone only can be obtained. By substituting the value of δ_π from Equation (6.7) into Equation (6.17), since the hydrodynamic boundary layer thickness was assumed approximately the same for water and the polymer solution. Consequently, the eddy diffusivity equation can be obtained by using Equations (6.7) and (6.17), if $\frac{G_i \, c_i}{\bar{u}_{max} \, x} \geq 10^{-8}$ as follows,

$$D^{(t)} = 3\times10^{-5}\,\bar{u}_{max}\,(x)^{0.43}\left(0.5275-0.065\times10^{8}\left(\frac{G_i c_i}{\bar{u}_{max} x}\right)\right)^{1+\frac{1}{n}}\left(0.37+0.02\times10^{8}\left(\frac{G_i c_i}{\bar{u}_{max} x}\right)\right) \quad (6.23)$$

Consequently the following comparison can be made for $x = 800$ mm. with $\bar{u}_{max} = 5.4$ m./sec.

$$D^{(t)}\ (\text{water}) = 36.5 \times 10^{-5} \quad m^2/\text{sec.}$$

$$D^{(t)}\ (c_i = 50\ \text{w.p.p.m.}) = 50.18 \times 10^{-5} \quad m^2/\text{sec.}$$

For polymer injection with $\bar{c}_m = 6.5$ w.p.p.m.

$$(D)_p^{(t)} = 21.74 \times 10^{-5} \quad m^2/\text{sec.}$$

which shows that for a low $(\bar{c}_m)_p$ the diffusion will increase, while at high $(\bar{c}_m)_p$ the diffusion will decrease when compared to water injection.

Additional experimental studies are needed to obtain more data in all the zones of diffusion to investigate the effect of the size and location of the injection slot on diffusion and also to obtain the exact value of the wall concentration for the different zones, in order that the relationship for the drag reduction per unit discharge of the polymer as a function of the length of the flat plate can be obtained.

CHAPTER 7

CONCLUSIONS

As a summary to the previous discussion, the following conclusions may be drawn:

1) A general equation for the concentration distribution for water injection from a line slot in a two-dimensional flow can be approximated by the following equation for the final zone.

$$\frac{\bar{c}}{\bar{c}_m} = \exp\left[-0.693\ \left(\frac{y}{\lambda}\right)^{2.15}\right] \qquad (7.1)$$

There being no distinct zones noticeable within the conditions

$$\frac{x}{\delta_{av}} = 12.5 \text{ to } 82 \quad \text{and} \quad \frac{\bar{u}_{max}}{u_i} = 8 \text{ to } 18$$

which were used in the experiments: the first three zones must therefore be within the range of $\frac{x}{\delta_{av}} = 0$ to 12.5. Furthermore, for water the functions λ, $\frac{\lambda}{\delta_\pi}$ and $\frac{\bar{c}_m\ \bar{u}_{max}}{c_i\ u_i}$ can be approximated by the following equations:

$$\lambda = 0.284\ (x)^{0.47} \qquad (7.2)$$

$$\frac{\lambda}{\delta_\pi} \simeq 0.45 \qquad (7.3)$$

$$\frac{\bar{c}_m \, \bar{u}_{max}}{c_i \, u_i} = 25.63 \left(\frac{x}{h}\right)^{-0.834} \qquad (7.4)$$

2) The diffusion field for polymer solution injection can be divided into four zones; an initial, an intermediate, a transient and a final zone. A general equation for the concentration in the flow field for all the zones can be written in the following form.

$$\frac{\bar{c}}{\bar{c}_m} = \exp\left[-0.693 \left(\frac{y}{\lambda}\right)^a\right] \qquad (7.5)$$

where

a = 1.7 for the intermediate zone

a = 2.15 for the final zone

The length of the different zones will depend on the actual polymer injection rate $Q_i \, c_i$ and the velocity ratio $\frac{\bar{u}_{max}}{u_i}$.

3) A comparison between water and polymer solution injections shows that for water injection the length of the first three zones is relatively short and insignificant, while for polymer injection the length of the first three zones and particularly the initial zone is very significant.

4) In general, it can be stated that within the range of the flow parameters for the present research, the diffusion rate of diluted drag reducing polymer is increased for very low wall concentration, that is,

when $0 < \bar{c}_m < 0.75$ w.p.p.m. with a maximum diffusion rate when $\bar{c}_m$ is about 0.5 w.p.p.m.

5) It may also be stated that as the concentration at the wall increases above the increased diffusion rate range, the diffusion is greatly reduced with increasing concentration.

6) Lastly, for $\bar{c}_m > 0.75$ w.p.p.m. (i.e., above the increased diffusion rate range), the function for the relative diffusion thickness λ/δ_π can be approximated by the following equation.

$$\frac{\lambda}{\delta_\pi} = 0.5275 - 0.18 \times 10^8 \left(\frac{G_i \, c_i}{\bar{u}_{max} \, x}\right) \qquad (7.6)$$

where $\frac{x}{\delta_{av}} \geq 50$

REFERENCES

1. M. Poreh and J. E. Cermak, Study of Diffusion from a Line Source in a Turbulent Boundary Layer, International Journal of Heat and Mass Transfer, Vol. 7, pp. 1083-1095 (1964).

2. A. G. Fabula and T. J. Burns, "Dilution in a Turbulent Boundary Layer with Polymeric Drag Reduction", TP 171, 1970, Naval Under Sea Research and Development Center, Pa Saderna, Calif.

3. M. V. Morkovin, "On Eddy Diffusivity, Quasi-similarity and Diffusion Experiments in Turbulent Boundary Layers", International Journal of Heat and Mass Transfer, Vol. 8, pp. 129-145 (1965).

4. D. Coles, "The Law of the Wake in the Boundary Layer", Journal of Fluid Mechanics, Vol. 1, No. 2, pp. 191-226 (1956).

5. J. Wu, "Suppressed Diffusion of Drag-Reducing Polymer in a Turbulent Boundary Layer", Journal of Hydronautics, Vol. 6, No. 1, pp. 46-50 (1972).

6. M. Poreh and K. S. Hsu, "Diffusion from a Line Source in a Turbulent Boundary Layer", International Journal of Heat and Mass Transfer, Vol. 14, pp. 1473-1483 (1971).

7. G. K. Batchelor, "Diffusion in Free Turbulent Shear Flows", Journal of Fluid Mechanics, Vol. 3, p. 67 (1957).

8. F. Pasquill, Lagrangian Similarity and Vertical Diffusion from a Source at Ground Level", Q. J. R. Met. Soc., Vol. 92, No. 392, pp. 185-195 (1966).

9. T. H. Ellison, "Meteorology", Science Progress, Vol. 47, No. 187, pp. 495-506 (1959).

10. M. Poreh and K. S. Hsu, "Diffusion of Drag Reducing Polymers in a Turbulent Boundary Layer", Journal of Hydronautics, Vol. 6, No. 1, pp. 27-33 (1972).

11. R. R. Walters and C. S. Wells, "An Experimental Study of Turbulent Diffusion of Drag Reducing Additives", Journal of Hydronautics, Vol. 5, No. 2, pp. 65-77 (1971).

12. R. R. Walters and C. S. Wells, "Effects of Distributed Injection of Polymer Solutions on Turbulent Diffusion", Journal of Hydronautics, Vol. 6, No. 2, pp. 69-76 (1972).

13. R. B. Bird, W. E. Stewart and E. N. Lightfoot, Transport Phenomena, 2nd Printing, Wiley, New York, p. 608, 1962.

14. H. Schlichting, Boundary Layer Theory, 6th ed., McGraw-Hill, New York, p. 598, 1968.

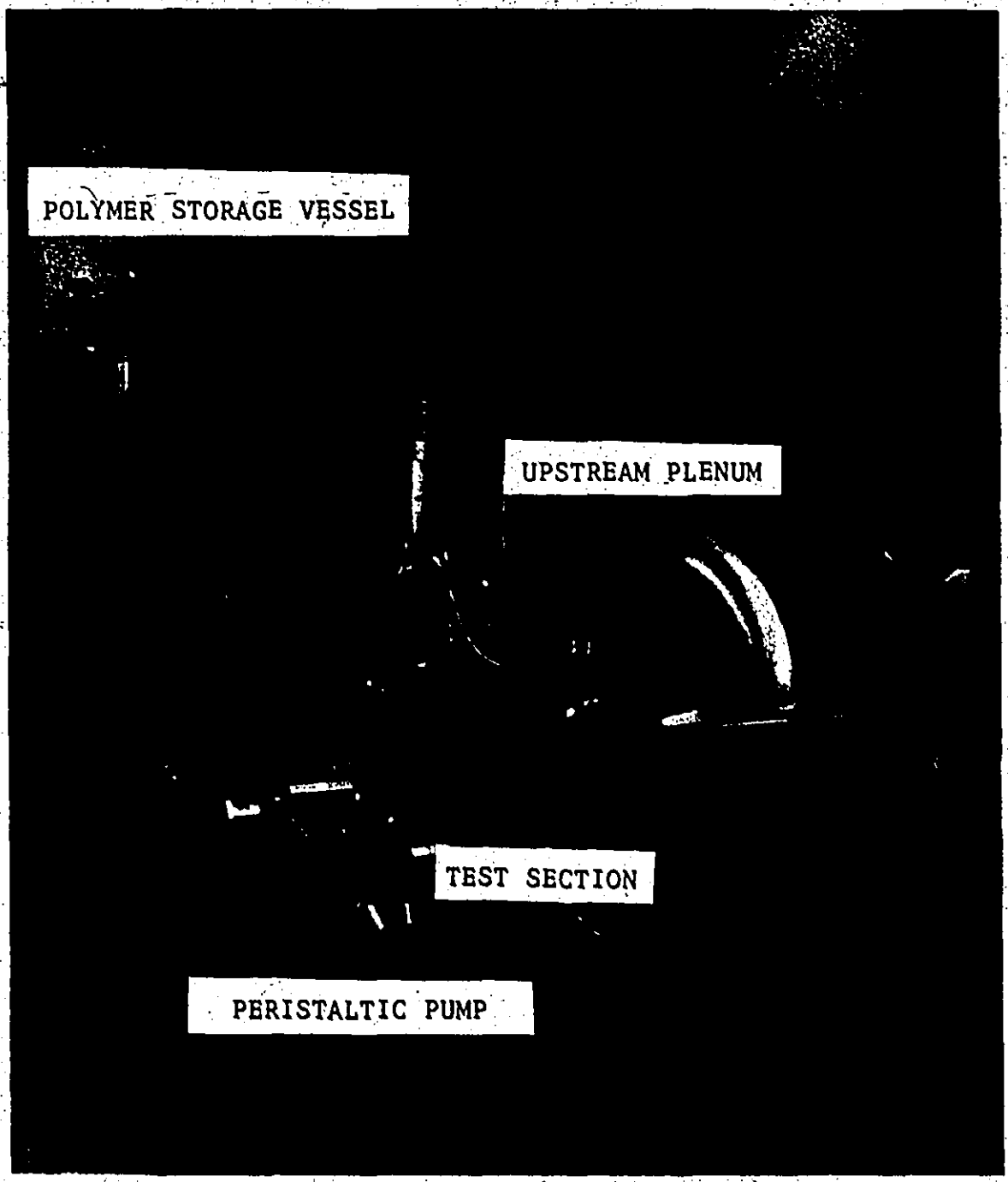

Figure 1-A. Experimental Apparatus.

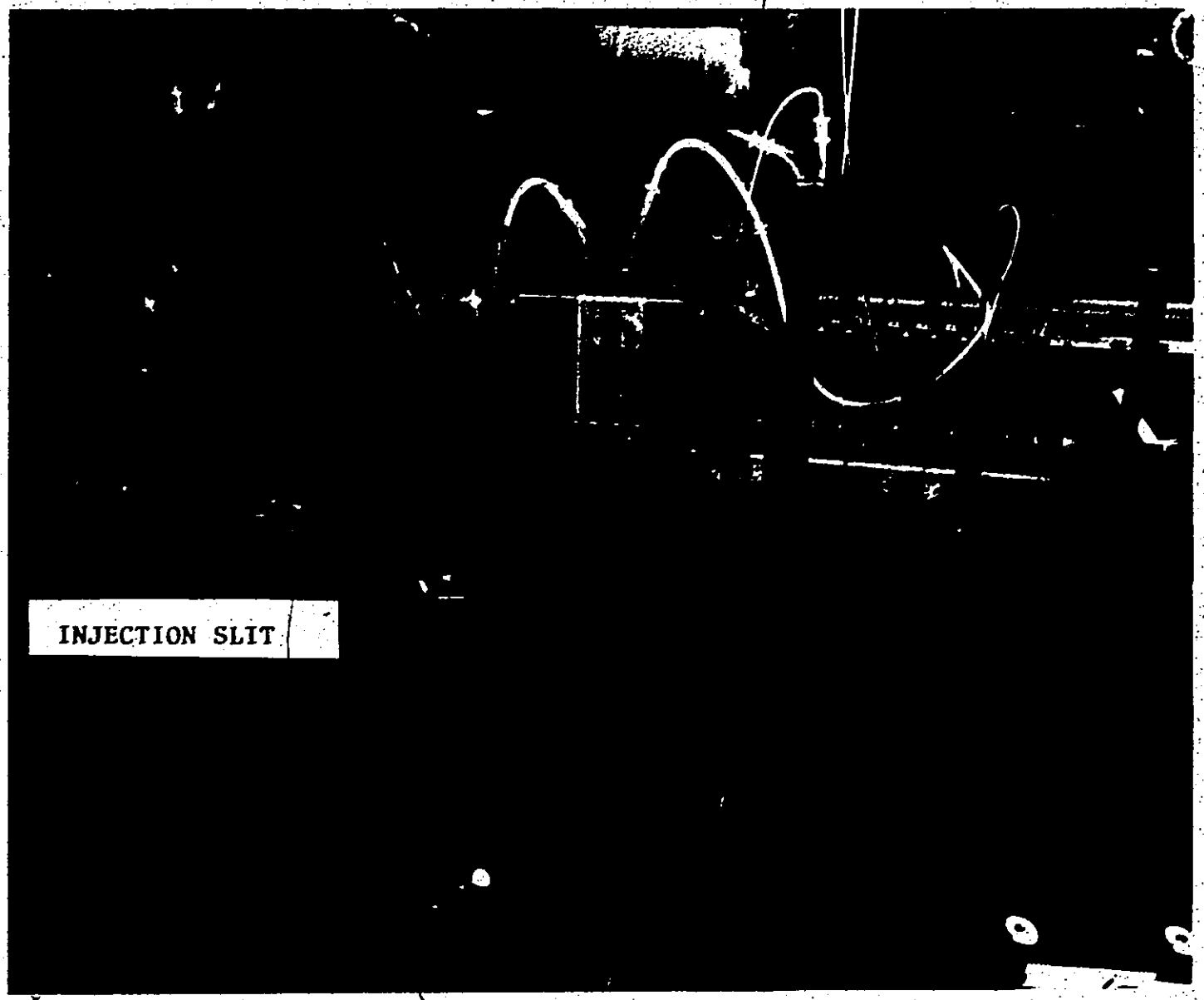

Figure 1-B. Test Section.

LEGEND

Figure 2

A	Plenum chamber
B	Additives inlet
C	Additives exit

Figure 3

a	Regulator
b	Safety valve
c	Polymer solution vessel
d	Relief valve
e	Rotometer
f	Plenum chamber
g	Drain valve
h	Honeycomb filter
i	Test section
L	Constant head tank
K	Centrifugal pump
m	Screen
n	Over flow
p	Sectional view in the test section

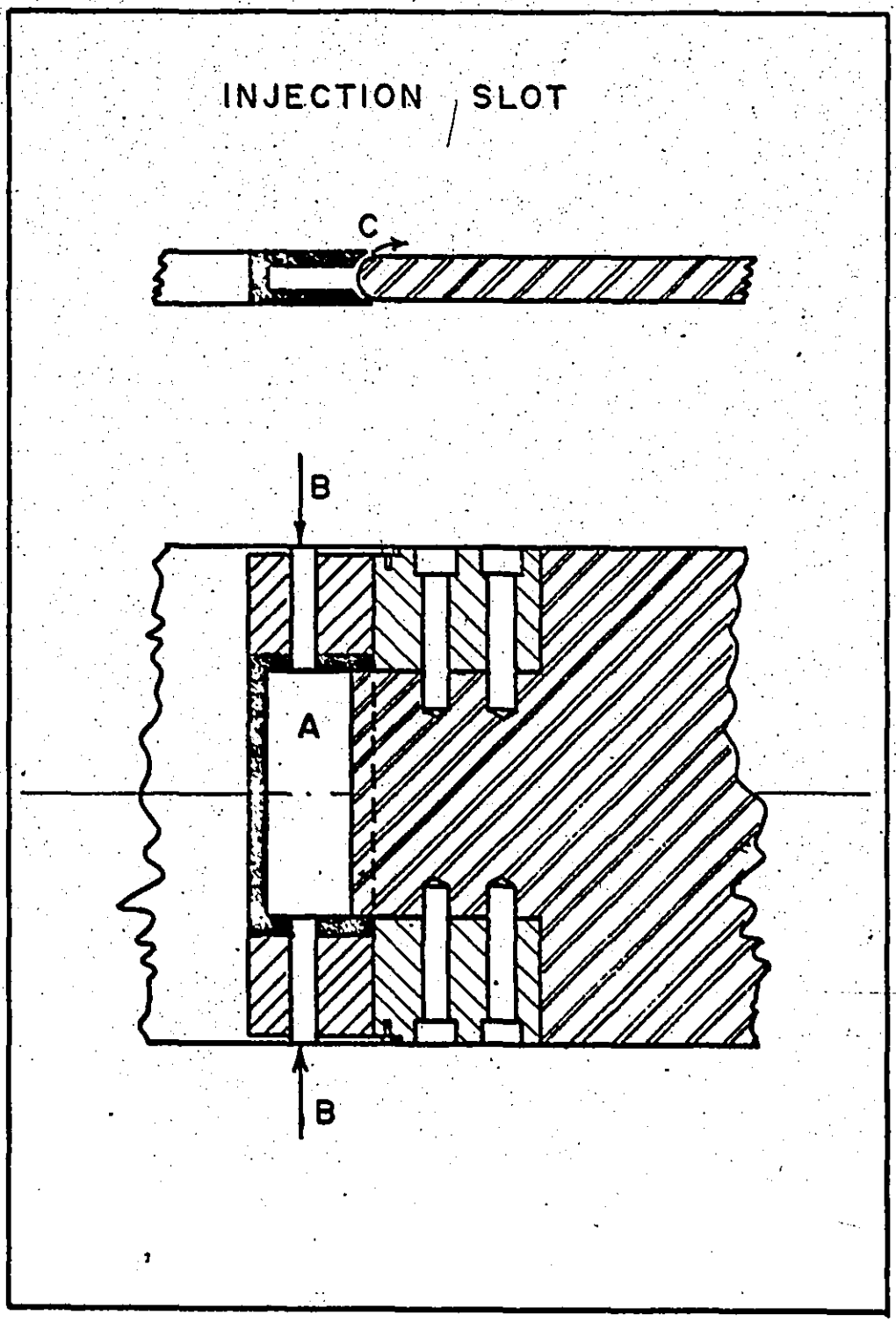

Figure 2. Sectional View of Injection Plenum.

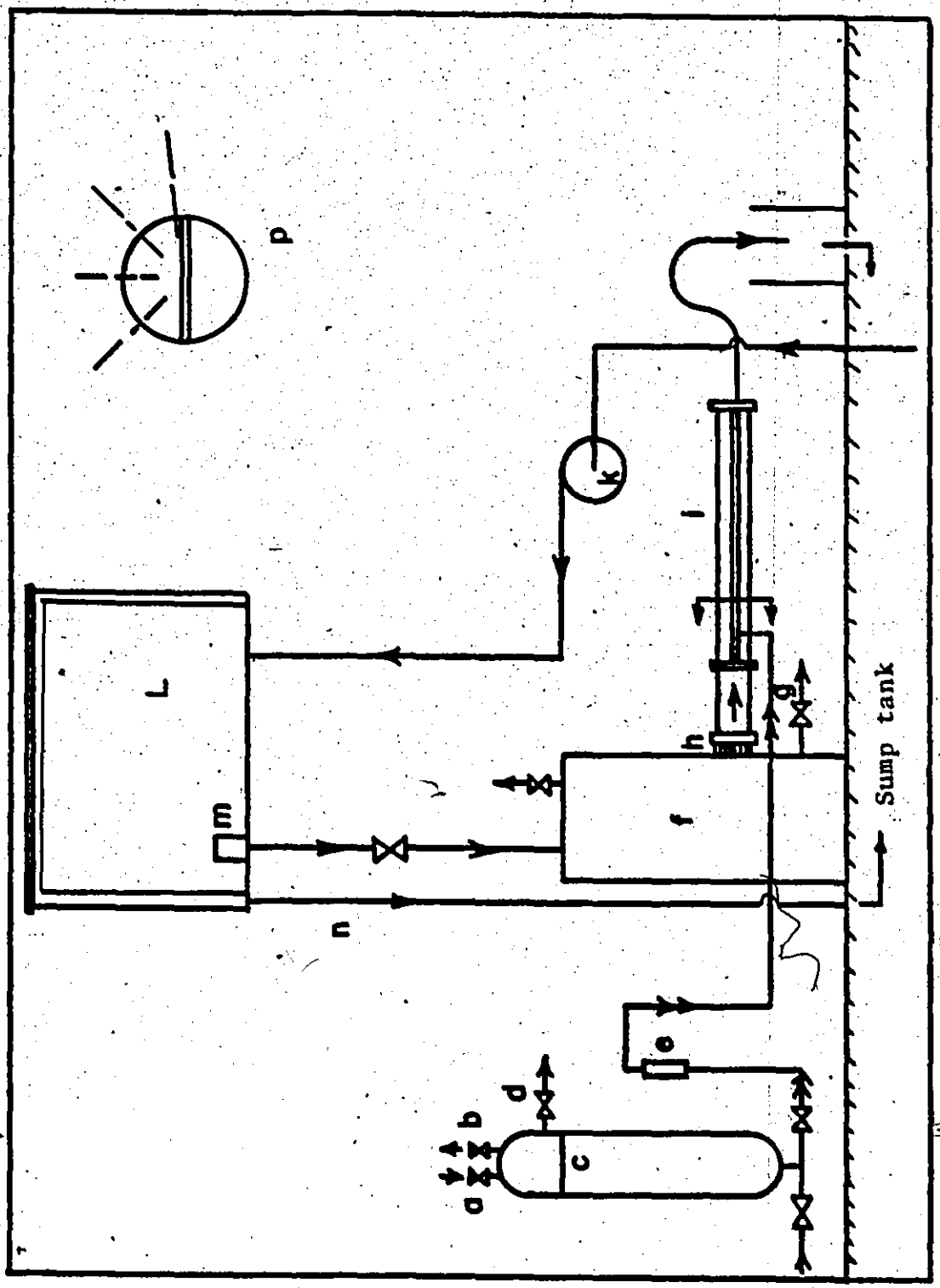

Figure 3. Flow Diagram.

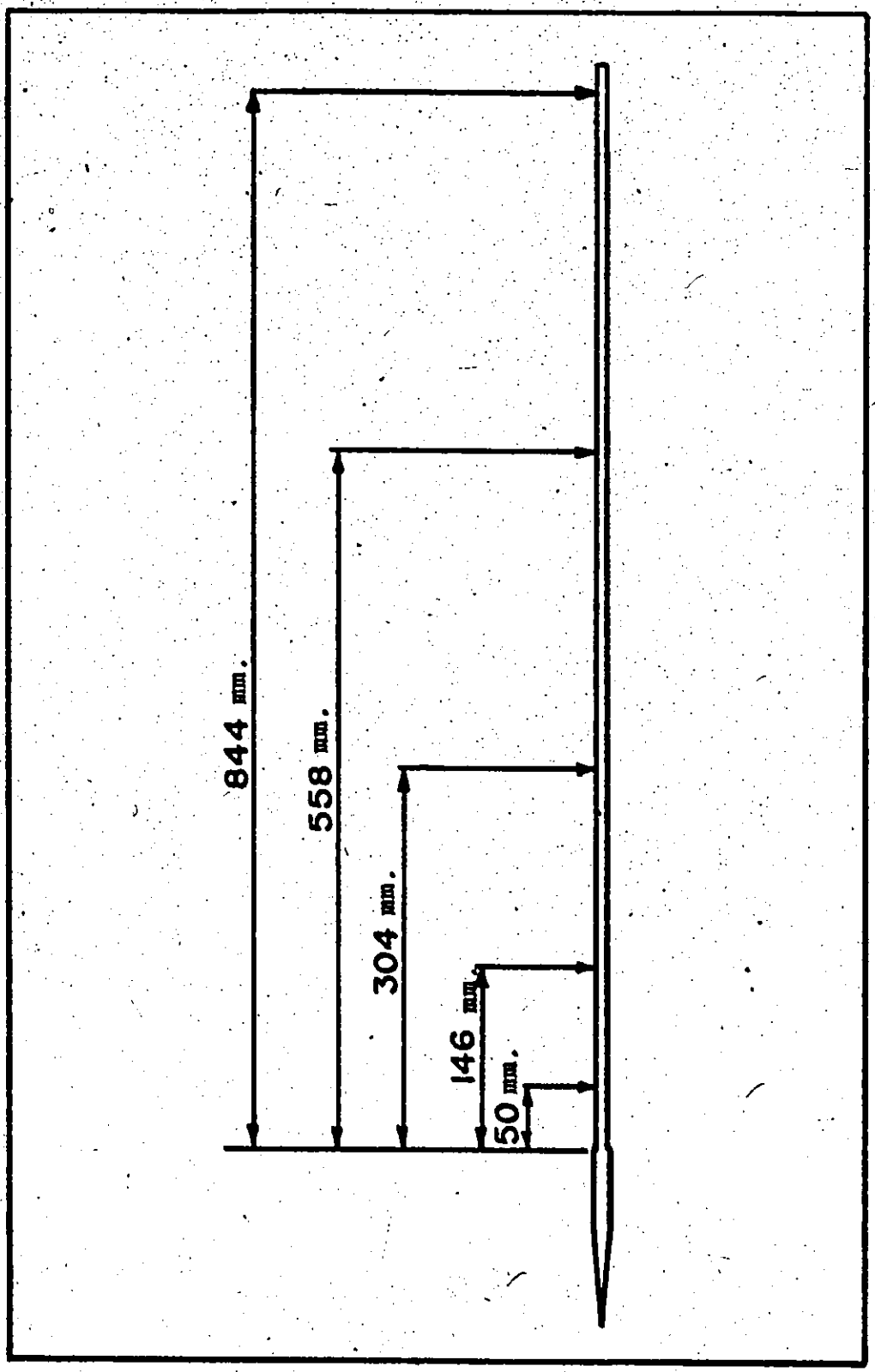

Figure 4. Sampling Locations.

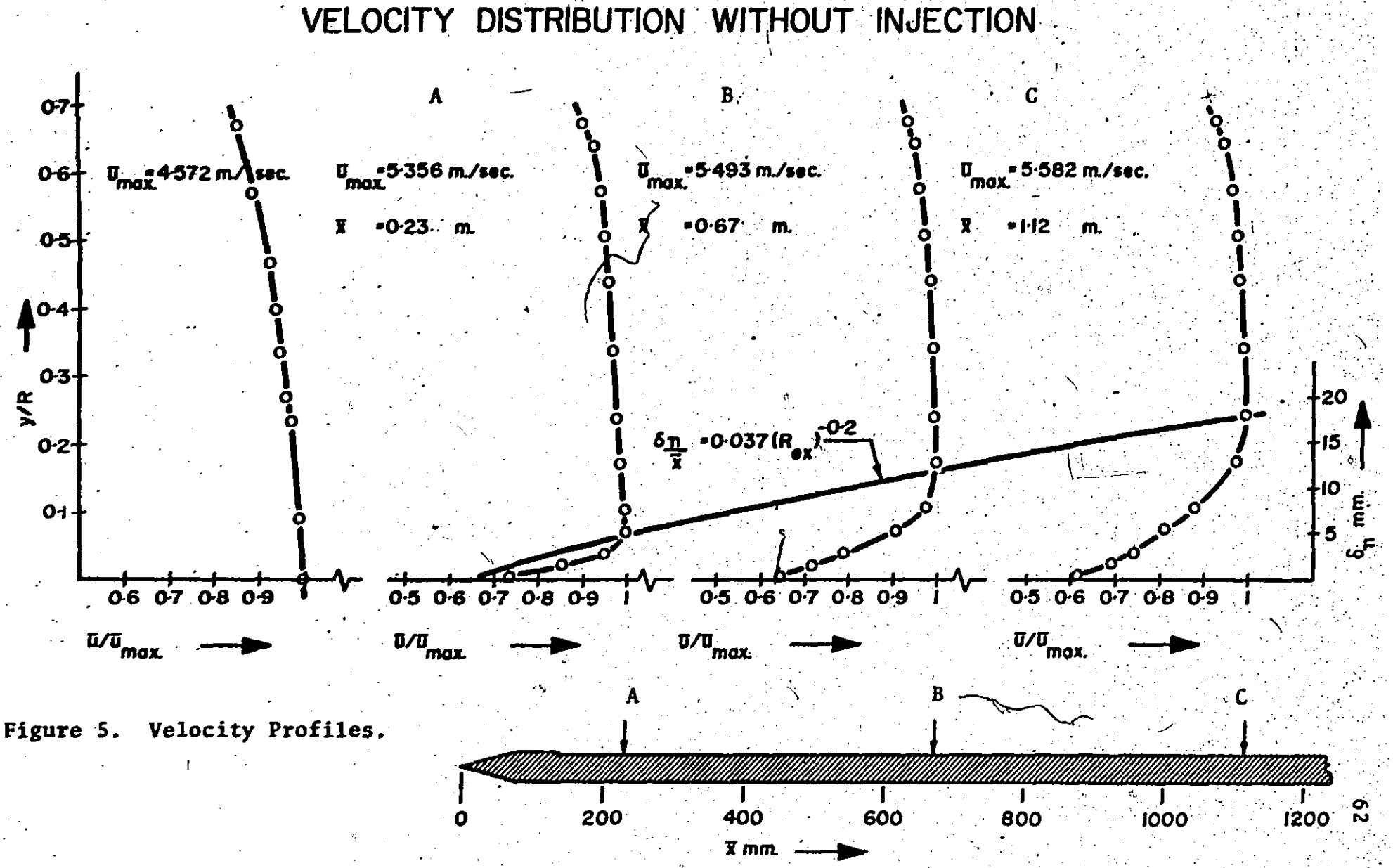

Figure 5. Velocity Profiles.

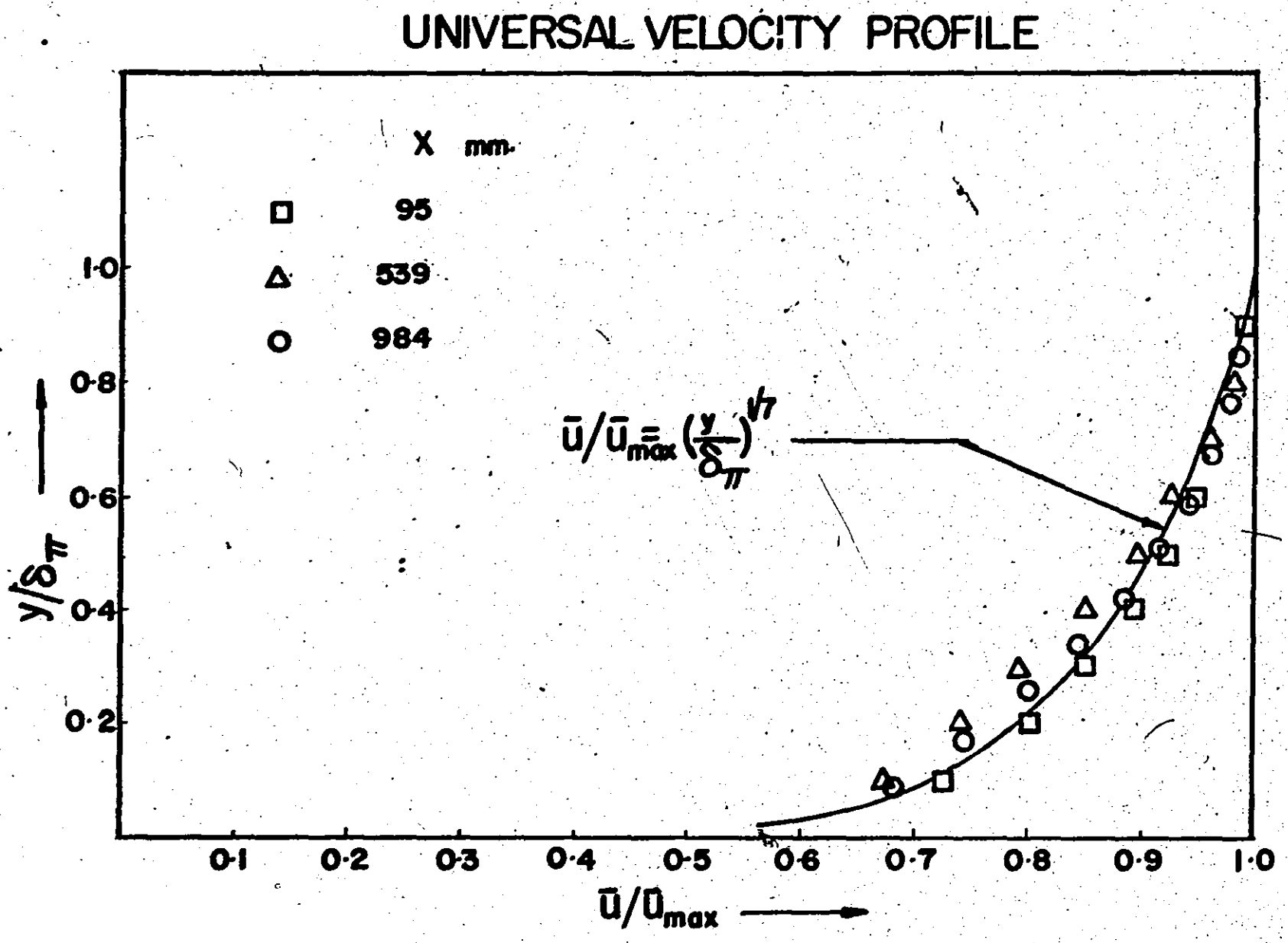

Figure 6. Universal Velocity Profile.

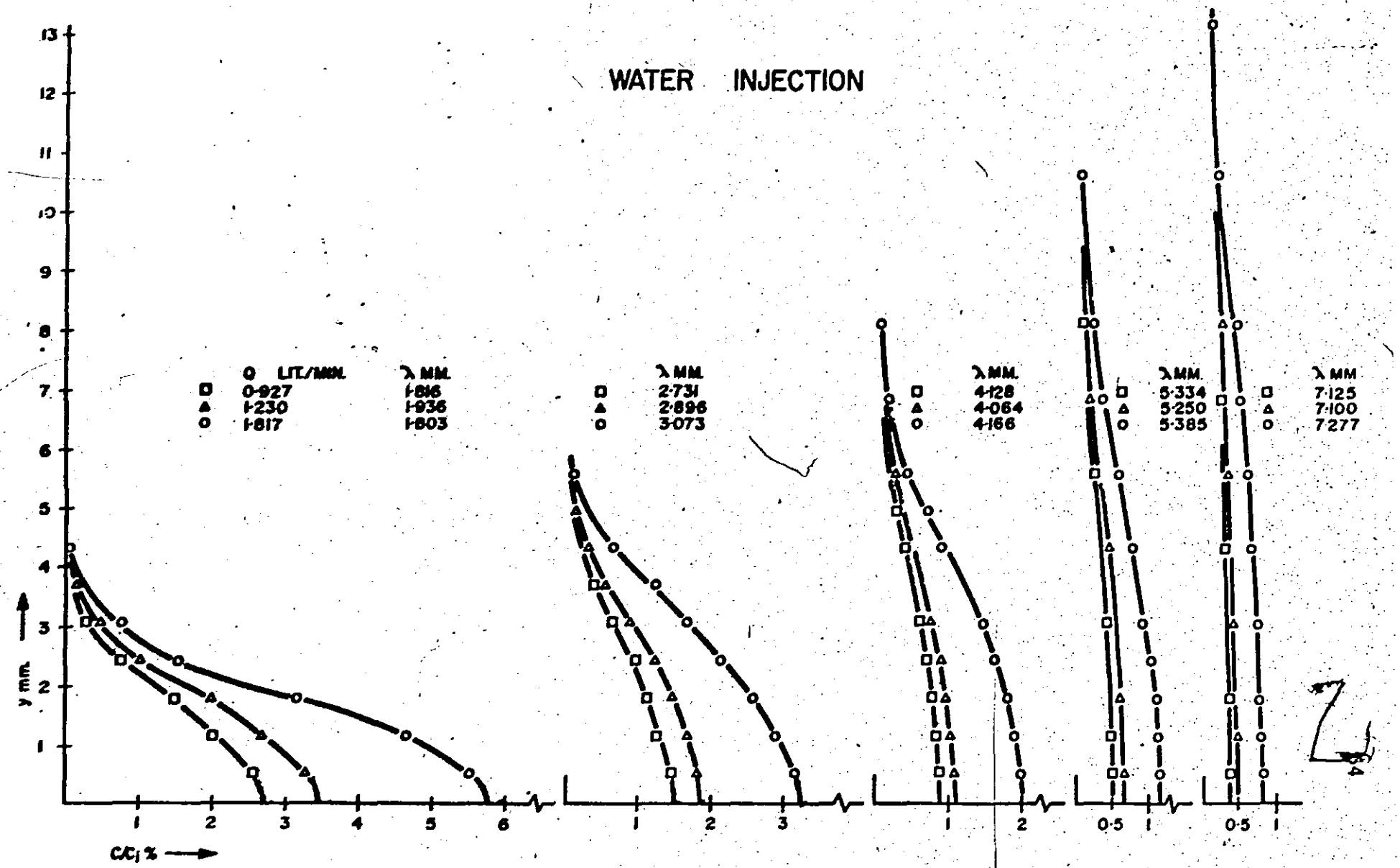

Figure 7. Concentration Profiles (Water Injection).

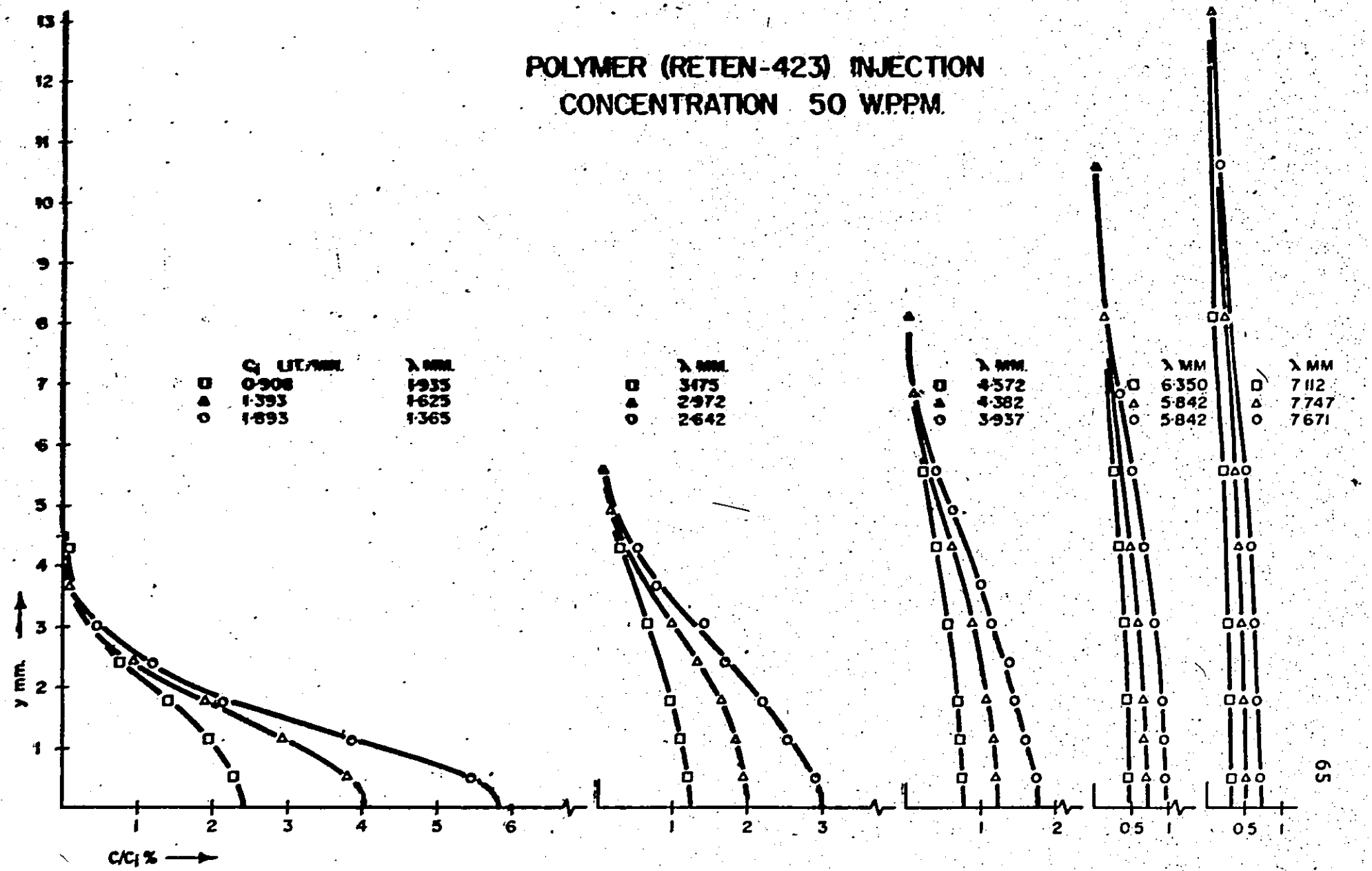

Figure 8. Concentration Profiles (c_i = 50 w.p.p.m.)

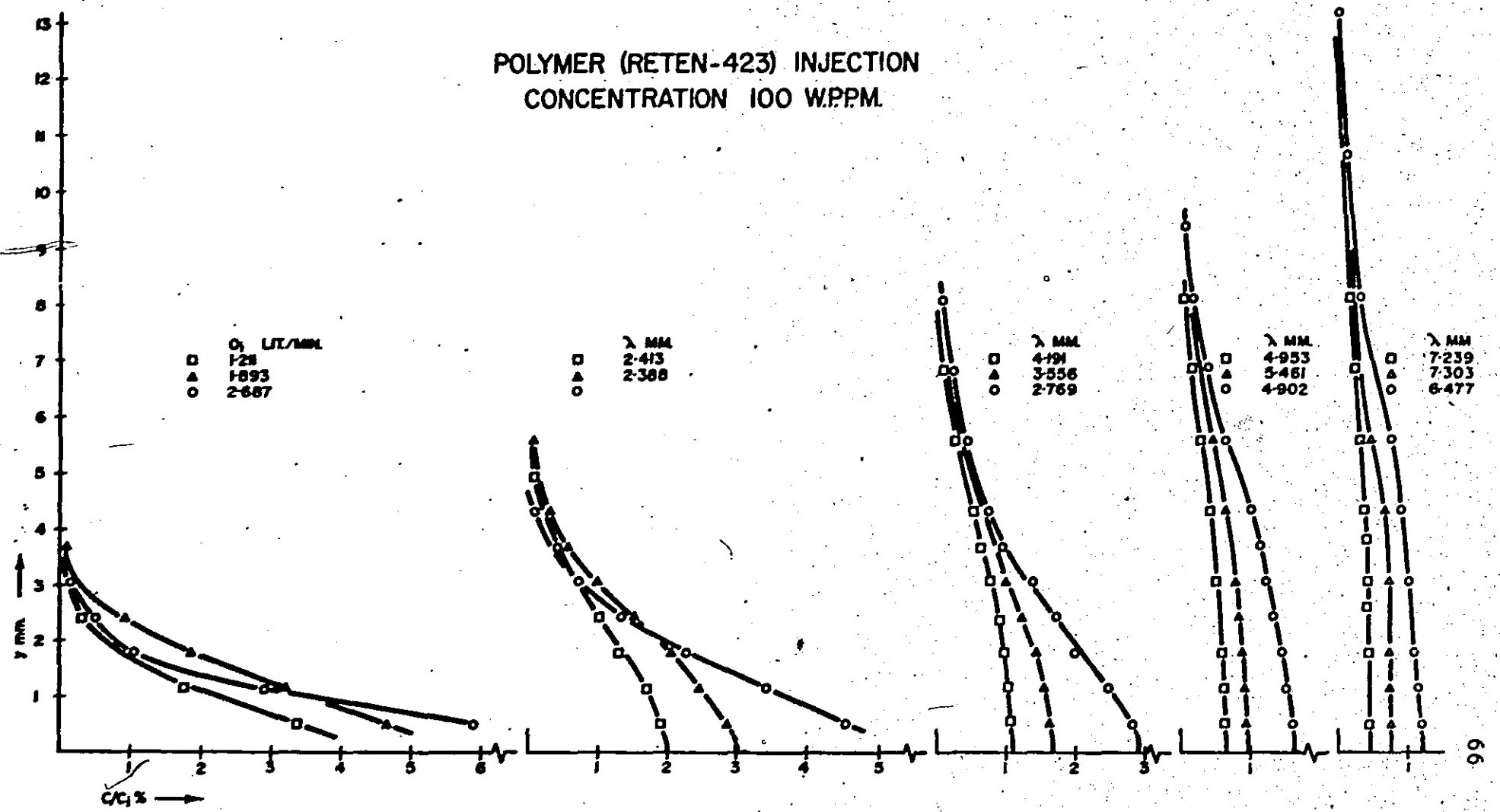

Figure 9. Concentration Profiles (c_i = 100 w.p.p.m.).

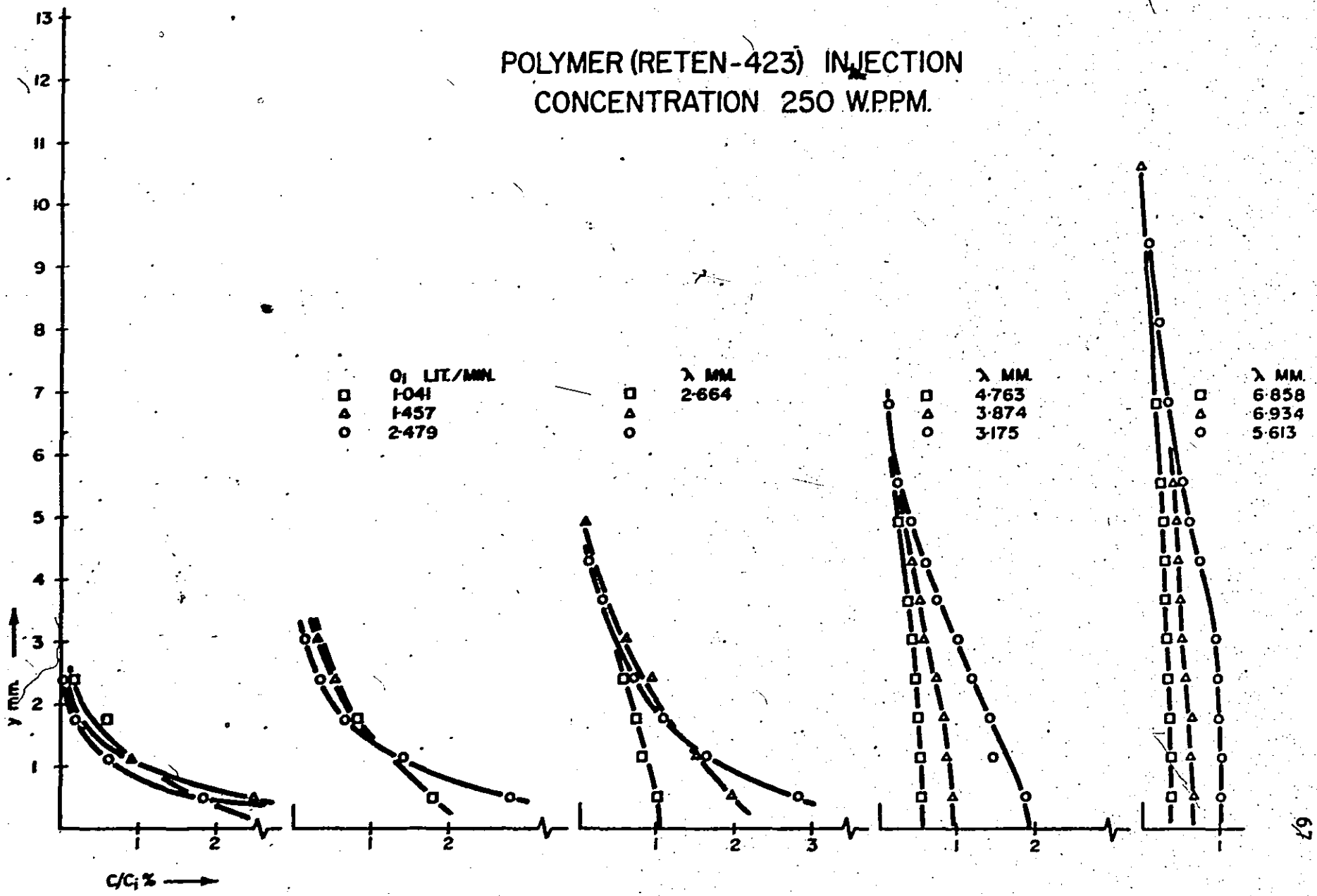

Figure 10. Concentration Profiles (c_i = 250 w.p.p.m.)

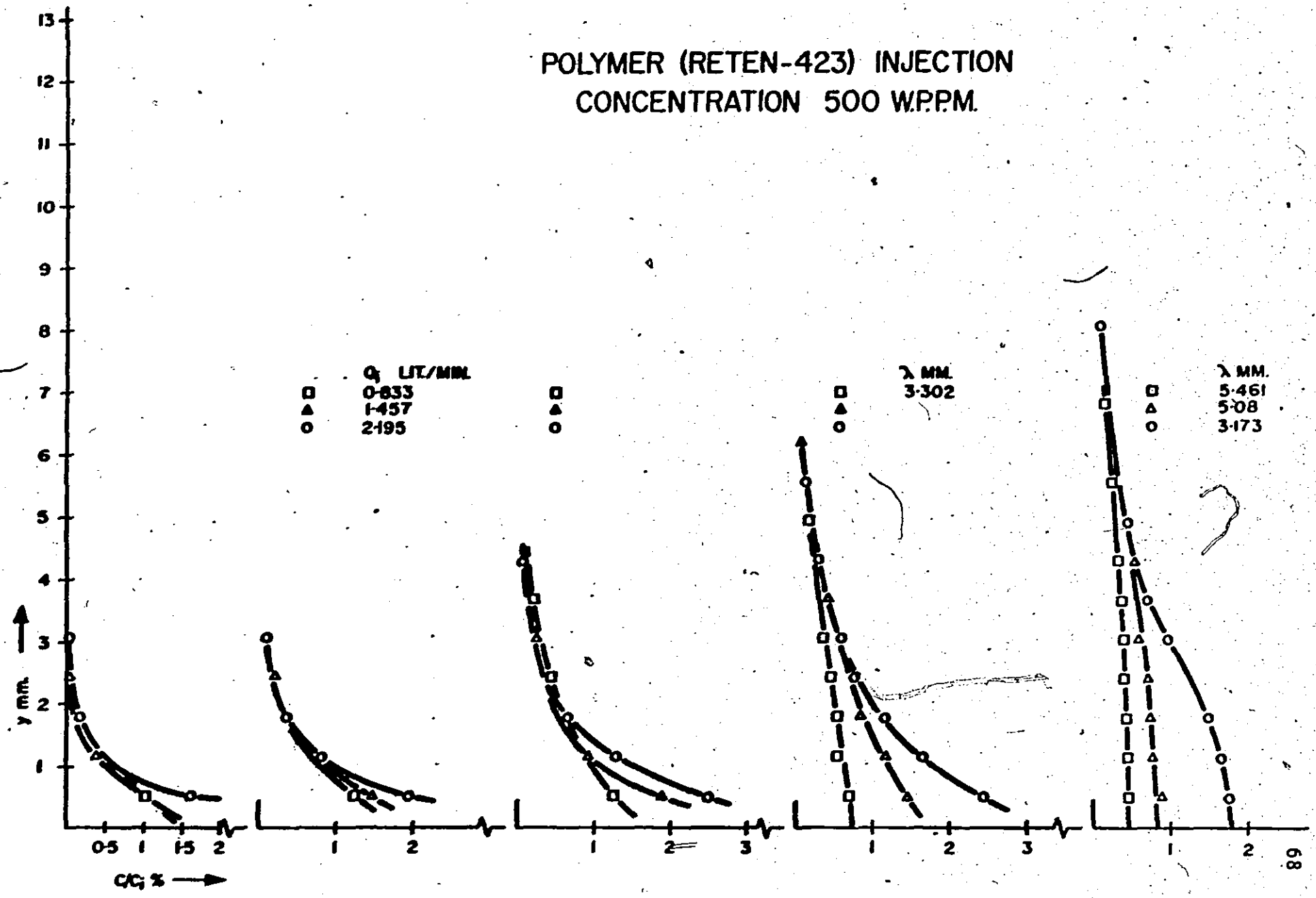

Figure 11. Concentration Profiles (c_i = 500 w.p.p.m.).

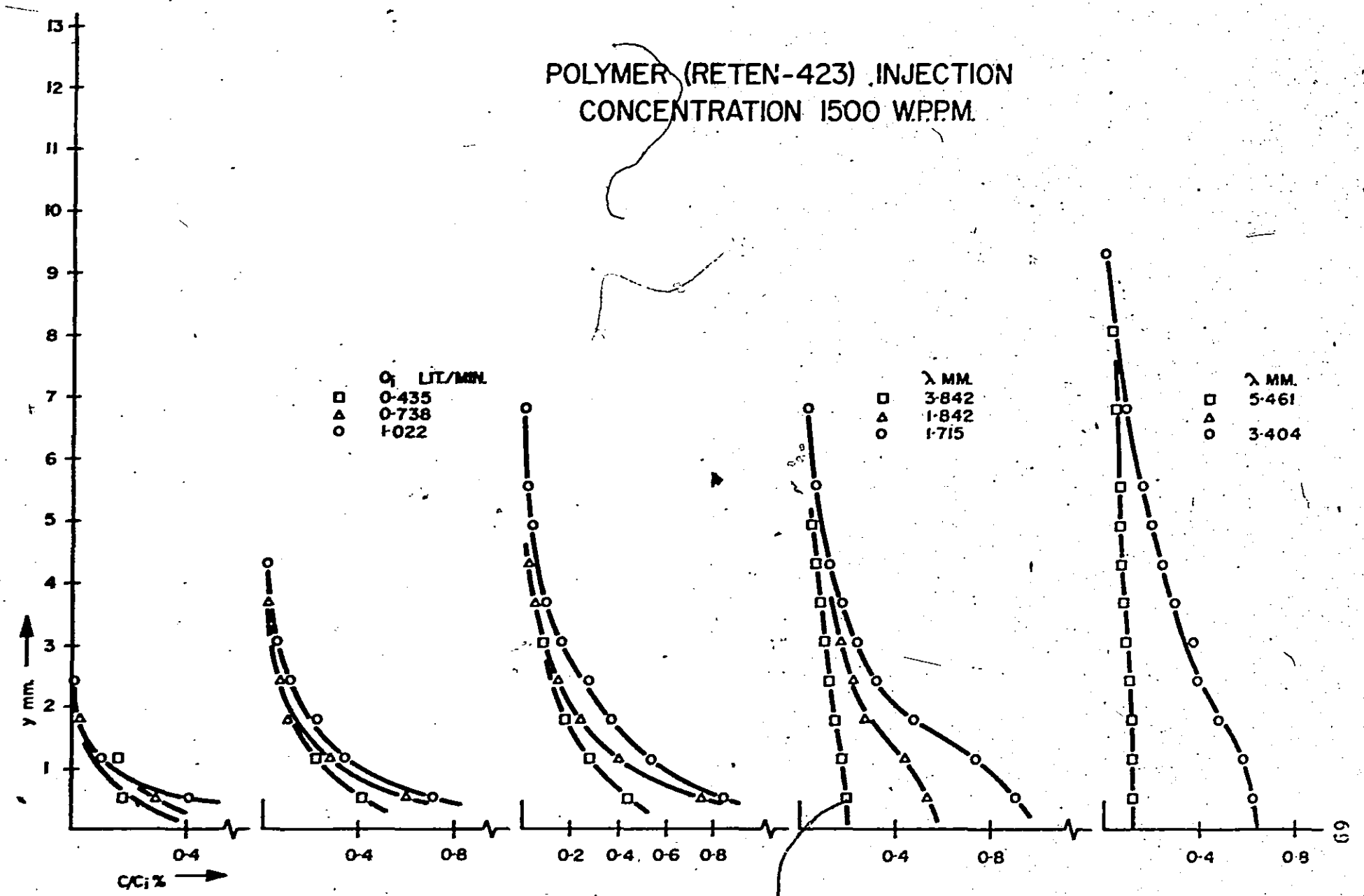

Figure 12. Concentration Profiles (c_i = 1500 w.p.p.m.).

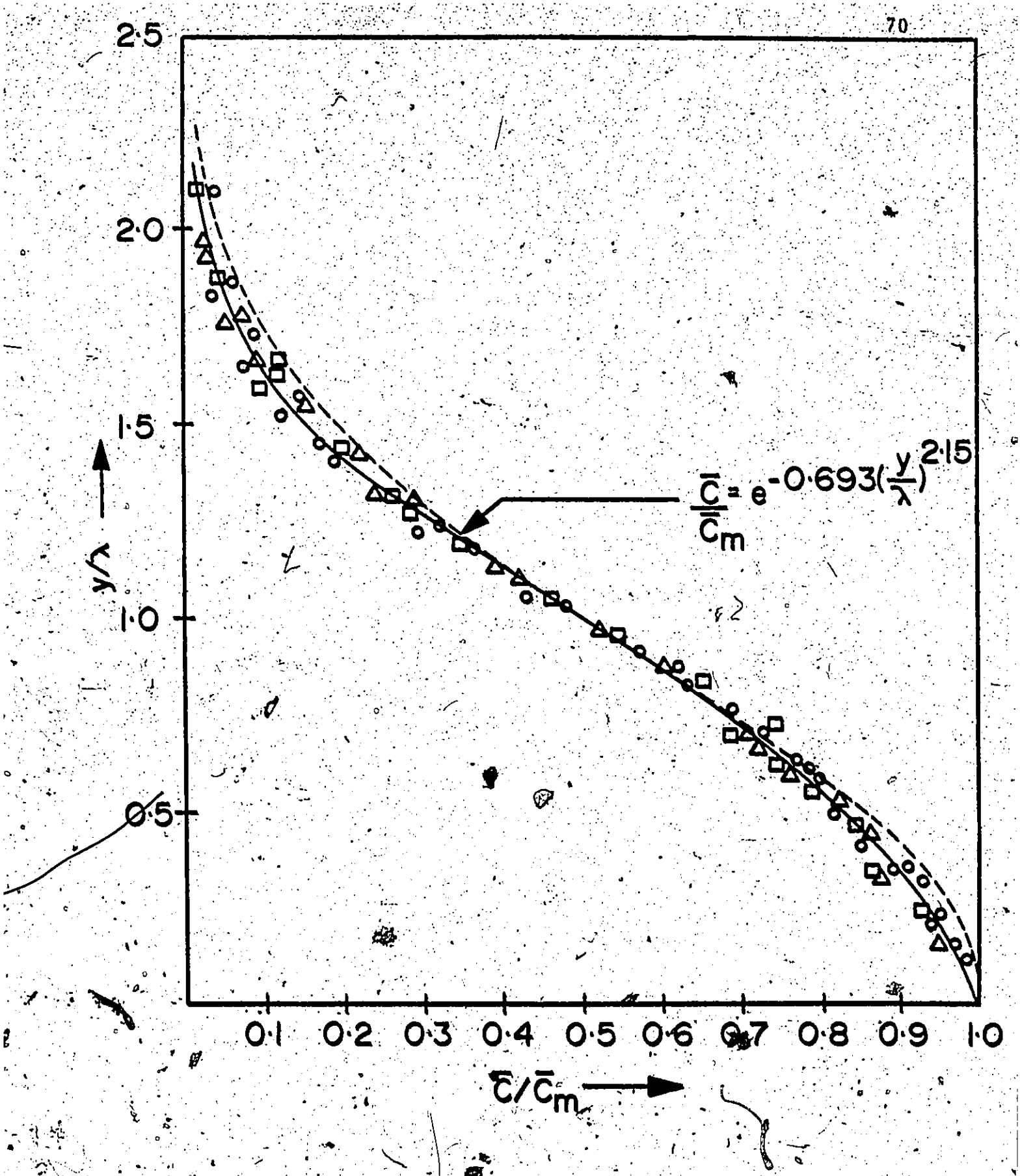

Figure 13. Universal Concentration Profile (Water Injection - All Data and c_i = 0 w.p.p.m.)

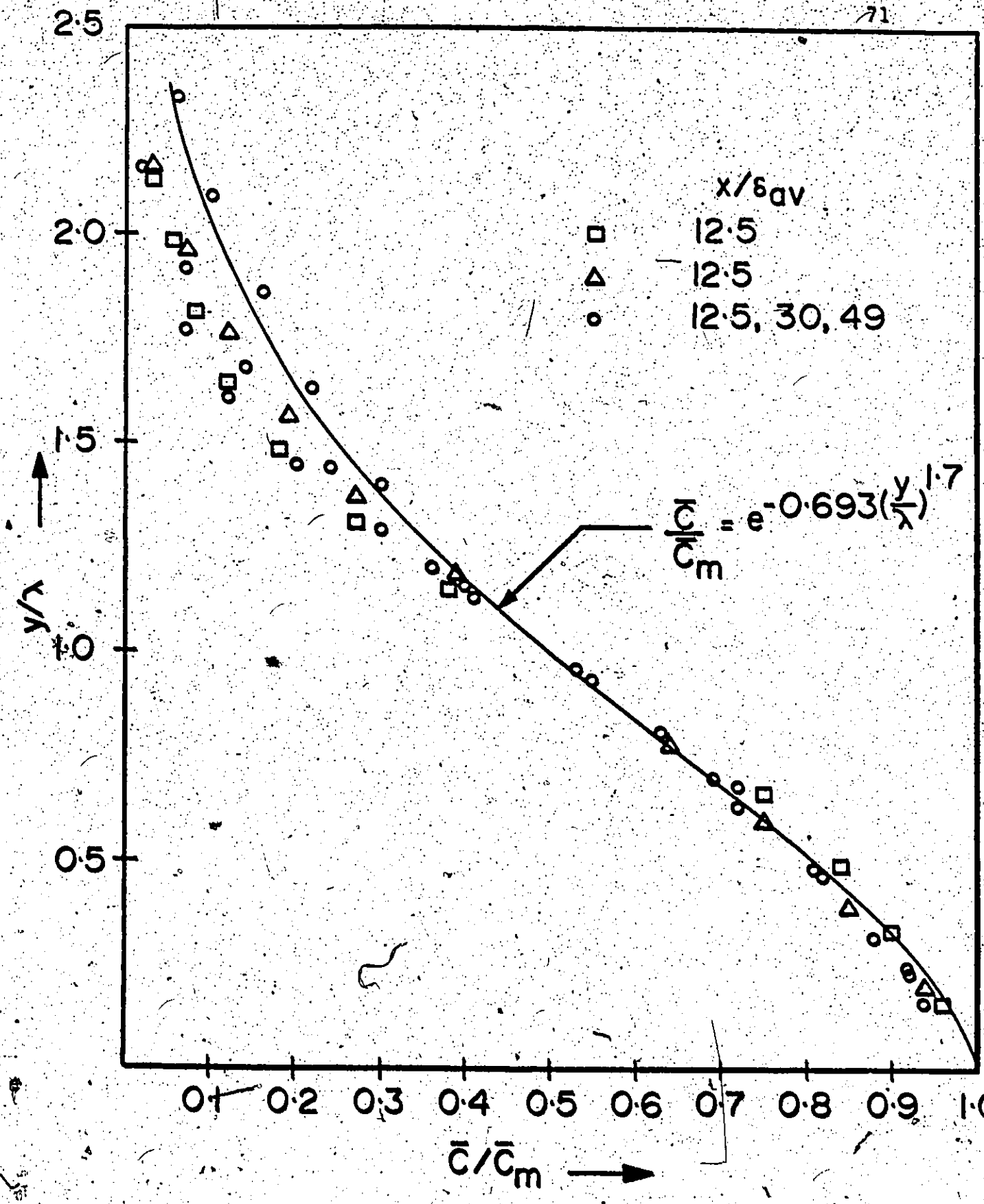

Figure 14. Universal Concentration Profile (c_i = 50 w.p.p.m. - Intermediate Zone).

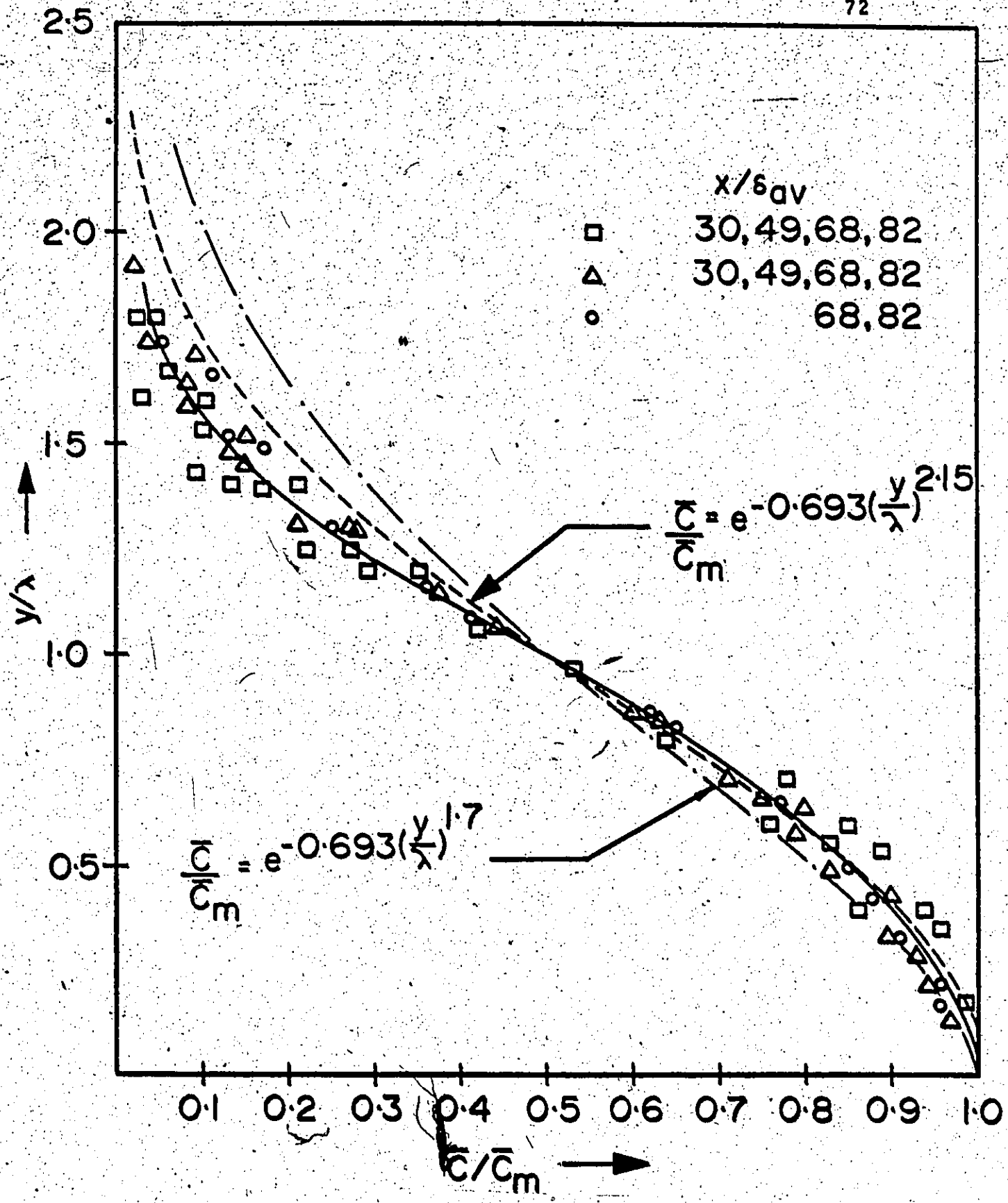

Figure 15. Universal Concentration Profile (c_i = 50 w.p.p.m. - Final Zone).

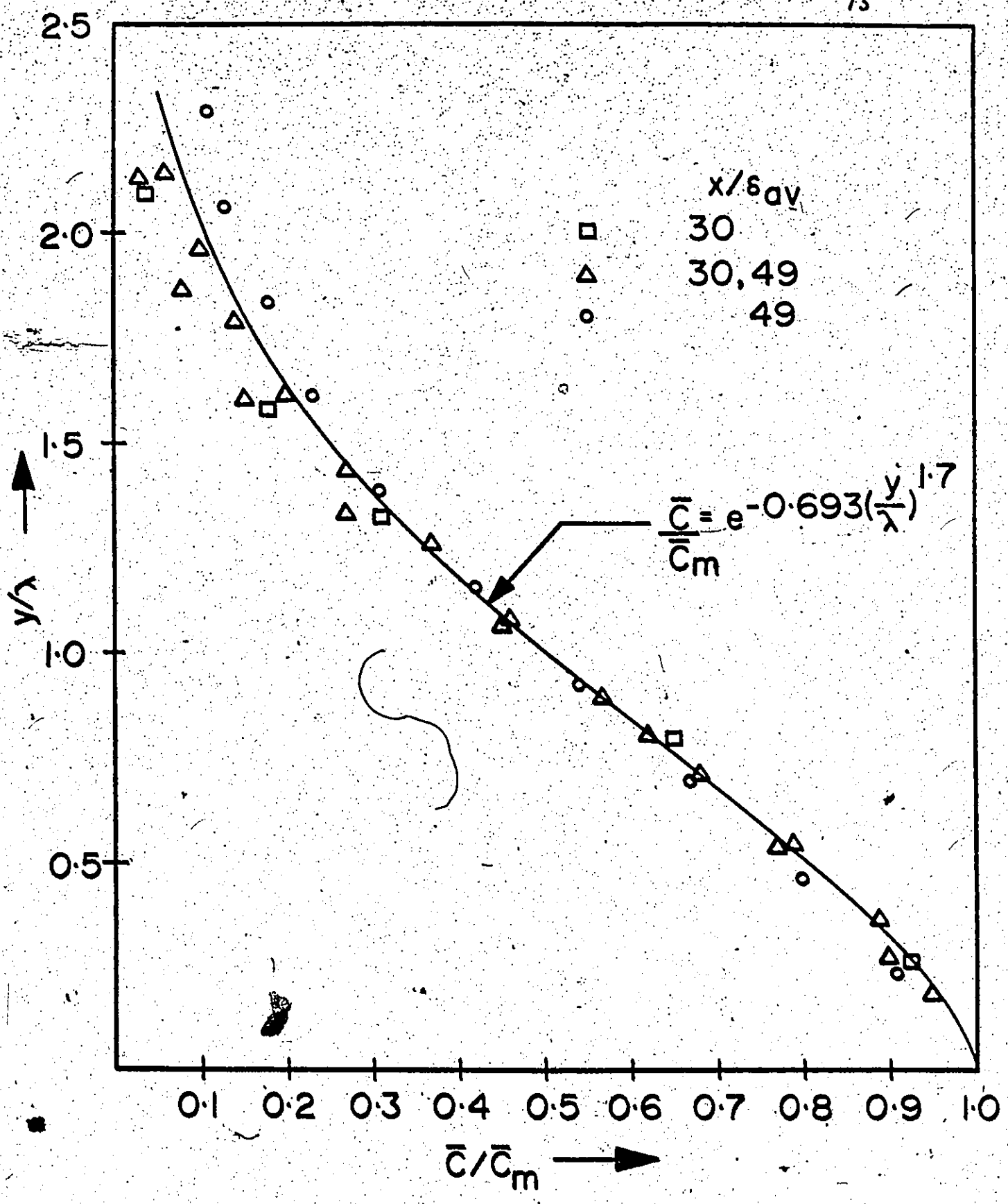

Figure 16. Universal Concentration Profile (c_i = 100 w.p.p.m. - Intermediate Zone).

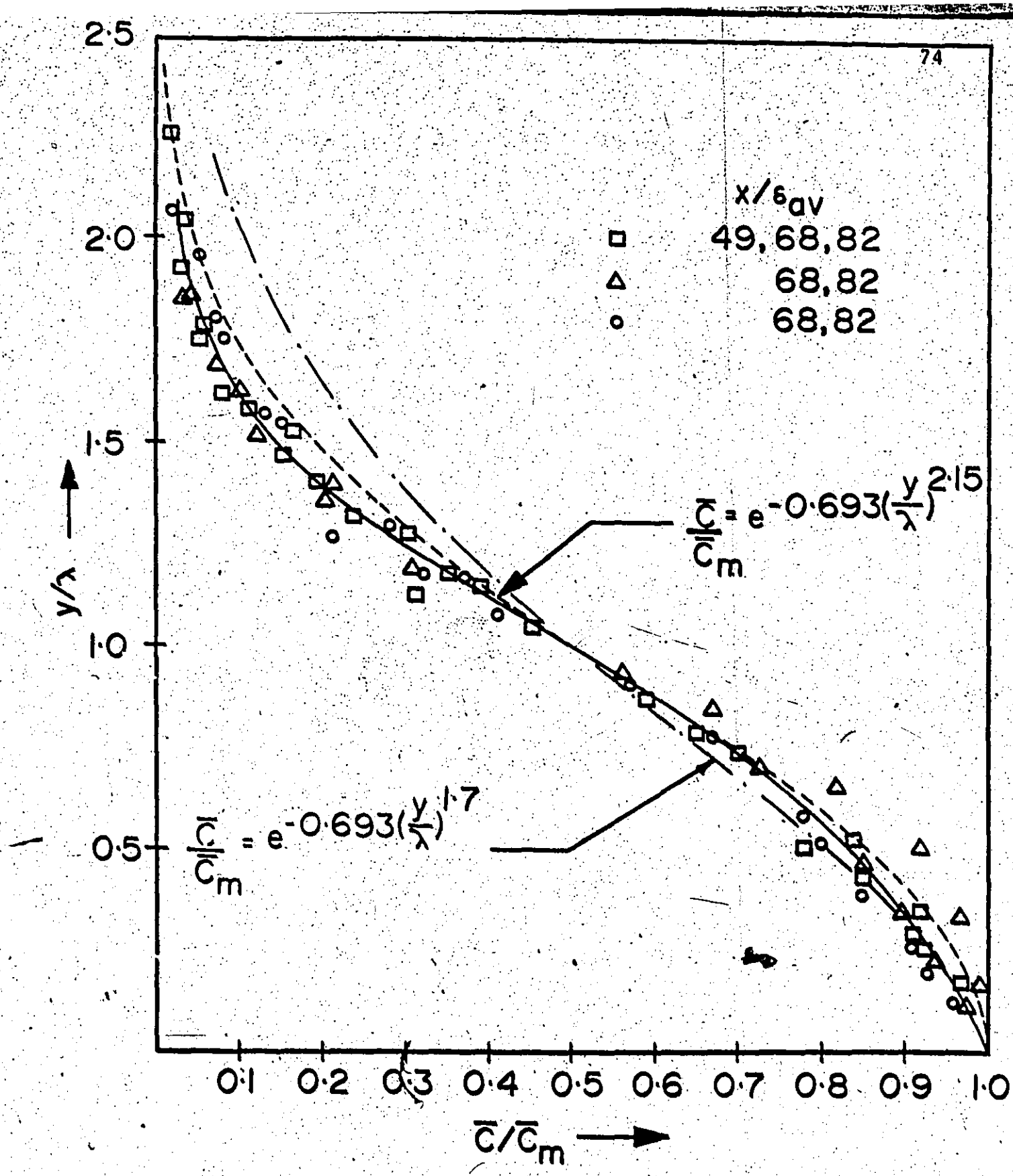

Figure 17. Universal Concentration Profile (c_i = 100 w.p.p.m. - Final Zone).

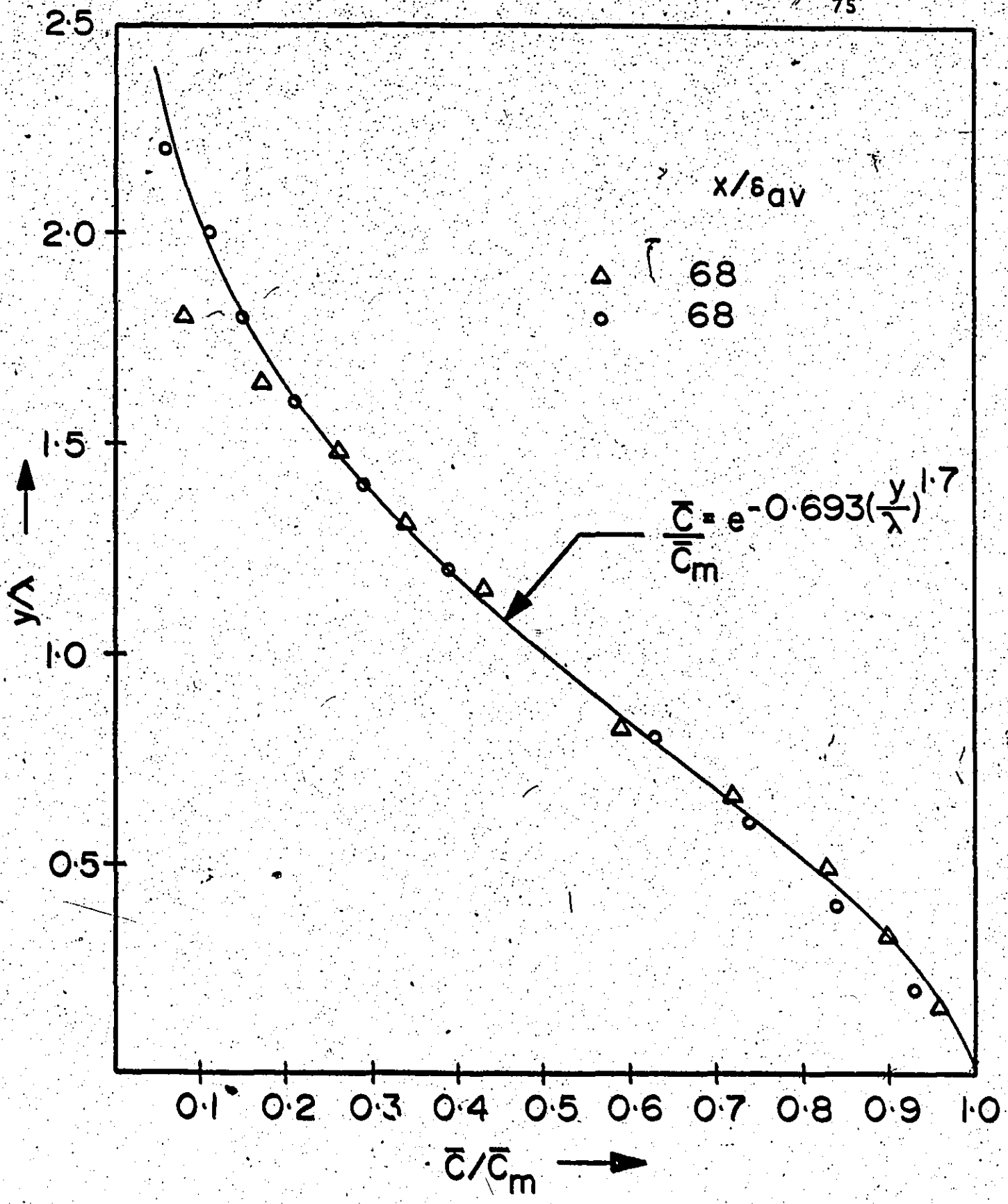

Figure 18. Universal Concentration Profile (c_i = 250 w.p.p.m. - Intermediate Zone).

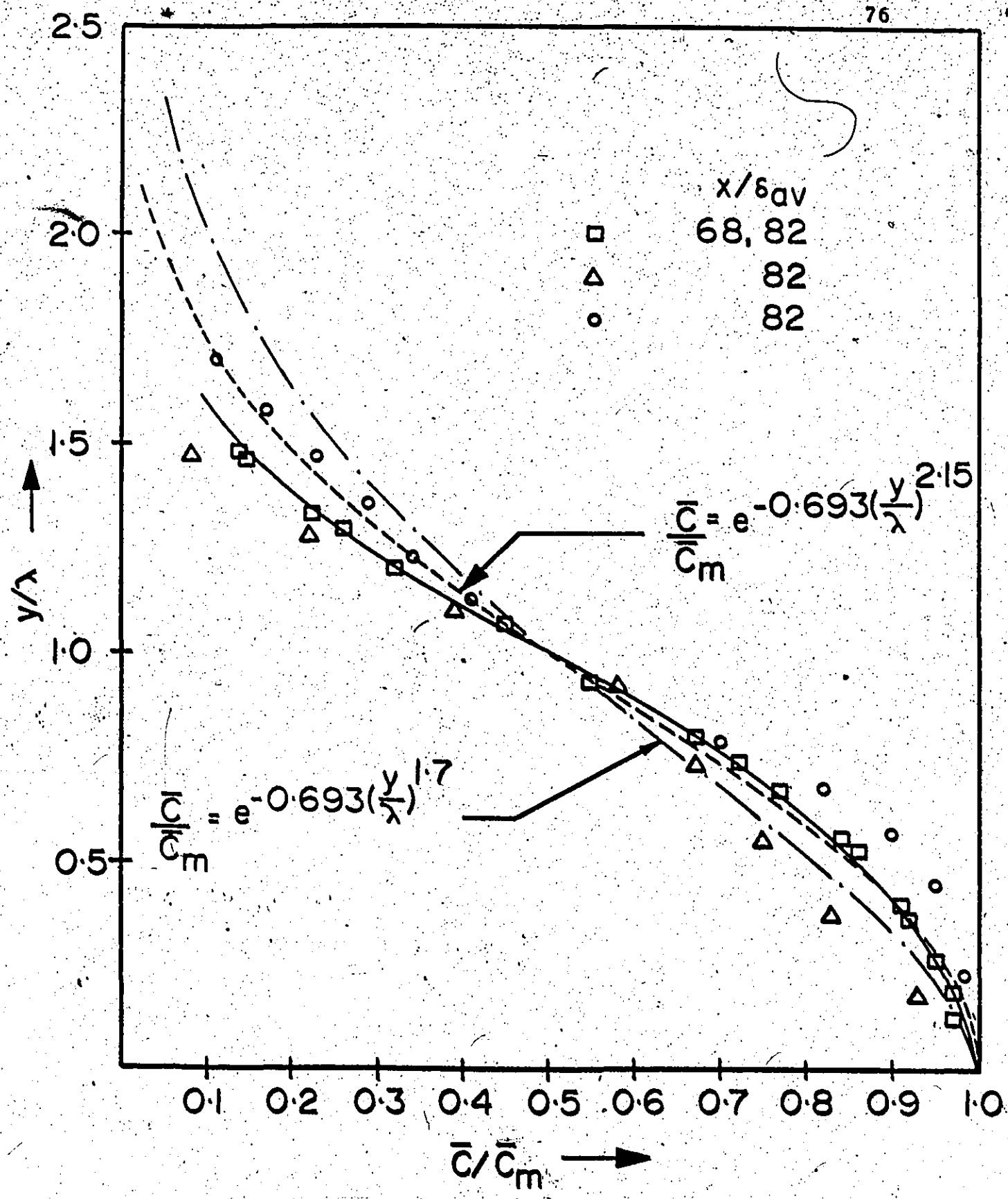

Figure 19. Universal Concentration Profile (c_i = 250 w.p.p.m. - Final Zone).

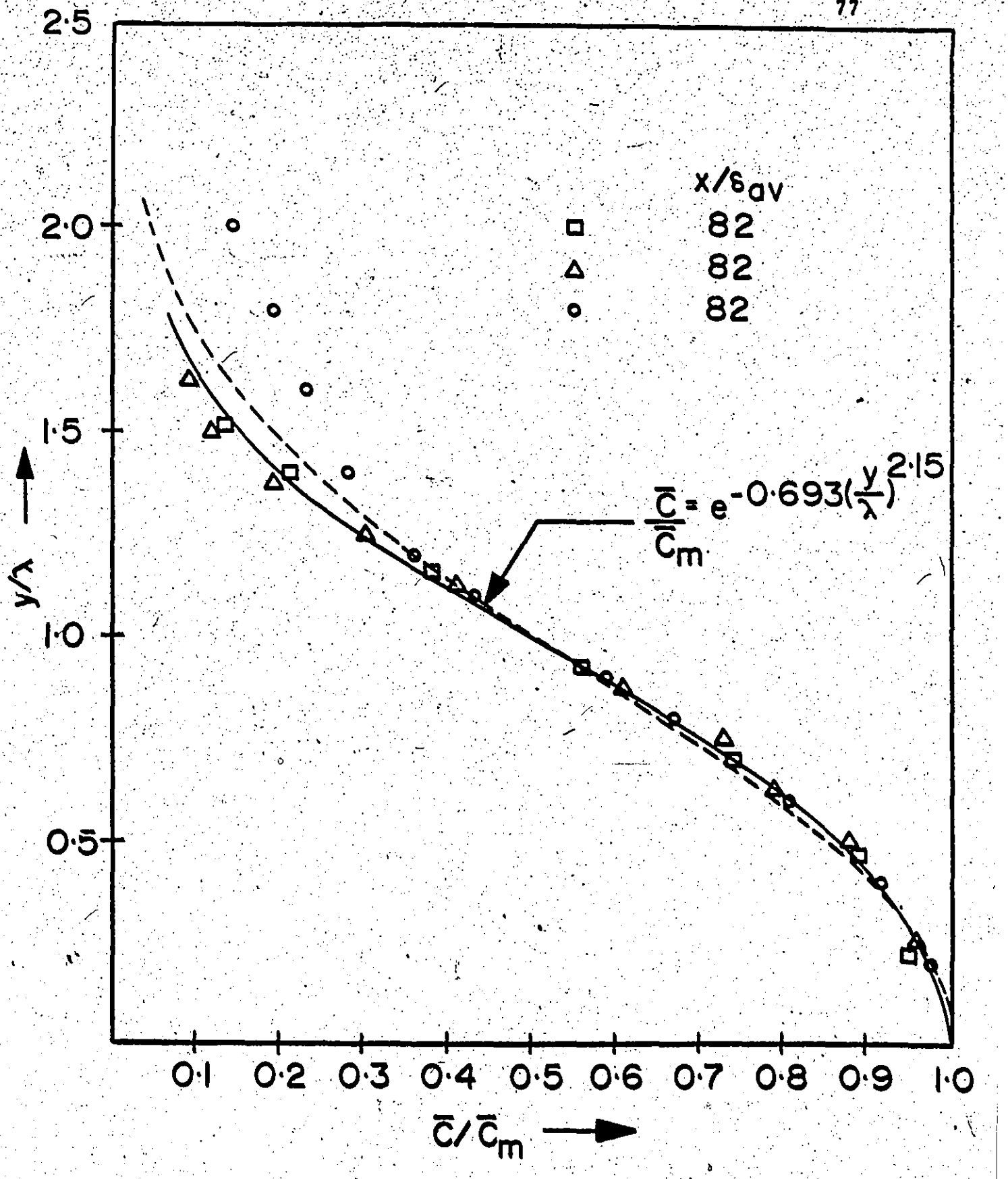

Figure 20. Universal Concentration Profile (c_i = 500 w.p.p.m. - Final Zone).

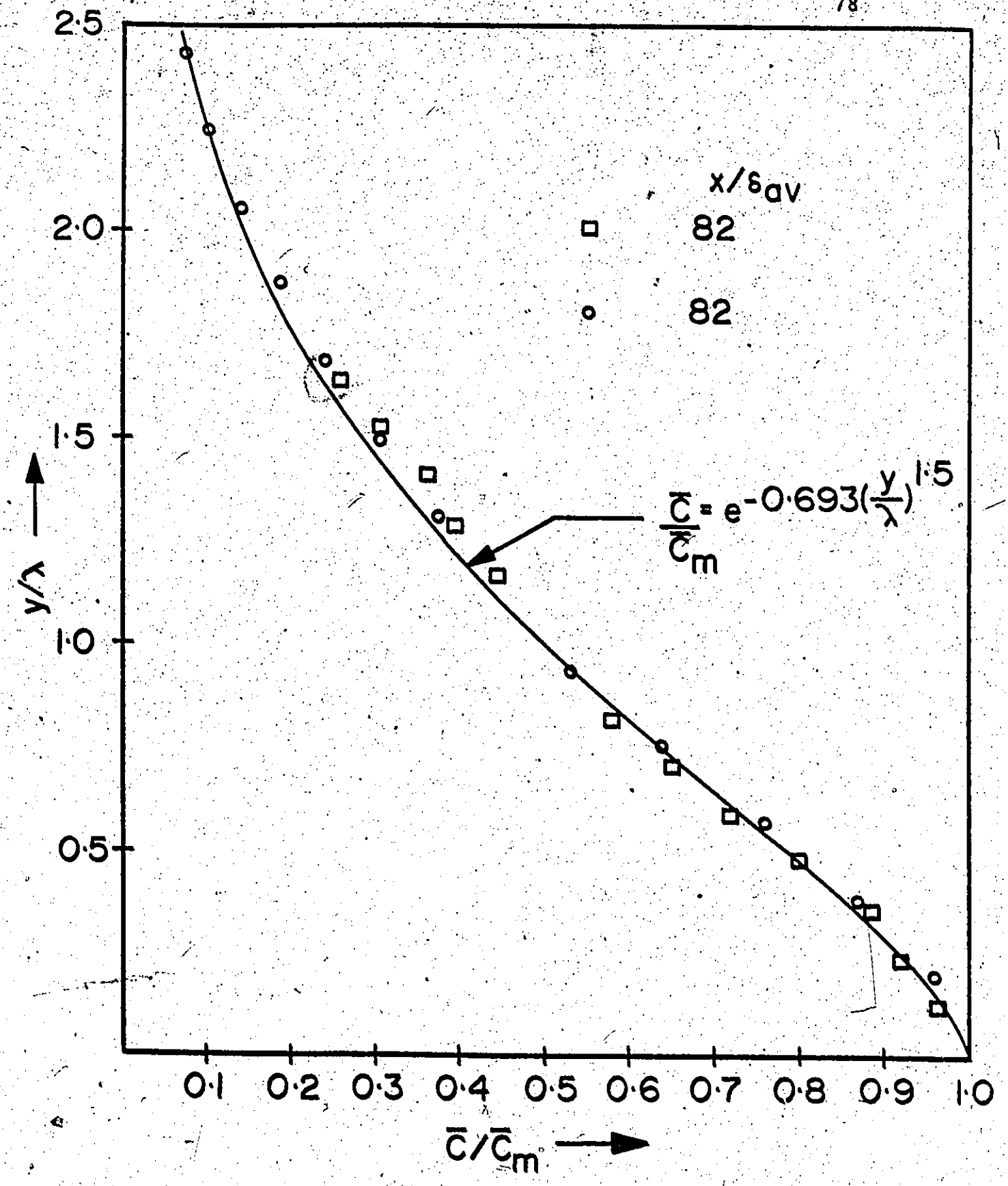

Figure 21. Universal Concentration Profile (c_i = 1500 w.p.p.m. - Last Location).

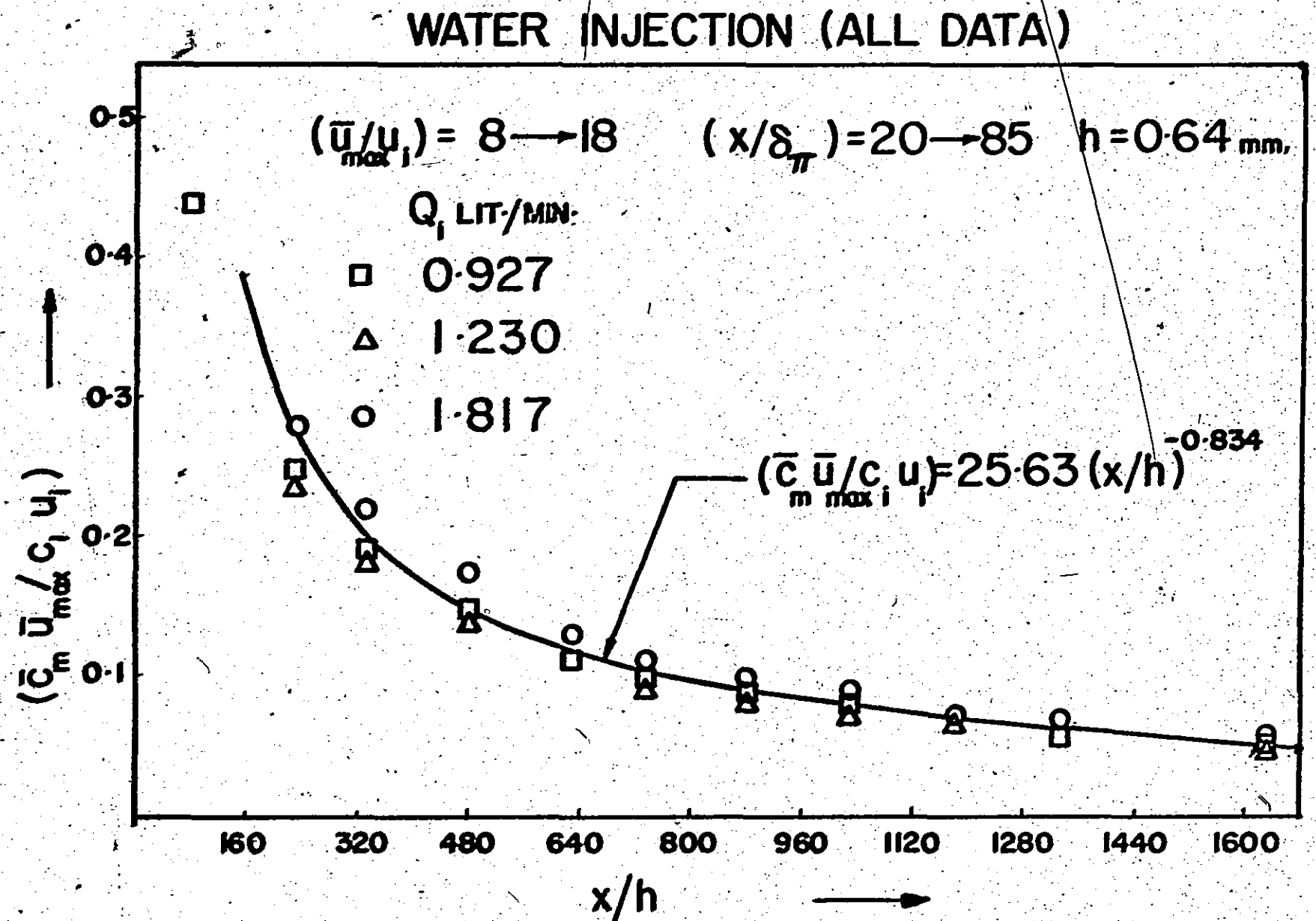

Figure 22. $\frac{\bar{c}_m \bar{u}_{max}}{c_i u_i}$ vs. $\frac{x}{h}$ (Water Injection).

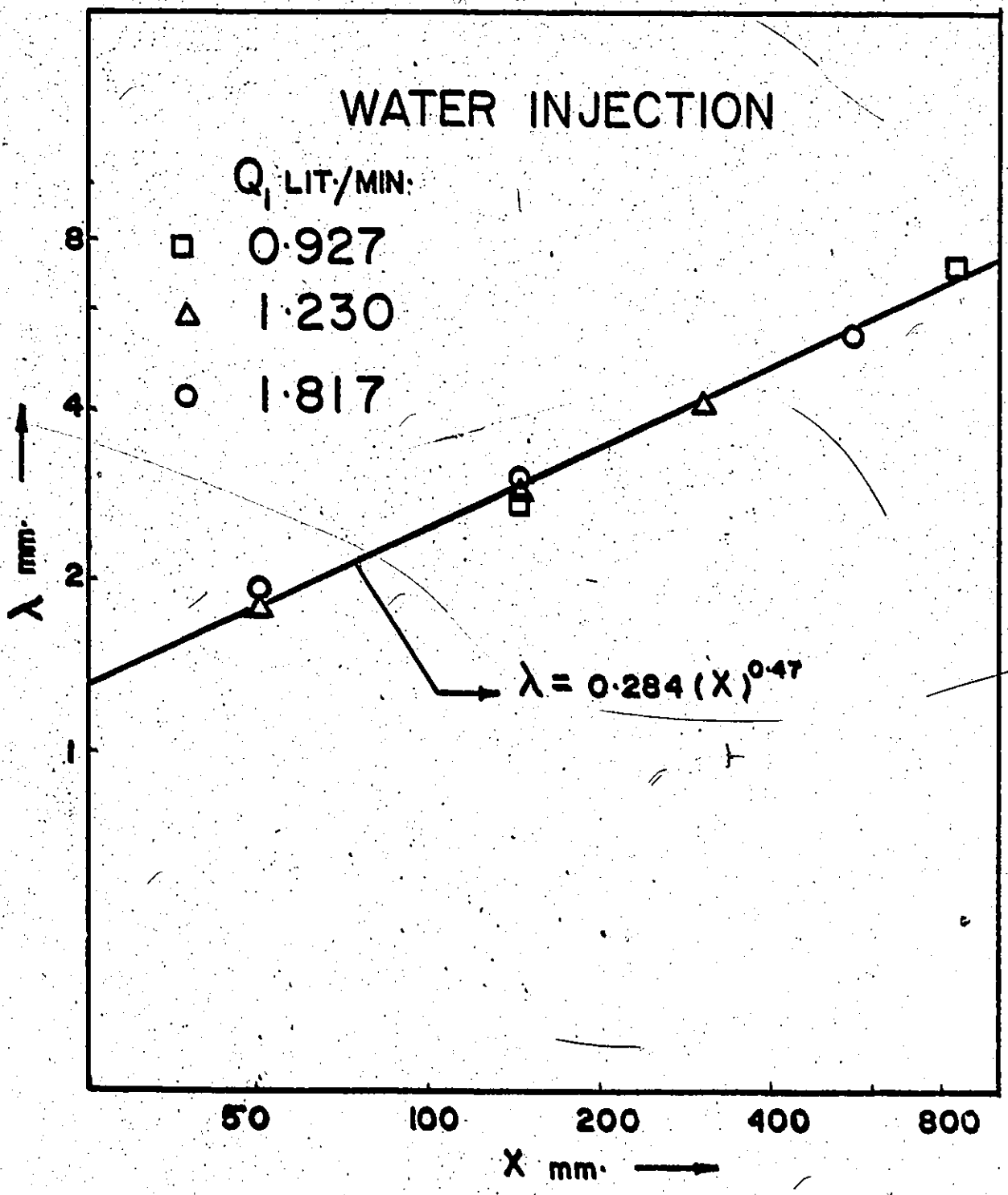

Figure 23. λ vs. x (Water Injection).

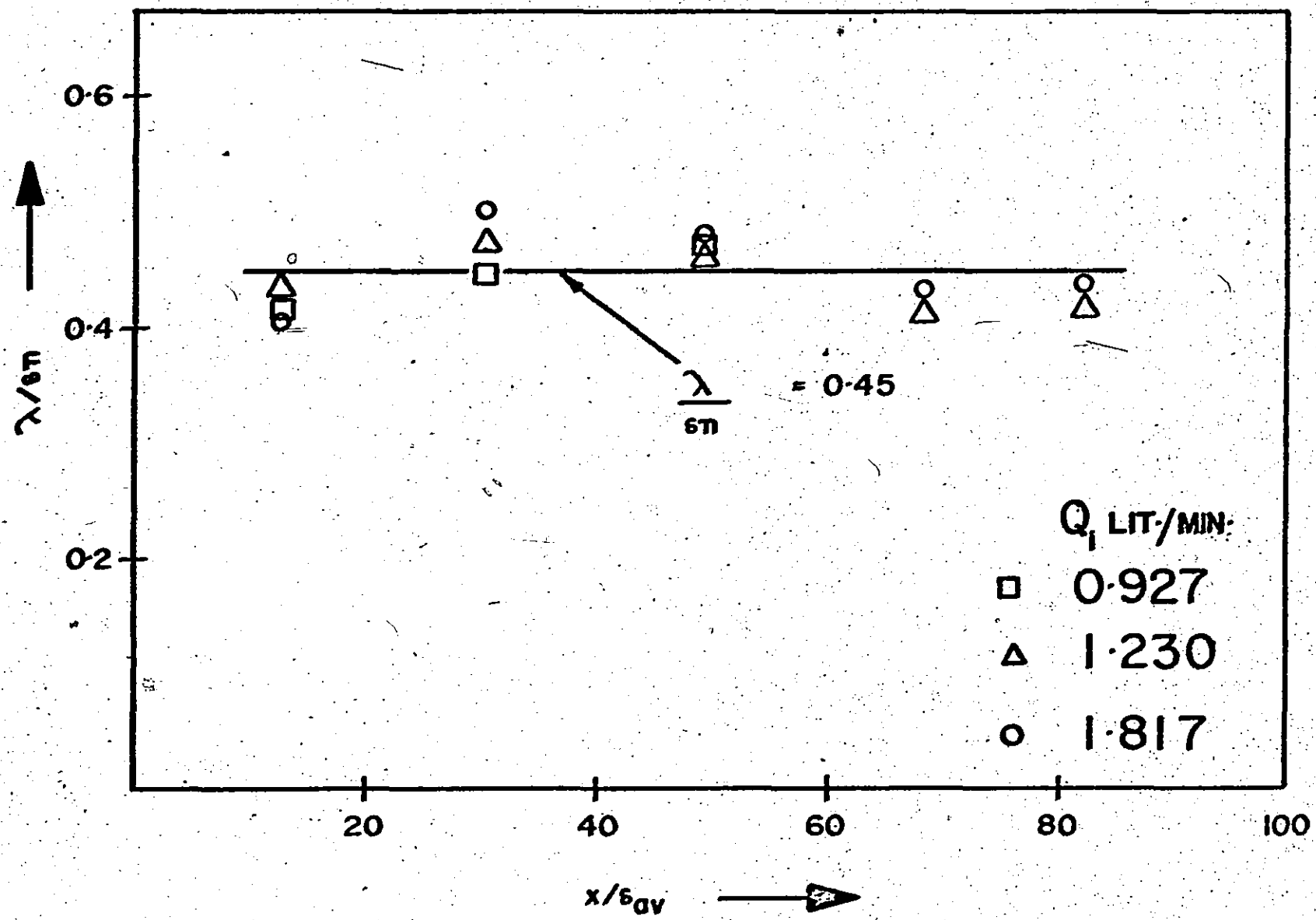

Figure 24. $\frac{\lambda}{\delta_n}$ vs $\frac{x}{\delta_{av}}$ (Water Injection).

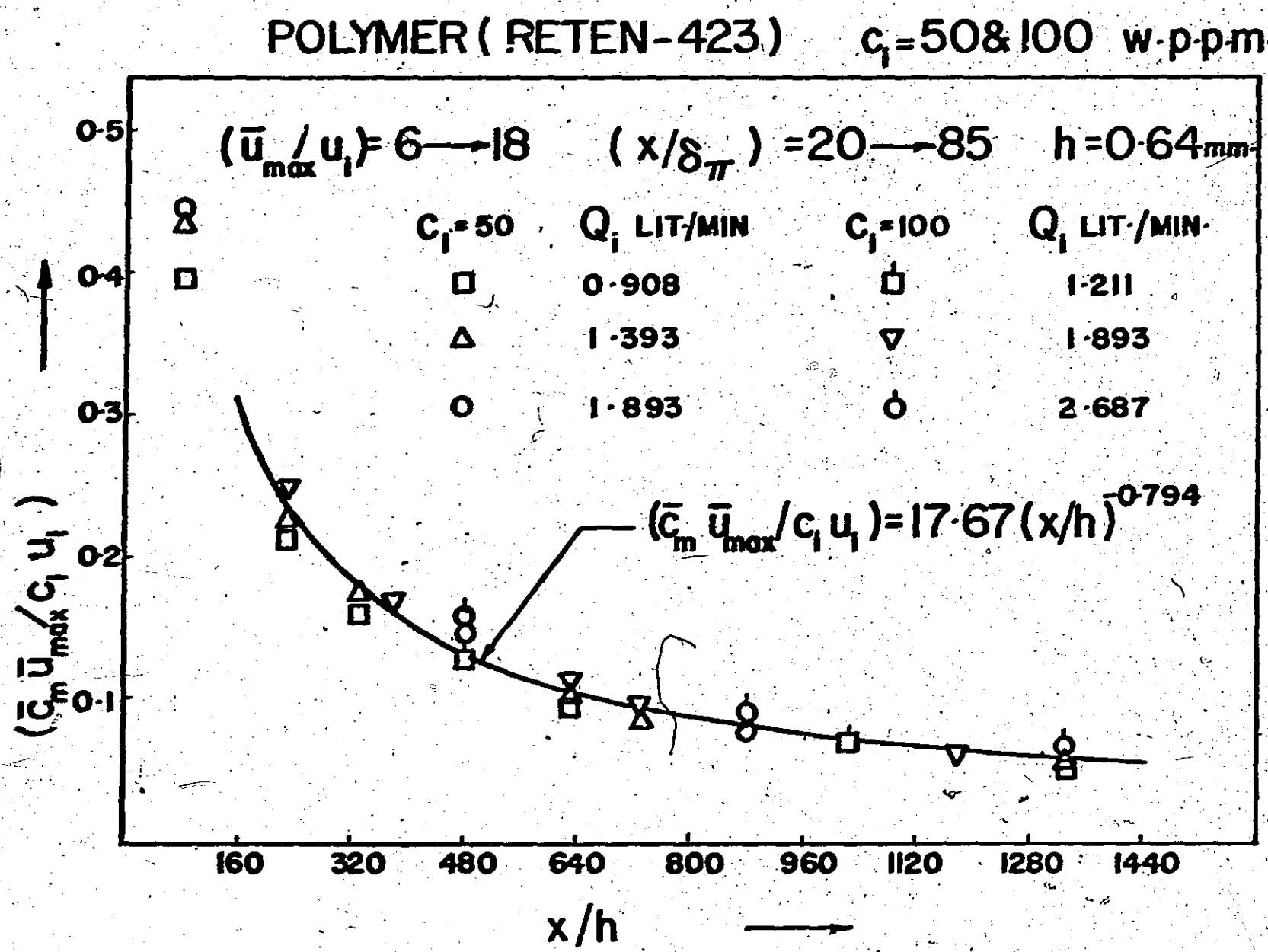

Figure 25. $\frac{\bar{c}_m \bar{u}_{max}}{c_i u_i}$ vs. $\frac{x}{h}$ (c_i = 50 and 100 w.p.p.m.).

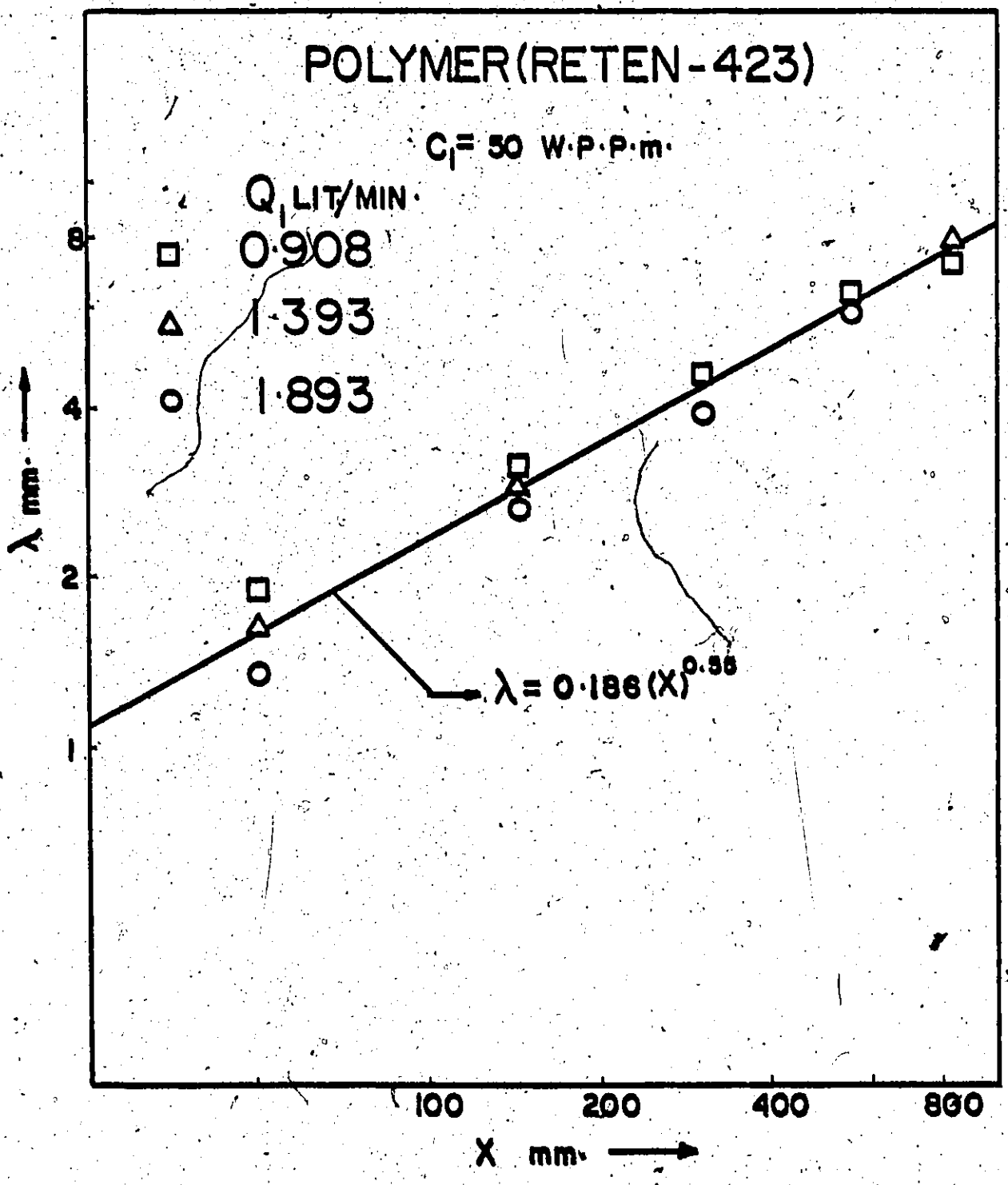

Figure 26. λ vs. x (c_1 = 50 w.p.p.m.).

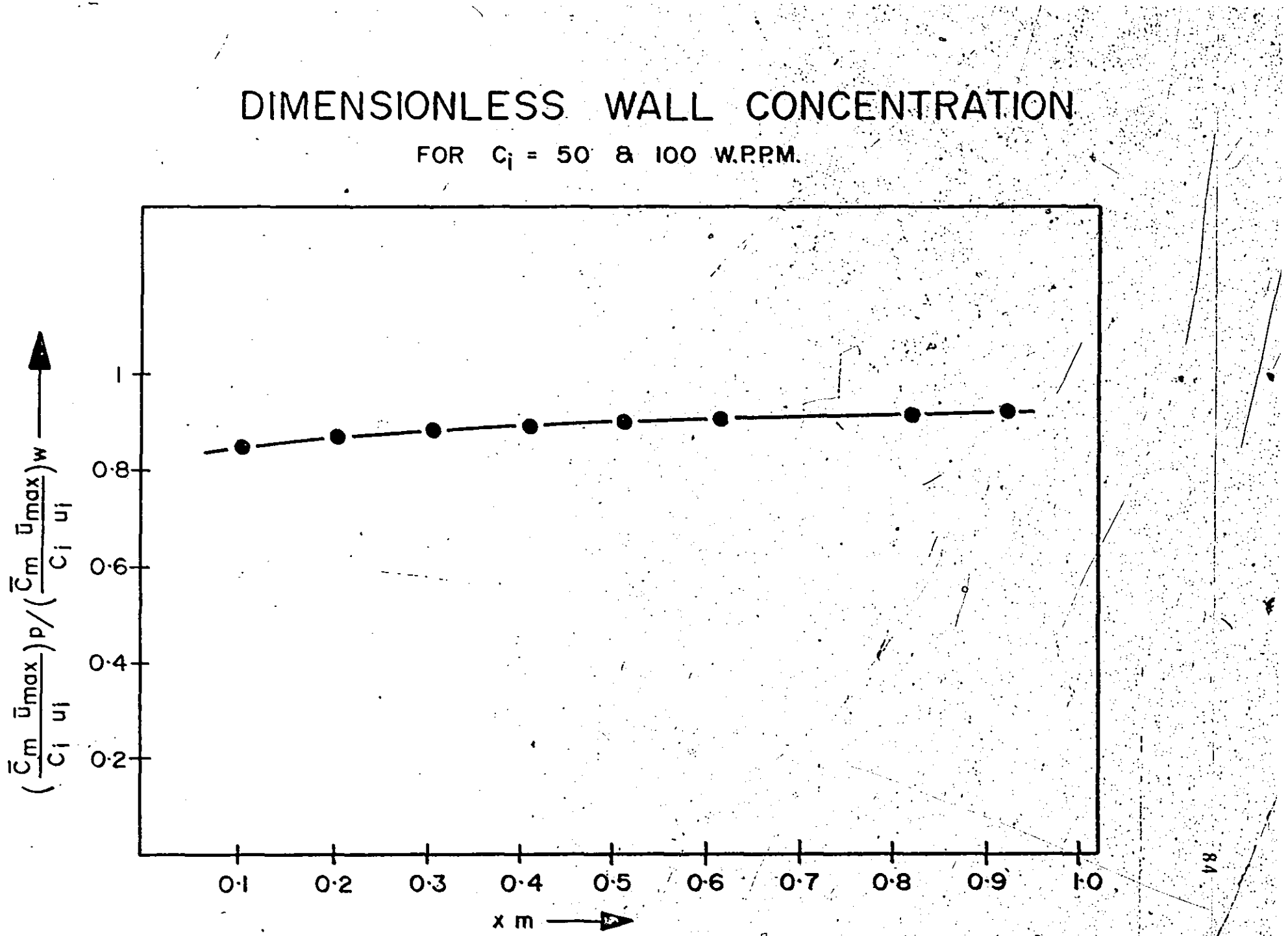

Figure 27. $(\frac{\bar{C}_m\ u_{max}}{C_i\ u_i})_p/(\frac{\bar{C}_m\ \bar{u}_{max}}{C_i\ u_i})_w$ vs. x (c_i = 50 and 100 w.p.p.m.).

DIMENSIONLESS WALL CONCENTRATION

X = 0·8446 m

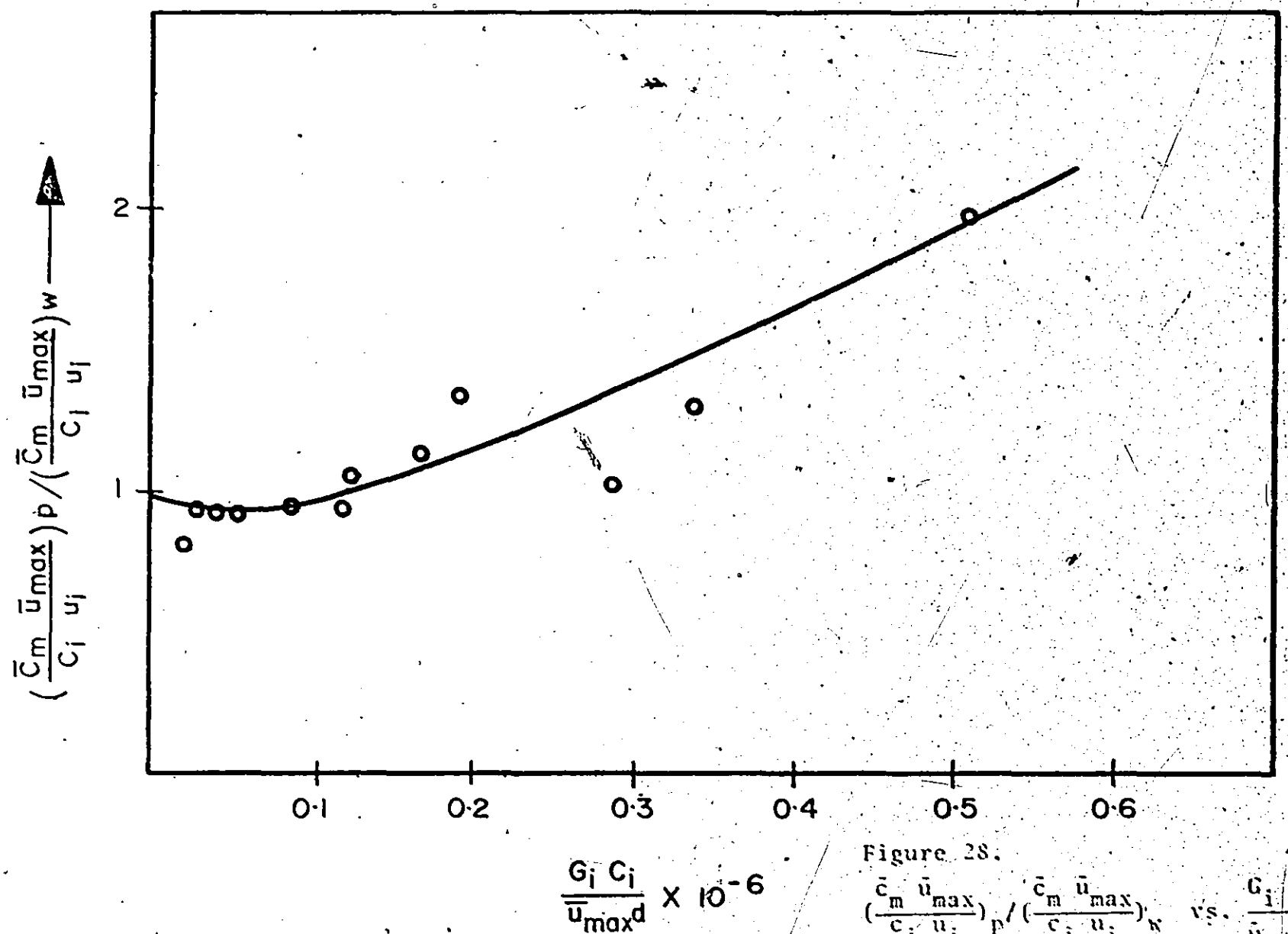

Figure 28.

$\left(\frac{\bar{c}_m\ \bar{u}_{max}}{c_j\ u_j}\right)_p / \left(\frac{\bar{c}_m\ \bar{u}_{max}}{c_j\ u_j}\right)_w$ vs. $\frac{G_j\ c_j}{\bar{u}_{max}\ d}$

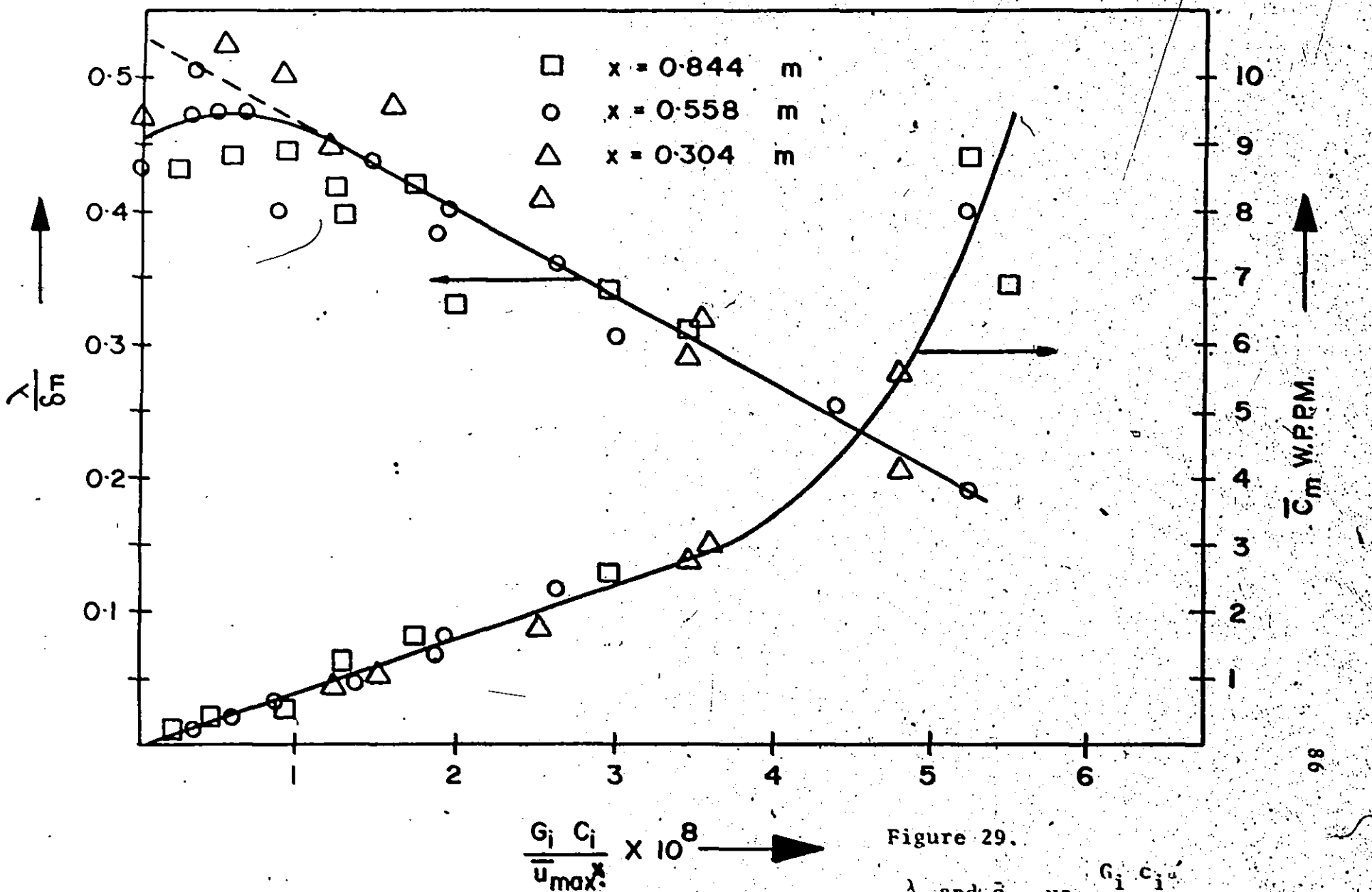

Figure 29.

$\frac{\lambda}{\delta_m}$ and $\bar{c}_m$ vs. $\frac{G_i\, c_i}{\bar{u}_{max}\, x}$

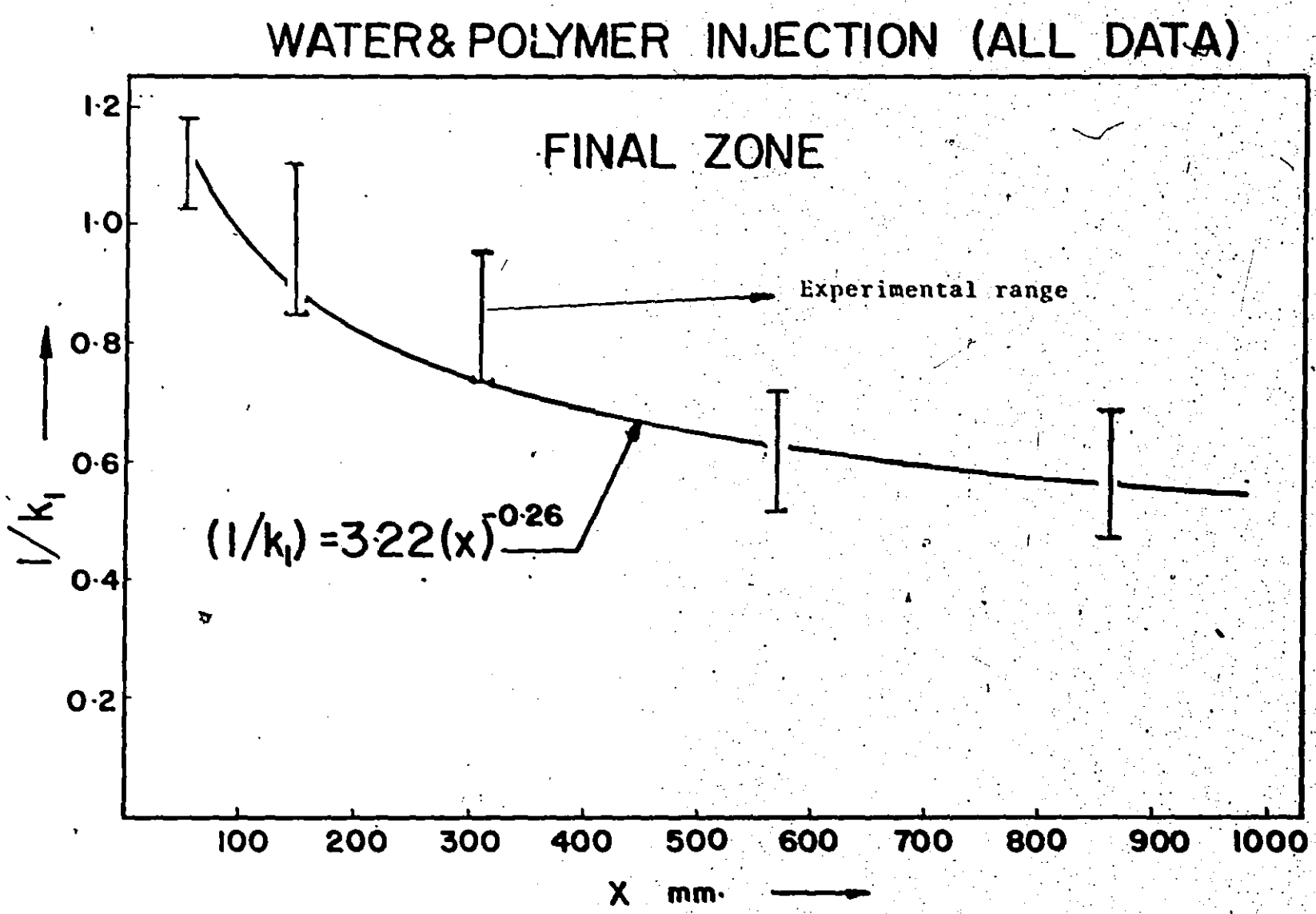

Figure 30. $\frac{1}{K_1}$ vs. x.

APPENDIX I

CALIBRATION CURVES

Calibration curves of the rotometer reading versus injection flow rate for various polymer concentrations are shown in Figure 31. These data for the curves were obtained by passing a known concentration of polymer solution through the rotometer and volumetrically measuring the flow rate by timing given values of fluid to pass through the meter.

The calibration curve for determining the optimum exciting wave length for Rhodamine WT is shown in Figure 32. The data for this curve were obtained by applying various exciting wave lengths for the same concentration. The calibration curve for the relation between the concentration and the optical density is shown in Figure 33 and was obtained by applying the optimum exciting wave length for the known concentration.

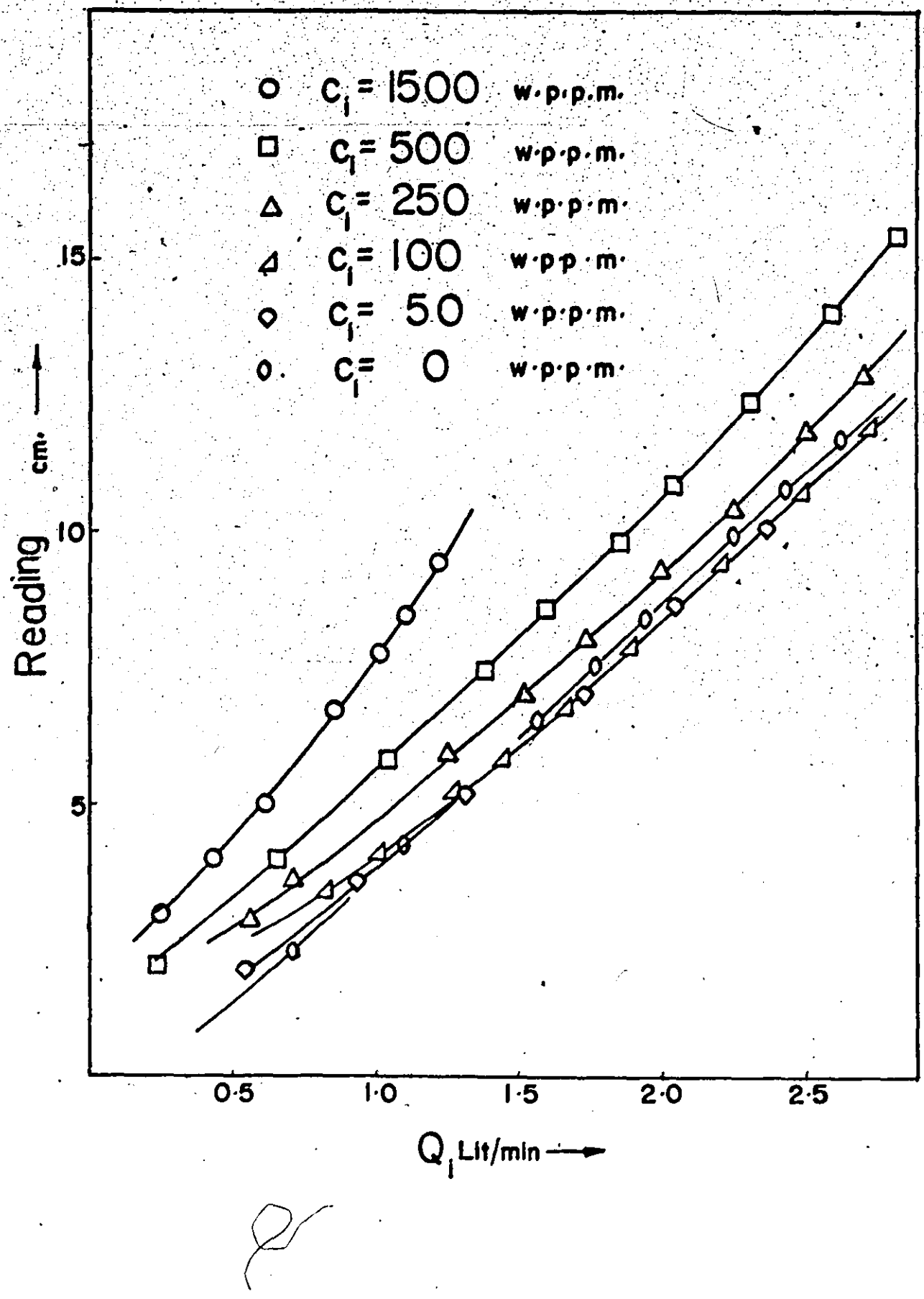

Figure 31. Calibration Curve for the Rotometer.

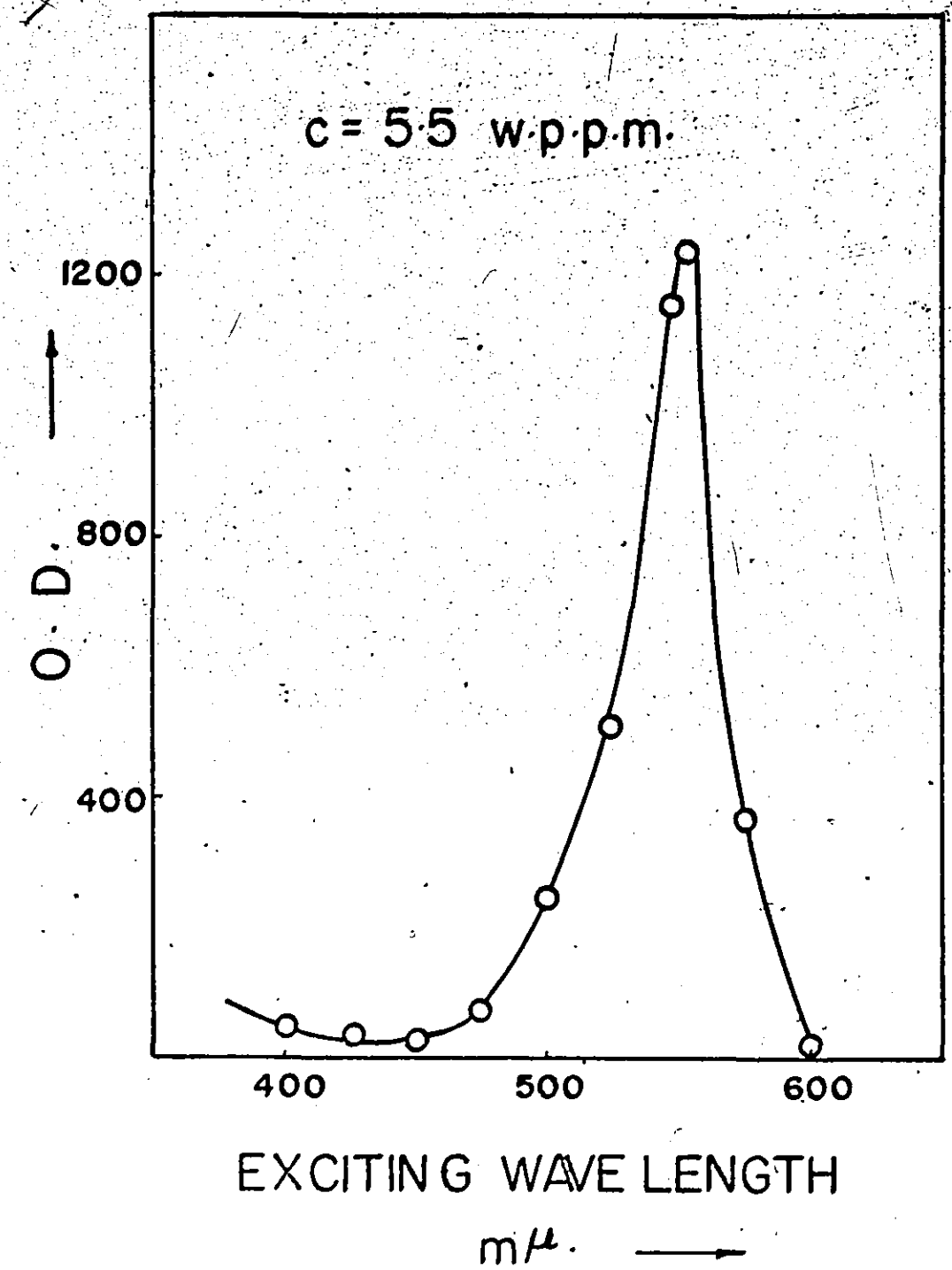

Figure 32. Optical Density (O.D.) vs. Exciting Wave Length.

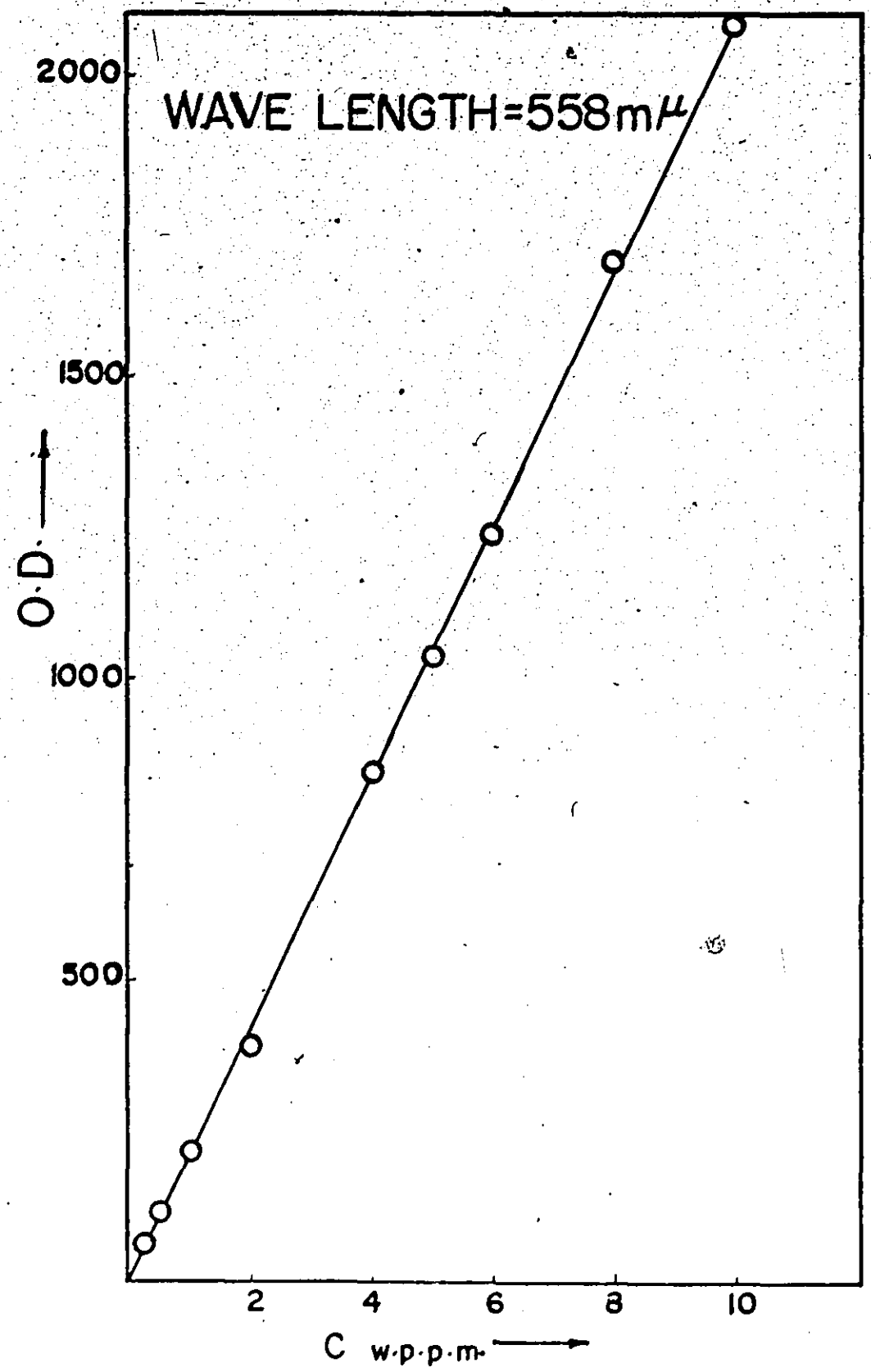

Figure 33. Calibration Curve for the Spectrophotometer.

APPENDIX 2

DATA TABLES

The experimental data for the concentration measurements for c_i = 0, 50, 100, 250, 500 and 1500 w.p.p.m. for the various injection flow rates are shown in Tables 1 through 18 inclusive.

The velocity ratio $\frac{\bar{u}}{u_{max}}$ data are also shown in Tables 19 and 20. All the data in the tables are self explanatory.

CONCENTRATION DATA

Table 1.

c_i = 0 w.p.p.m. Q_i = 1.817 Lit./min. I.O.D. = 22000

y mm. \ x mm.	50.8	146.0	304.8	558.8	864.6
0.500	1314	703	453	271	203
1.135	1024	641	426	257	200
1.770	724	578	414	263	196
2.405	344	480	375	247	
3.040	177	380	330	221	190
3.675	33	281			
4.310	17.5	156	216	191	167
4.945			172		
5.580		34	110	151	154
6.850			58.5	101	120
8.120			30	72	120
9.390					
10.660				36	63
13.200					45
50.000	8.5	15	21.5	20	25

Table 2.

c_i = 0 w.p.p.m. Q_i = 1.230 Lit./min. I.O.D. = 22000

y mm. \ x mm.	50.8	146.0	304.8	558.8	864.6
0.500	725	418	264	173	133
1.135	610	390	254.5	165	134
1.770	458	334	228	156.5	124
2.405	330	292	228		
3.040	128	215.5	195	151	117
3.675	47	144			
4.310	20	90	144	125	111
4.945		53			
5.580		30	89	98	99
6.850			50	68.5	86
8.120			30	53	79.5
9.390					
10.660				33	52
50.000	23	26	20	32	37

Table 3.

c_i = 0 w.p.p.m. Q_i = 0.927 Lit./min. I.O.D. = 22000

y mm. \ x mm.	50.8	146.0	304.8	558.8	844.6
0.500	566	318	196	117.5	90.5
1.135	442	277	186	114	93.5
1.770	327	247	173	113	95
2.405	166	212	156		
3.040	64	137	128	100.5	85
3.675	25	99	118		
4.310	7	47	92	80	73
4.945		26	70		
5.580		10	50.5	65	57.5
6.850			21	44	58
8.120			12	26	43
9.390				18.5	
10.660					20
13.200					10
50.000	2	4	7.5	12.5	14

Table 4.

c_i = 50 w.p.p.m. Q_i = 1.893 Lit./min. I.O.D. = 21100

x mm. / y mm.	50.8	146.0	304.8	558.8	844.6
0.500	1102	640	394	220	170
1.135	840	550	360	220	
1.770	471	493	322	218	172
2.405	260	383	318		
3.040	104	325	264	200	164
3.675	18	181	230		
4.310		134		170	157
4.945		62	141		
5.580		36	108	138	142
6.850			45	100	
8.120			27	57	98
9.390					
10.660				30	60
13.200					43
50.000	7	14	20	24	31

Table 5.

c_i = 50 w.p.p.m. Q_i = 1.393 Lit./min. I.O.D. = 21100

y mm. \ x mm.	50.8	146.0	304.8	558.8	844.6
0.500	827	440	283	182	147
1.135	637	416	275	173	
1.770	436	370	254	173	142
2.405	221	302			
3.040	95	228	210	160	133
3.675	38				
4.310	28.5	112	162	137	126
4.945		51			
5.580		42	101	117	118
6.850			50		
8.120			35	71	96
9.390				39	61.5
10.660					53
13.200					41
50.000	24	26	33	37	37

Table 6.

c_i = 50 w.p.p.m. Q_i = 0.908 Lit./min. I.O.D. = 21100

y mm. \ x mm.	50.8	146.0	304.8	558.8	844.6
0.500	486	261	163	108	86
1.135	429	236	159		
1.770	300	210	152	107	83
2.405	172				
3.040	83	140	129	102.5	70.5
3.675	30				
4.310	7	70	94	83	
4.945		34			
5.580		14	57	76	68
6.850			20		
8.120			16	38	37.5
10.660				18	24.5
13.200					23
50.000	5	7	9	18	21

Table 7.

c_i = 100 w.p.p.m. Q_i = 1.211 Lit./min. I.O.D. = 21800

y mm / x mm.	[illegible]	146.0	204.8	558.8	911.6
[illegible]	731	406	238	154	112
1.135	377	274	220	146	
1.770	220	276	215	127	112
2.405	71	224	190		
3.040	33	157	176	125	110
3.675	6	102	135		
4.310		56	125	106	92
4.945		22			
5.580		13	60	72	84
6.850			30	48	74
8.120			16	30	61
9.390				23	
10.660				18	34
12.200					26
15.240					22
50.000	2.5	8.	11	15	20

Table 8.

c_i = 100 w.p.p.i. Q_i = 1.893 Lit./min. I.O.D. = 21800

y mm / x mm.	[illegible]	146.0	204.8	558.8	911.6
[illegible]	1[illegible]	420	360	216	167
1.135	602	535	356	217	163
1.770	404	456	327	207	166
2.405	205	330	294	201	
3.040	64	222	225	193	157
3.675	19	135	205		
4.310		83	170	150	143
[illegible]		38	98	124	132
4.850			60	83	
8.120			35	58	93
10.660				30	60
12.200					38
50.000	6	15	20	25	31

Table 9.

c_i = 100 w.p.p.m. Q_i = 2.687 Lit./min. I.O.D. = 21800

y mm. \ x mm.	50.8	146.0	304.8	558.8	844.6
0.500	1249	998	632	371	300
1.135	626	747	557	356	287
1.770	331	504	456	340	274
2.405	116	296	394	315	
3.040	37	169	324	292	260
3.675		103	225	270	
4.310		39	195	256	230
5.580			121	172	211
6.850			81	122	
8.120			41	74	115
9.390				53	
10.660					77
12.200					59
50.000	7	17	27	37	47

Table 10.

c_i = 250 w.p.p.m. Q_i = 2.479 Lit./min. I.O.D. = 9875

y mm. \ x mm.	50.8	146.0	304.8	558.8	844.6
0.500	100	285	287	195	114
1.135	62	147	160	152	115
1.770	22	71	115	140	112
2.405	6	39	75	128	111
3.040		21	51	111	101
3.675			36	83.5	104
4.310			19	72	90
4.945				53	77
5.580				36	70
6.850				25	47
8.120					41
9.390					29
50.000	3	5	6	11	16

Table 11.

c_i = 250 w.p.p.m. Q_i = 1.457 Lit./min. I.O.D. = 9875

y mm. \ x mm.	50.8	146.0	304.8	558.8	944.6
0.600	252	287	206	105	70
1.135	95	143	141	97	76
1.770	31	82.5	115	95	79
2.405	20	63	102	85	69
3.040		38.5	70	69.5	67
3.675			46	64	65
4.310			39	55	62
4.945			26	48	62
5.580				41	58
6.850				22	50
8.120					36
9.390					27
10.660					18
50.000	6	8	10	11	13

Table 12.

c_i = 250 w.p.p.m. Q_i = 1.041 Lit./min. I.O.D. = 9875

y mm. \ x mm.	50.8	146.0	304.8	558.8	944.6
0.600	185	180	102	56	43
1.135	94	132	81	54.5	43
1.770	61	93	75	52	40
2.405	30.5	61	60	49	36
3.040		37	47	47	30
3.675			29	30	25
4.310			25	25	36
4.945				20	33
5.580				14	30.5
6.850				13	24
8.120					18
9.390					12.5
10.660					8
50.000	0	1	2	3	4

Table 13.

c_i = 500 w.p.p.m. Q_i = 0.833 Lit./min. I.O.D. = 21800

y mm. \ x mm.	50.8	146.0	304.8	558.8	944.6
0.500	230	272	276	167	122
1.135	121	158	202	136	120
1.770	51	94	162	142	114
2.405	35	52	114	121	110
3.040		44	70	94	113
3.675			70	95	102
4.310			54	88	93
4.945			44	58	89
5.580				57	80
6.850					61
8.120					48
50.000	24	26	29	32	36

Table 14.

c_i = 500 w.p.p.m. Q_i = 1.457 Lit./min. I.O.D. = 21800

y mm. \ x mm.	50.8	146.0	304.8	558.8	944.6
0.500	206	293	270	302	125
1.135	78	149	192	244	167
1.770	11.5	69	114	170	162
2.405	7.5	48	93	156	157
3.040		19	59	134	134
3.675			40	97	138
4.310			31	72	121
4.945				55	86
5.580				48	94
6.850				22	67
8.120					38
50.000	4	6	11	17	22

Table 15.

c_i = 500 w.p.p.m. Q_i = 2.195 Lit./min. I.O.D. = 21800

y mm. \ x mm.	50.8	146.0	304.8	558.8	844.6
0.500	351	433	500	557	411
1.135	103	188	297	386	302
1.770	38	82	128	284	248
2.405	24	43	89	191	242
3.040	13	32	74	151	240
3.675			50	121	180
4.310			36	90	146
4.945				67	134
5.580				54	119
6.850					82
8.120					64
50.000	8	14	24	30	40

Table 16.

c_i = 1500 w.p.p.m. Q_i = 1.022 Lit./min. I.O.D. = 66000

y mm. \ x mm.	50.8	146.0	304.8	558.8	844.6
0.500	272	490	591	647	469
1.135	87	245	391	535	444
1.770	30	170	280	364	390
2.405	17	95	217	264	322
3.040	16	58	142	212	315
3.675	15	45	101	172	267
4.310		36	76	136	233
4.945		33	68	113	204
5.580			53	104	184
6.850			47	79	136
8.120					114
9.390					85
10.660					79
50.000	15	31	47	57	79

Table 17.

c_i = 1500 w.p.p.m. Q_i = 0.435 Lit./min. I.O.D. = 66000

y mm. \ x mm.	50.8	146.0	304.8	558.8	844.6
0.500	147	287	307	148	98
1.135	138	157	201	123	95
1.770	23	97	134	116	97
2.405	17	54	97	100	89
3.040	12	32	70	92	82
3.675	0	22	49	79	76
4.310		17	39	59	72
4.945				55	64
5.580					64
6.950					61
8.120					46
50.000	0	14	17	20	22

Table 18.

c_i = 1500 w.p.p.m. Q_i = 0.738 Lit./min. I.O.D. = 66000

y mm. \ x mm.	50.8	146.0	304.8	558.8	844.6
0.500	184	405	506	277	
1.135	98	196	278	212	
1.770	20	72	171	100	
2.405	14	61	112	177	
3.040		31	71	138	
3.675	7	21	46	95	
4.945		12	35		
50.000	4	11	20	27	

VELOCITY DATA

Table 19.

Velocity data prior to the test plate U_{max} = 4.572 m./sec.

y mm.	$\bar{u}/\bar{u}_{max}$
0.000	1.000
10.000	0.990
21.000	0.973
23.540	0.960
28.620	0.948
33.700	0.936
38.780	0.923
46.400	0.883
54.020	0.850

Table 20.

x m. / U_{max} m/sec. / y mm.	0.2318	0.673	1.1208
	5.356	5.493	5.592
0.500	0.737	0.647	0.617
1.770	0.856	0.719	0.696
3.040	0.951	0.789	0.745
5.580	1.000	0.910	0.816
8.120	0.996	0.979	0.882
13.200	0.987	1.000	0.976
18.280	0.978	0.996	1.000
25.900	0.969	0.992	0.992
33.520	0.960	0.988	0.984
38.600	0.951	0.971	0.980
43.680	0.942	0.963	0.968
48.760	0.929	0.954	0.951
51.300	0.900	0.937	0.934